THESIS

TOOLLESS OUT OF BUILD PLANE MANUFACTURING OF INTRICATE CONTINUOUS FIBER REINFORCED THERMOPLASTIC COMPOSITES WITH A 3D PRINTING SYSTEM

Submitted by

Mark Elliott Bourgeois

Department of Mechanical Engineering

In partial fulfillment of the requirements

For the Degree of Master of Science

Colorado State University

Fort Collins, Colorado

Summer 2019

Master’s Committee:

Advisor: Dr. Donald Radford

Dr. Kaka Ma
Dr. Anthony Maciejewski

ABSTRACT

TOOLLESS OUT OF BUILD PLANE MANUFACTURING OF INTRICATE CONTINUOUS FIBER REINFORCED THERMOPLASTIC COMPOSITES WITH A 3D PRINTING SYSTEM

Continuous fiber reinforced composite materials are manufactured using a variety of techniques ranging from manual layup to highly automated tape and fiber placement, yet all of the processes require significant tooling to act as a form which gives the composite the desired shape until processing is complete. Once processed and rigid, the composite is removed from the tooling and the tooling is, usually, then prepared and another composite component shaped on the tool. Manufacturing on such tooling has the advantage of offering a repeatable shape in a large batch production of fiber reinforced composite parts; however, the tooling itself can be a significant time to manufacture and cost challenge. It may take a large volume of composite parts to effectively amortize the cost of the tooling, which has a finite service life. Further, once the tooling is produced, making geometry changes during a production cycle is almost impossible. Geometry changes need either remanufacture of the tooling or the development of completely new tooling sets. Thus, technologies which could reduce the required tooling for composites production are highly desirable.

With the advent of additive manufacture, it has become commonplace to expect the development of components of very complex geometry built from a simple surface. However, unlike continuous fiber reinforced composites, these complex geometry 3D printed components have material properties which are, for the most part, non-directional. While fiber reinforced composites are produced in a layer-by-layer additive fashion, the key to the performance of this material family is the positioning and orientation of the continuous fiber over complex contours, which has resulted in a need for substantial tooling. Thus, if concepts related to 3D printing could be mapped into the continuous fiber

reinforced composite manufacturing space, the potential may exist for a radical reduction in the amount of tooling required and a corresponding increase in the flexibility of manufacture. The current research effort implements concepts common to 3D printing to investigate an approach to producing continuous fiber reinforced structures which require no tooling.

Sandwich panels are commonly used as structure based on fiber reinforced composites, with the goal of high flexural stiffness and low mass. It is most common to separate two high performance composite laminates (facesheets) with a low-density core material, generally in the form of a foam of honeycomb. A recent concept has been to replace these traditional core materials with fiber reinforced truss-like structures, with the goal of further reducing mass; however, a manufacturable solution for these truss core sandwich panels has not been developed and those processes that do exist are tooling intensive. In this work, a system was developed and demonstrated that can radically reduce the amount of tooling required for truss core sandwich panels. Pyramidal truss core sandwich panels were manufactured to test the positional fidelity of out of build plane, unsupported space manufacturing. Laminates with different lamina counts were manufactured on a substrate and in unsupported space and tested for consolidation quality. Lap shear specimens were manufactured on a substrate and in unsupported space and tested for interlaminar bond quality. Individual continuous fiber reinforced composite strand specimens were manufactured in unsupported space at varying temperatures and tested for stiffness. These truss core panels, manufactured without tooling, were compared to similar truss core panels produced by more traditional techniques.

The outcome of the research performed indicates that structures could be manufactured, unsupported, in free space with good precision. The void content of laminates manufactured in unsupported space decreased by 15% as the laminate was built up while the laminate manufactured on the substrate had no significant change in void content. Unidirectional laminates placed in space showed no statistical difference in strength when compared to laminates placed on a substrate.

Crossply laminates had a 33% reduction in strength compared to similar laminates placed on a substrate. Composite truss core sandwich panels manufactured with the system developed in this work were more precise than composite truss core sandwich panels manufactured with compression molding and heat fusion bonding. Increasing the placement temperature of continuous fiber reinforced thermoplastic strands increases the quality of the strand by up to 44%. Improvements to the MAGIC system have increased the composite quality by 25%.

Thus, manufacturing techniques were implemented to place fiber not only within the build plane, X-Y, but also to place continuous fiber out of the build plane, X-Y-Z. Intricate continuous fiber reinforced thermoplastic composites were manufactured without the use of tooling. While the composites produced with the new system were less stiff than composites made with compression molding further improvements to the manufacturing system have closed the stiffness gap between the two manufacturing methods.

ACKNOWLEDGEMENTS

I would like to thank my advisor Dr. Donald Radford for his help and patience over the past 3 years. It has been a pleasure working with everyone who has worked at the Factory facility. A special thanks to Patrick Rodriquez for his help throughout the graduate school process. My parents have been very supportive, and I could not have been able to have this opportunity without their help and support. All my friends both within work and outside of work have been pillars that have helped support me when working for these past years and without their support I would not be who I am today. To everyone that has shaped who I am, Thank you.

TABLE OF CONTENTS

CHAPTER 1: INTRODUCTION

Continuous fiber reinforced thermoplastic composite materials have become more pertinent due to the recyclability, but the processing of thermoplastic composite materials into net shape products requires significant tooling to act as a form which gives the composite the desired shape. A composite material consists of a reinforcement and a matrix. The reinforcement fibers have a higher stiffness than the matrix material to withstand loads while the matrix material transmits significant loads to the reinforcement and holds the fibers a desired shape and orientation. Fiber reinforcement is flexible and can conform to different shapes but will not keep a shape unless bound with a rigid matrix material. During the manufacture of composite materials, the matrix material must be in a state where it can flow freely to fully coat (wet out) the fiber reinforcement and form the desired shape. Tooling is used to control the shape of the composite material as the matrix solidifies.

THERMOPLASTIC MATRIX COMPOSITES

There are two types of polymers most relevant to plastics for composite manufacturing, thermoplastics and thermosets. Thermosets have low viscosities before cure and cure with heat making them an ideal choice when selecting a matrix material for composite structures; however, thermosets limit any potential recycling of the composite material due to cure induced rigid crosslinks. Thermoplastics are recyclable their use in composite material design has increased specifically for this purpose.

Two groups of thermoplastics that need to be addressed are semi-crystalline and amorphous thermoplastic polymers. Amorphous polymers have a glass transition temperature while semi-crystalline thermoplastics have a glass transition temperature and a melt temperature. Heating amorphous thermoplastic polymers above their glass transition temperature exponentially decreases the viscosity of the plastic enabling flow of the polymer chains. Glass transition temperatures of common thermoplastics can be found in Figure 1. When cooled from above the glass transition temperature the thermoplastic will become rigid, but can be reheated and reformed. A graph of material stiffness vs temperature is shown in Figure 2. For semi-crystalline thermoplastic polymers, the viscosity exponentially drops when the temperature increases beyond its melting temperature. When the temperature within the polymer are above the melting point crystalline structures within the thermoplastic break down and reform below the melting point. Crystalline regions are tightly packed, well organized molecular chains and when broken down the volume of the material increases significantly. When cooled slowly the crystalline structures reform decreasing the volume significantly. Changes in volume are not limited to semi-crystalline polymers. When volume changes occur during manufacturing internal stresses form within the structure and warping of the part often occurs.

When processing thermoplastic composite materials, it is important to decrease the viscosity as much as possible to fully wet out the reinforcement. When the matrix material has a long way to move to wet out the reinforcement it is important to control the time, temperature, and pressure. Increasing the time that the polymer it at a high temperature, and low viscosity, will facilitate flow of the polymer matrix over long distances. Increasing the pressure removes voids and forces the low viscosity polymer to flow faster around the reinforcement. Numerous composites manufacturing techniques have been developed to produce continuous fiber reinforced thermoplastic composite (CFRTC) structures which all use different methods to control time, temperature, and pressure.

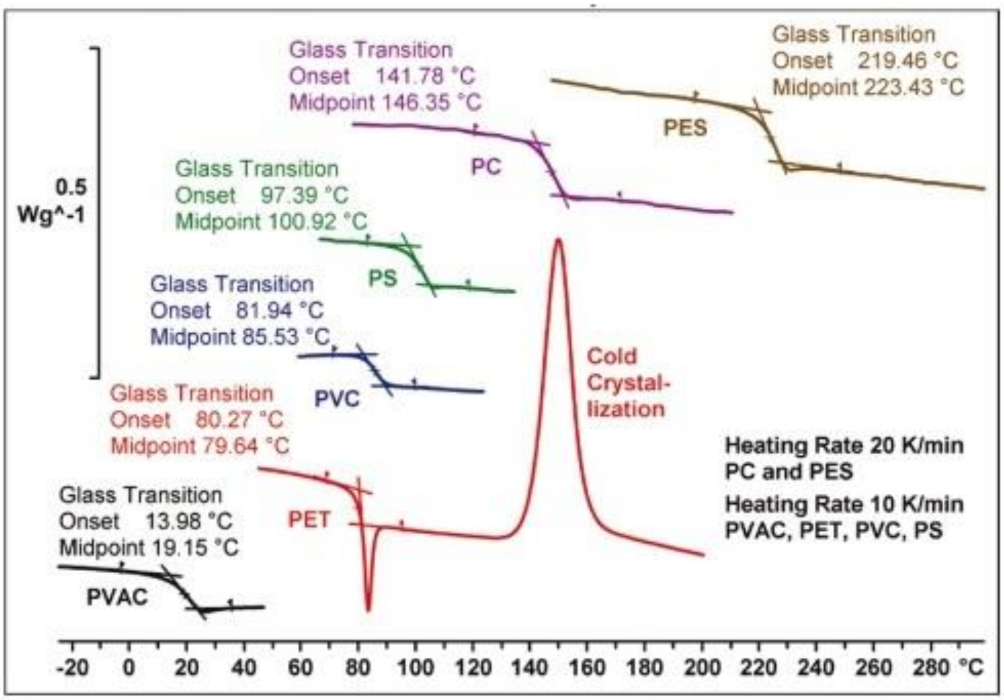

Figure 1: Glass Transition Temperature Measurements Using DSC [1]

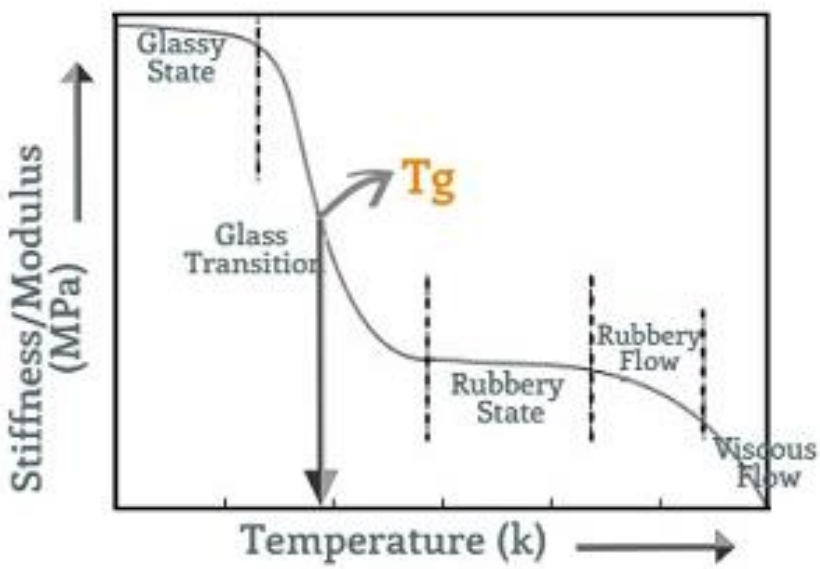

Figure 2: Modulus vs Temperature of Generic Thermoplastics [1]

COMPOSITE MANUFACTURING METHODS

HAND LAYUP

For complex geometries hand layup is the only way to manufacture a part, but this can also be one of the most expensive means of manufacturing because of the tooling and labor costs. Hand layup is the process of a trained layup technician placing either pre-impregnated sheets or a reinforcement and resin mixture onto a tool, shown in Figure 3. The lack of automation for the hand layup process means that parts can be manufactured inconsistently leading to variances in part performance. One prime example of the complexity for a hand layup part is the thrust reversing cascade basket, a demonstration article is shown in Figure 4, a structure where every surface is a tooled surface and has multiple cells that have slightly different geometries, all requiring complex tooling. Automating the manufacturing of these complex composites is difficult and the tooling cost for parts is substantial. As the complexity of a composite structure increases the ease of automation decreases. Continuous fiber reinforced thermoplastic composite materials are not often manufactured with hand layup. Directional placement of thermoplastic pre-impregnated tape within a tool is a technique that often combines some automation with hand layup techniques.

Figure 3: Hand Layup onto Complex Large Tooling [2]

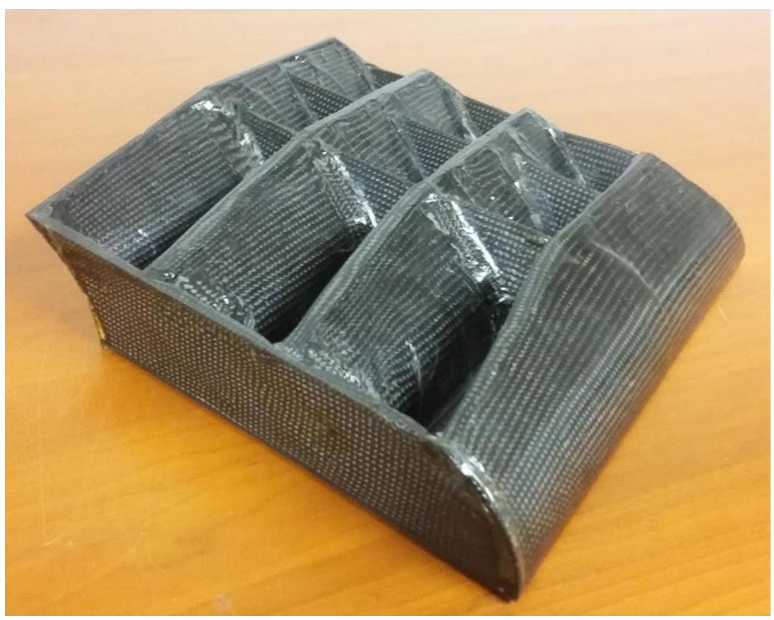

Figure 4: Thrust Reversing Cascade Basked Demonstration Article

COMPRESSION MOLDING

Compression molding composites is done by either heating up the fiber reinforced material stock or a set of matched molds and applying pressure to the material, forcing it to take on the shape of the mold. Alternatively, a charge, bulk material that will be formed, is placed in a set of matched molds. Pressure and heat are then applied to form the desired shape. Charges can consist of thermoplastics, thermosetting resins or composite materials. Continuous fiber compression molded composites are not as common as short fiber reinforced compression molded thermoplastic composites because the fiber orientation of continuous fiber composite structures is more critical and issues where the fiber moves to conform with the flow path occur frequently. Charges are more difficult to generate with continuous fiber reinforcement and short fiber is preferred, but continuous fiber composites have been manufactured with compression molding techniques. Composites made with compression molding techniques often have low void contents and good fiber wet out. Compression molding requires a press to force the charge into the desired shape, therefore the molds used in compression molding are limited to the size

FILAMENT WINDING

Filament winding is the process of selectively placing reinforcement in pre-specified locations around a mandrel. The mandrels shape is determined by the end part and the fiber direction is dictated by how fast the mandrel rotates and how fast the fiber placement head moves across the mandrel. More complex placement heads allow for more complex fiber paths around the mandrel. The direction of the fibers (fiber angle) and different winding parameters will affect the quality of the finished part [3]. Filament winding is very effective for large pressure vessels and other round shapes as shown in Figure 5. The simplicity of filament winding also makes the process easily scalable, limited only by the post processing requirements of the composite system. The tooling for large mandrels is substantial and leads to increased part costs.

Figure 5: Large Scale Filament Winding [4]

PULTRUSION

Manufacturing a composite structure with constant cross section but with varying lengths can be accomplished with a process called pultrusion. Pultrusion starts with continuous roving being pulled through a bath coating the fibers in a resin or powder. The coated fiber reinforcement is then pulled through a heated forming die to achieve the desired shape and cure the resin or melt the thermoplastic [5]. A good surface is created on every surface of a pultruded composite because the composite goes through a die as shown in Figure 6. A mechanism pulls the composite from the die after the composite has been cooled, thus the composite can be continuously be pultruded from the die. For thermosetting resin and thermoplastic matrix composites, the die must have temperature controlled to facilitate processing [6]. Manufacturing complex dies for pultrusion is expensive, but the ability to amortize the cost of the mold over the production run makes the process affordable.

Figure 6: Tooling Dies for the Pultrusion Process [7]

AUTOMATIC TAPE PLACEMENT

Automatic Tape Placement (ATP) is widely used in industry today to manufacture a variety of composite structures for pressure vessels, airfoils, and wind turbine blades [8]. ATP systems use pre-impregnated composite tape with either thermosetting [8], or thermoplastic [9, 10] polymer matrix materials. A very basic ATP system, illustrated in Figure 7, places the fiber with a placement head consisting of a roller, to place the pre-impregnated tape and apply pressure to remove voids [11], and a heating system to make the tape more pliable and tackier to stick to the surface of the tool. Large parts require tooling of equivalent size that is very costly to manufacture, as shown in Figure 8. The tooling must have large radiused curvature for the roller to apply adequate consolidation force and geometries produced by ATP generally have large radii of curvature.

The composite tape must be able to conform to the tooled shape when being applied to various contours present on the tool. When the curvature changes the fiber paths of the tape change increasing the length in some areas and decreasing the length in other areas of the tape. Creating an environment where fibers in the tape can shear relative to one another increases positional fidelity. When the fibers shear the relative length of the fiber does not change and the path the fibers take during placement is independent of the tape itself [12]. Tow/tape shearing increases the quality of composite structures that have complex curvatures by reducing fiber or matrix build up in corners and decreasing the number of cuts the ATP system must make to manufacture the composite. Traditional ATP placement paths are shown in Figure 9 (a) and placement paths for individual tows using tow shearing techniques are shown in Figure 9 (b).

ATP placement systems build up a laminate, one lamina at a time and are limited to placing fiber onto tooling. ATP laminates with thermosetting resins need to be cured after the laminate has been placed and this curing takes place in a large-scale oven or autoclave while thermoplastic composite tapes do not need an extra curing process because the composite is consolidated and solidified in-situ with the ATP process. The process of building a structure one layer/lamina at a time is similar to Fused Deposition Manufacturing, a 3D printing technique where thermoplastic filaments are selectivity placed to produce extremely complex structures using only a placement head and a simple build surface.

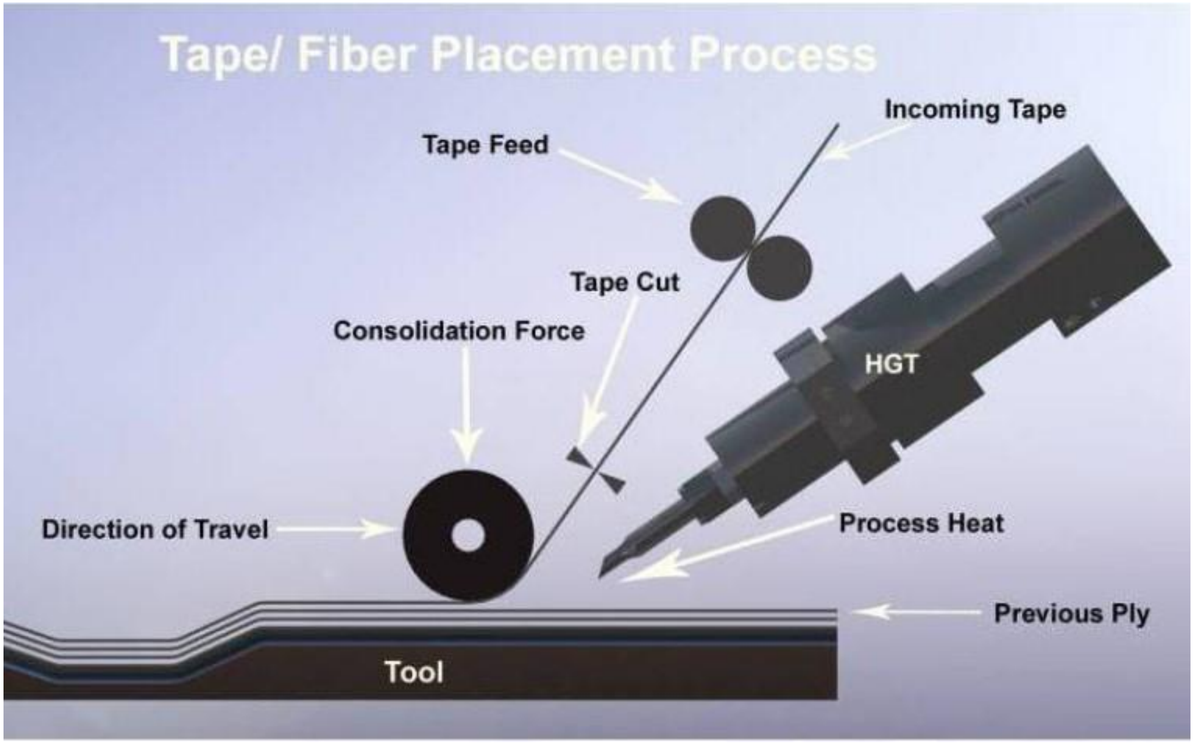

Figure 7: Anatomy of an ATP Placement Head [8]

Figure 8: Fiber Being Placed Over a Tool Using the ATP System [13]

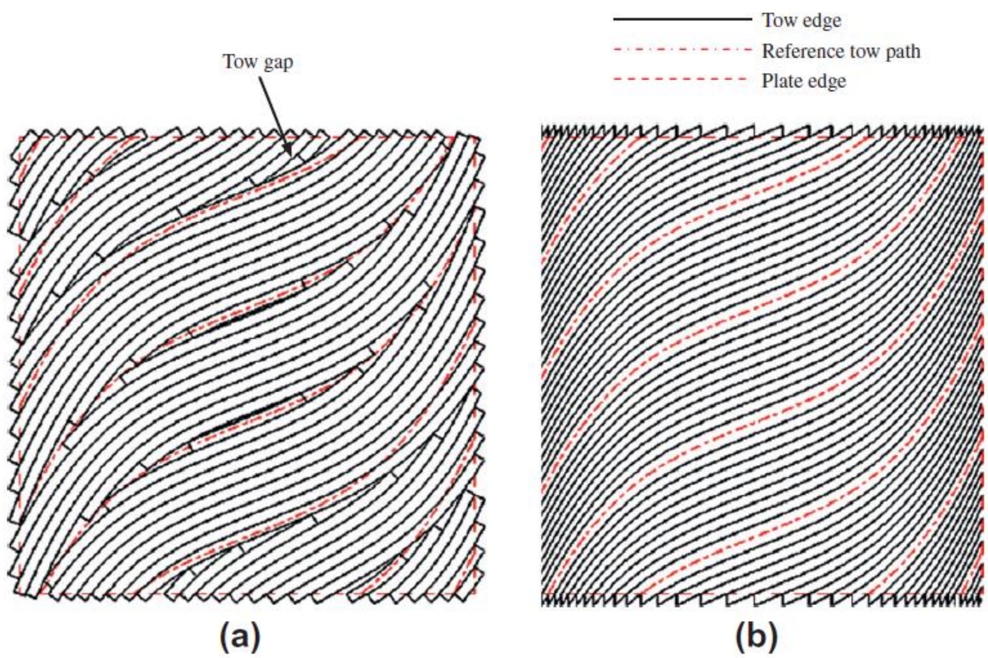

Figure 9: ATP Tape Placement Paths (a) Conventional Pathing (b) with Tow shearing [12]

FUSED DEPOSITION MODELING 3D PRINTING METHOD

There are many different types of 3D printing that produce different levels of quality in the final part and use different materials. This work references the Fused Deposition Modeling (FDM) Printing methodology.

ANATOMY OF AN FDM PLACEMENT SYSTEM

There are two main parts to an FDM extrusion system, the hot end and the extruder. The hot end consists of cooling fins, a heat break, a heater block and a nozzle, shown Figure 10. The cooling fins have two functions; (1) stop heat from traveling from the heater block to the gantry, and (2) keep the thermoplastic filament from melting before it gets to the heater block. The heat break, generally made from insulative materials, helps to stop heat from moving up to the cooling fins. If the thermoplastic melts before getting to the heater block the filament jams in the heat break. The heater block consists of a heater cartridge and thermistor or thermocouple and is used to control the temperature of the nozzle.

The nozzle houses molten thermoplastic and when the filament is pushed forward by the extruder, discrete molten thermoplastic is pushed out from the opening of the nozzle. The amount of thermoplastic strand extruded from the nozzle is directly correlated to the length of filament forced into the molten thermoplastic.

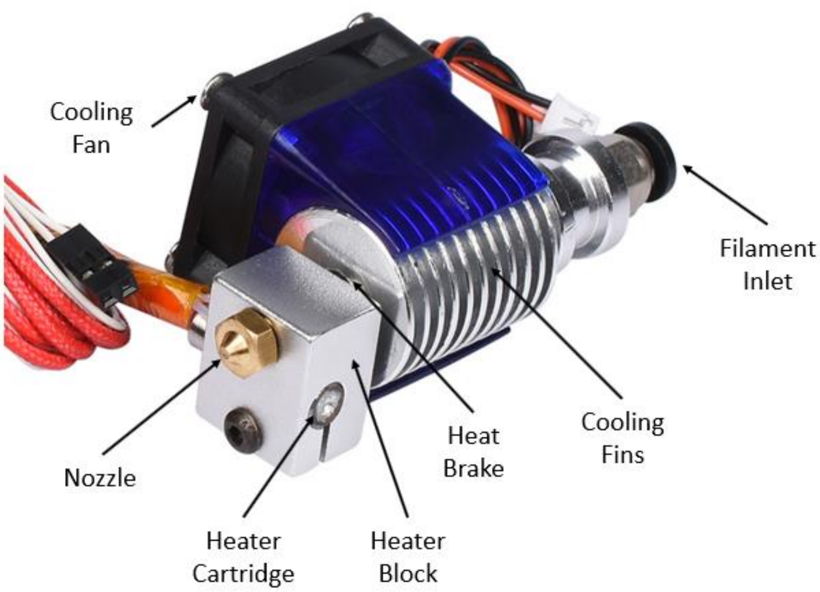

Figure 10: Anatomy of a Hot End

RESOLUTION

Fused deposition modeling works by building up a desired parts structure in a layer-wise fashion. The thermoplastic placement system moves in-plane, placing thermoplastic strands in a predetermined pattern. Once the pattern for a given plane, or layer, is complete the placement system increases the height of the placement plane and starts placing another layer of thermoplastic atop the previous layer. The amount the height increase is called the layer height.

A single thermoplastic strand takes on the shape of the nozzle when extruded but when placed against a substrate the form of the strand takes on the shape of a flat rectangle with curved outer sides.

The height of the thermoplastic strand is the layer height and the width of the strand, known as the bandwidth is slightly larger than the outlet diameter of the nozzle. The cross section of a single strand is known as the resolution of an FDM system. The resolution of a 3D printed part is referencing the error between the desired shape and the as manufactured shape. A large layer height has a low resolution due to the stair stepping effect, and a large nozzle has a low resolution because the size of the bead of thermoplastic is very large, limiting the output quality [14].

MANUFACTURING WITH 3D PRINTING

To manufacture a part with a FDM 3D printing system the part must be first made in a digital format and converted to a Stereolithography (.stl) file. A slicer imports the stereolithography file and generates G-code to manufacture the desired part. The slicer works by cutting the part into parallel planes that are separated by the layer height of the 3D printer. After slicing the part, points for each plane are generated based on the cross section of the part that intersects the reference plane. After the points are generated a computer algorithm generates G-code for each reference plane starting from the substrate and moving upward in the Z-direction to complete the part. The reference plane is known as the build plane. The G-code is then exported into a format that the 3D printer firmware interprets to manufacture the part.

Due to the layer wise manufacturing process, parts made with 3D printing are often somewhat anisotropic, with parts being stiffer in the direction that thermoplastic strands have been placed [15] and less stiff out of the build plane. Chopped fiber reinforced filament is commercially available and work has been done to orient the short fibers to increase the mechanical properties along this preferred direction; however, the anisotropic response of 3D printed parts also increases [16]. 3D printed structures are still not capable of carrying significant shear loads or loads out of the build plane because of the layered structure, and small fractions of very short fibers only offer limited improvements. Placing thermoplastic strands with or without chopped fiber out of the build plane will increase the out of build plane mechanical response of the 3D printed structures [14].

MANUFACTURING CONTROL SYSTEMS

Computer Numerical Control (CNC) machining is when a computer sends code to a controller to precisely move an end effector along predetermined tool paths to manufacture a net shape part from an initial digital design. For CNC milling, the machine is calibrated to know where a single point on the cutting tool is and the milling software creates the path to move that point in a way to machine the desired part [17].

The point controlled by the software is known as the Cutter Location (CL) while the point at which the tool contacts the part is known as the Cutter Contact (CC) [18]. To manufacture complex shapes, it is important to know the difference between CC and CL because the G-code, the code the machine interprets to move to specific locations, just shows the path of the CL. The CC is the last location that the cutting tool touches the stock in the case of conventional cutting, and the first place the cutter touches the stock in the case of climb cutting. The CL changes between 3-axis and 5-axis system and is accounted for in either the firmware or in the Computer Aided Manufacturing package. Computer Aided Manufacturing (CAM) software is used to generate G-code to machine parts from a stock material. When a 3-axis cutting system cuts a slope from stock material the process can take a long time because the cutter orientation only allows for the removal of small section of the stock, an example is shown in Figure 11 (a). This is consistent with FDM 3d printing in that a stair-step contour is produced, with a reduction in the step dimension yielding a surface quality improvement, but at the expense of time. A 5-axis system can change orientations to be more efficient for every cutting operation because the cutting tool can be parallel with the surface of the stock, as show in Figure 11 (b).

The cutting path generated by the CAM software is often an optimal path to generate the surface of the desired structure with as few defects as possible. Defects in this case would be tool marks or small curvatures created by the cutting tool. To reduce defects in the final part small step overs are used. A step over is the distance between passes that the tool will make. Decreasing the step over will create a smoother surface for the final part and less post processing will be needed to finish the part.

Cutting operations can overlap because material is being removed but the same methodology cannot be applied when material is being added to the surface. When adding material to a complex surface, the material added cannot overlap or an increase in volume will occur. Increases in volume on a single layer may not be crucial to the development of a part, but when building up a structure with multiple layers areas with increased thickness will become significant defects later in part production and must be accounted for early in production of structures made with additive manufacturing.

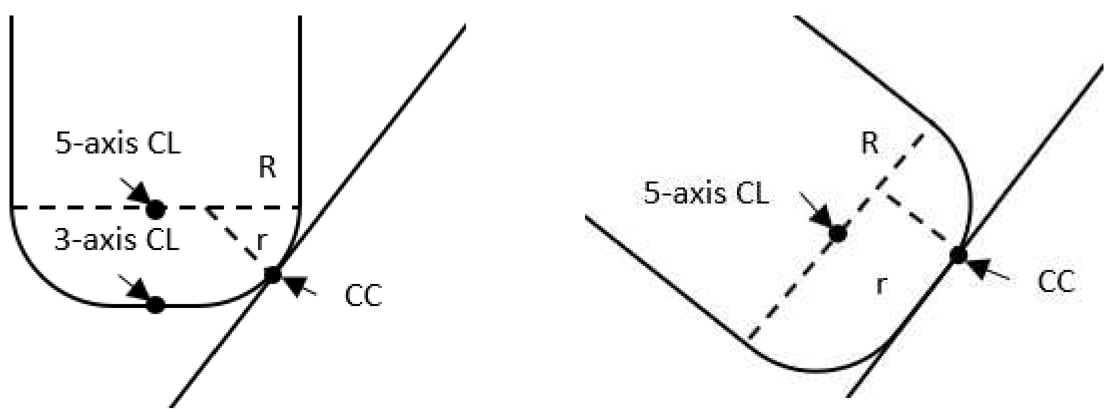

(a) 3-axis CNC Using a Bull Nose End Mill to Cut a Slope

(b) 5 or 6-axis CNC Using a Bull Nose End Mill to Cut a Slope

Figure 11: Difference Between a 3-Axis and a 5 or 6-axis CNC Doing a Cutting Operation

CHAPTER 2: BACKGROUND

The current state of commercial continuous fiber reinforced composite manufacturing with FDM is the MARK TWO and MARK X from Markforged. These machines make use of a proprietary FDM line that is co-extruded with a small fraction (14% by volume) of continuous reinforcement fiber, but these machines are limited to adding in plane reinforcement to individual layers of a thermoplastic parts [19]. The addition of continuous fiber reinforcement to a 3D printed part increases the strength and stiffness of the 3D printed thermoplastic part [20]. Companies that specialize in manufacturing thermoplastic composites with robotic systems [21] have begun to increase in numbers, but robotic manufacturing systems are not publicly available and placement software is proprietary. With a multi-axis manufacturing machine, it is possible to place continuous fiber on multiple faces of a defined geometry as well as place fiber along load paths creating a tailored composite structure that can take full advantage of the potential of a continuous fiber reinforced composite [22]. Continuous fiber reinforced thermoplastic composites manufactured to-date have demonstrated an ability to reduce tooling requirements by placing composite strands in free space [23].

CONTINUOUS REINFORCEMENT DIRECT DIGITAL MANUFACTURING

Direct digital manufacturing is the process of taking a CAD file and using either a CAM package or a slicer to generate G-code used to manipulate a controlled manufacturing system. Current efforts are being made to use direct digital manufacturing techniques to manufacture continuous fiber reinforced thermoplastic composites [24, 25, 26, 27]. Sugiyama et al. combined continuous reinforcement within a print head to manufacture large cell honeycomb sandwich panels [27]. The spans within the honeycomb structure were crossed because the reinforcement was tensioned during placement, shown in Figure 12 [27]. Reinforcement was only placed within the print plane of each layer. Multiple studies have been done on the tensile strength increase in continuous fiber composites manufactured with in-plane reinforcement and the use of reinforcement increased the strength and stiffness of 3D printed parts [25, 26]. The use of a continuous fiber reinforced thermoplastic filament can be placed in a composite structure, but tow shearing of the filament is not possible.

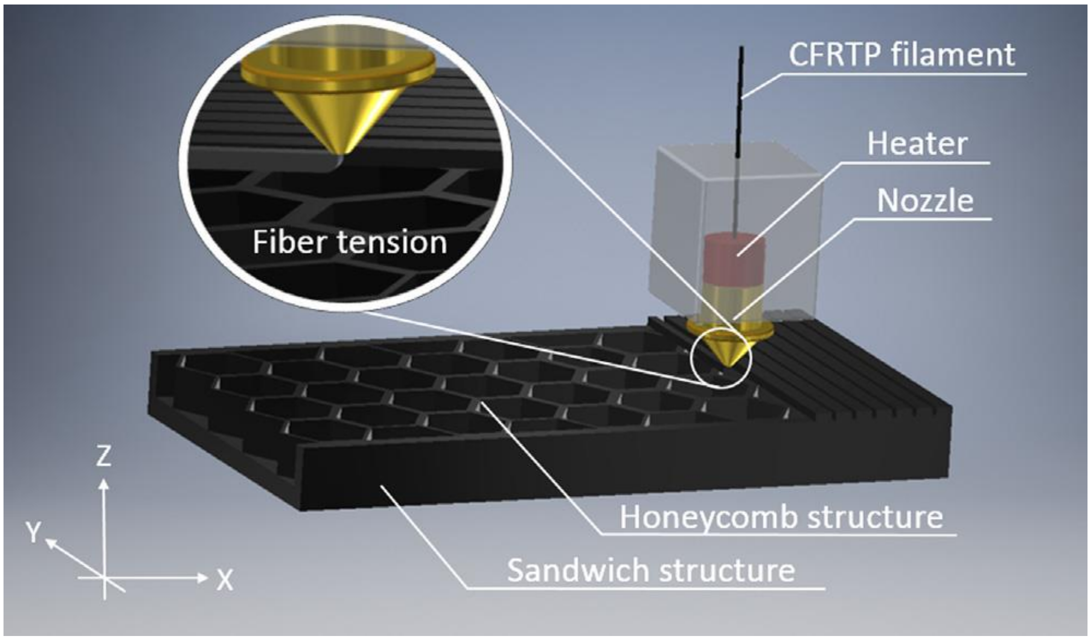

Figure 12: Fiber Placement Over a Honeycomb Span [27]

ADVANTAGES OF COMMINGLED ROVING

Two ways to manufacture continuous fiber reinforced thermoplastic composite (CFRTC) structures using 3D printing techniques have been examined. The first is to combine the reinforcement and the matrix within the placement head [27]. Combining the constituents of the composite in the molten region and extruding the thermoplastic as a normal FDM system while pulling the reinforcement tow from the nozzle. Using this technique is advantageous because the fiber volume fraction can be tailored during the manufacturing process. Current efforts using this technique have shown that the fibers do not intersperse well within the placed strand [24]. The local fiber volume fraction is significant, but the total fiber volume fraction of an extruded strand is less than desired. The second method of manufacturing 3D printed CFRTC structures is having a feed stock that is a premade CFRTC strand that is reformed into the desire shape with 3D printing techniques. This is the method that the Markforged systems uses to produce fiber reinforced thermoplastic parts.

Commingled roving, or hybrid yarn, is readily available raw material that consists of fibers of a reinforcement and a matrix material within the same tow and is typically used for filament winding of thermoplastic parts. Using commingled roving as a feedstock is a combination of the two methods to manufacture CFRTC structures using 3D printing. The constituents of the composite, and the relative amounts, are predetermined by the manufacturer of the commingled feedstock and combining of the reinforcement and the matrix happens within the placement head. Tow shearing is possible because the fiber reinforcement is not restricted using commingled feedstock as it would be with a premade composite strand [28]. With a commingled feedstock the matrix material can be processed in the hot end and the reinforcement fibers can shear over one another. By preprocessing the commingled roving into a CFRTC strand and then using an extruder-based system, complex shapes could be manufactured [29].

When using a commingled roving the thermoplastic matrix does not have to flow long distances to wet out the fibers, making fiber wet out easier than combining the constituents in the hot end. Commingled rovings are available with a variety of different reinforcement fibers including, but not limited to carbon fiber and glass fiber, and different thermoplastic matrix fibers such as PEEK, Nylon, and PET. The weight fraction of the commingled roving material is predetermined by the manufacturer but, in concept, could be changed depending on the structural needs of the part. Commingled roving can be found with fiber volume fraction that range from 30% to 55%. Work has been done to generate out-of-plane continuous fiber thermoplastic composites using commingled roving as a feedstock material [23].

OUT-OF-PLANE CONTINUOUS FIBER PLACEMENT

Placement of fiber with a 3D printing platform has been studied and attempts to place continuous fiber without being limited to the placement plane have been made. Liu et al. placed continuous fiber reinforced plastic in a lattice truss structure using a 3D printing system. The placement system used a 3D printing extrusion system with continuous fiber being pulled through the molten plastic sections. Thermoplastic could be extruded but there was still tension within the placed CFRTC strand [30]. Liu modified the placement path to adjust for deflections caused by the tension and implemented cooling in specific sections to solidify the CFRTC strand increasing the positional fidelity of the placed composite.

Eichenhofer et al. used a robotic system to place continuous fiber reinforced thermoplastic strands out of the build plane using commingled feedstock [23]. Consolidation of the commingled rovings occurred within the nozzle. The commingled roving was first formed by a die into composite rods that were then extruded through a forming nozzle consolidating the CFRTC strand. Out-of-plane placement of the CFRTC strand occurred by first adhering the strand to a nylon base to aid the extrusion of the CFRTC strand. A small adhering region was used before rotating the placement head to the desired angle and placing the fiber in that direction out of plane. Using this method, a simple truss core sandwich panel, shown in Figure 13, was manufactured and tested in compression. The top facing was bonded to the core using and adhesive. By using an extrusion-based system, Eichenhofer limited the placeable fibers paths because tow shearing could not occur due to the composite being formed into a shape then pushed through the nozzle.

Robotic systems have been used to place continuous fiber composites with matrix materials that cure with ultraviolet light. Fiber is pulled though a resin bath, similar to pultrusion, and fed through a long nozzle to place the continuous fiber. Curing of the resin takes place as soon as the tow leaves the nozzle making the process ideal for 3D manufacturing processes. The robotic placement system is used to build an initial structure with CFRTC strands being placed in plane. Once an initial structure is placed the placement plane changes and non-geodesic fiber paths are placed around the initial structure [21]. A proof of concept article was manufactured to demonstrate the capabilities of the UV curable placement system is shown in Figure 14. Non-geodesic paths and out-of-plane placement is demonstrated with the proof of concept article.

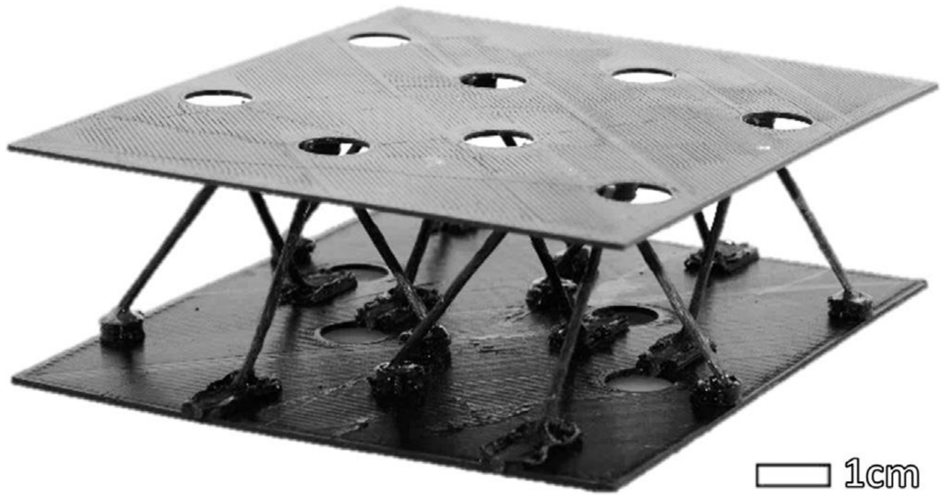

Figure 13: Sandwich Panel Manufacture By 3D Printing Commingled Roving [23]

Figure 14: UV curable Fiber Placement Demonstration Article [22]

PRIOR COMPOSITE MATERIAL MANUFACTURING AND STRUCTURES LABORATORY RESEARCH

Multiple placement systems have been developed to research the placement of high fiber volume fracture Continuous Fiber Reinforced Thermoplastic Composites (CFRTC). Warlick et al. developed a cooling system to increase positional fidelity when toe shearing CFRTC using an E-glass and Polypropylene commingled feedstock [28]. By cooling the CFRTC as it is being placed the thermoplastic solidifies and becomes capable of carrying more tension within the tow. When changing placement direction by making an arc, or just a quick angle change, the fibers on the inside of the arc move a shorter distance than the fibers on the outside of the arc. Without cooling the low viscosity matrix cannot withstand the tension and the outer fibers move toward the inside of the arc. More fibers on the inside of the arc creates a region that has an increased thickness and leads to manufacturing defects. When cooled, the CFRTC closely follows the desired path and proper tow shearing occurs.

Rodriquez et al. developed a method for in-situ consolidation of CFRTC when the composite was being placed with a traditional 3D printing gantry [31]. Consolidation force is necessary to remove voids within newly placed CFRTC strands. Using a spring to apply force to the end of the nozzle is an ideal way of applying a known force. The consolidation force can be determined by the distance the spring deflects multiplied by the spring constant divided the area of compaction. Consolidation force can therefore be controlled by setting an offset between the known layer's height and the desired spring displacement. Using just the machine compliance as a consolidation method does not work as well as a spring because the machine compliance is much lower than the spring. Fluctuations within the substrate height will have a significant impact on the consolidation force when using machine compliance, but have a decreased effect when using a spring for consolidation. A spring with a low spring stiffness to area of compaction ratio should be chosen to reduce substrate fluctuation effects.

Fluctuations in the height across the substrate have less of an effect on the consolidation force with the use of a spring. Without the spring, consolidation occurs by placing the nozzle at a known distance from the substrate. When fluctuations of the substrate occur the consolidation force either increases or decreases significantly based on the stiffness of the placement system. The spring decreases the vertical stiffness of the placement system decreasing the effects of fluctuations in the flatness of the substrate [31]. Utilizing contributions by Warlick and Rodriguez continuous fiber reinforced thermoplastic composite structures could be realized with increased composite quality and greatly reduced tooling.

SANDWICH PANELS

Sandwich panels are often used to increase the flexural stiffness of a structure by increasing the area moment of inertia without dramatically increasing the weight of the structure. Composite sandwich panels gain flexural stiffness and retain low mass by separating laminated composite facings with a lightweight core that resists the shear component of the load. The bending moment stresses are transferred from the face sheets to the core via shear at the interface between the face sheet and the core implying that the core/facing bond is crucial to the structural stability of a sandwich structure.

A sandwich panel consists of 4 major parts, the composite facings, the core, edge closures, and hardpoints. The composite facings add to bending stiffness but do not add to the compression or shear stiffness of the sandwich panel. The core increases the distance between the facings making the thickness contribute to the bending stiffness. Compression and shear stiffnesses of a composite sandwich panel are controlled by the core. Edge closures are used to protect the core and add to the stiffness of the sandwich panel increasing the bending, compressive and shear stiffness [32]. Edge closures and hard points are used to transfer loads into the sandwich.

The bending stiffness of a sandwich panel is defined with Equation 1 and the shear stiffness is defined with equation 2:

$$D = \frac{E_f t_f (t_f + t_c)^2 b}{2} \tag{1}$$

$$S = bhG_c \tag{2}$$

Where:

D = Bending stiffness of a sandwich structure,

S = Panel shear stiffness,

E_f = Modulus of elasticity of facing,

t_f = Thickness of facing,

t_c = Thickness of core,

b = Beam width,

h = Distance between facing centers ($t_f + t_c$),

G_c = Core shear modulus.

The facing thickness, t_f, is generally smaller than the core thickness, t_c, making the bending stiffness dominated by the thickness of the core. Core shear stiffness is equally controlled by all parts of equation 2 [33]. The bond between the core and the facings must be sufficient to transfer loads from once facing to the other.

A core cell is the smallest repeating geometry within the core of a sandwich panel. Core density is calculated using equation 1:

$$\rho_{core} = \frac{M_{core}}{V_{cell}} \tag{3}$$

Where ρ_{core} is the core density, M_{core} is the mass of the core and V_{cell} is the total volume of a single cell. Core density directly effects the stiffness of the core. Relative performance of a core is proportional to the core density. A comparison between core density and the strength and stiffness of the core is shown in Figure 15. There are two ways to increase the core density, by decreasing the cell size with the same amount of material or by forcing more material into the same area [34]. Core compression and shear modulus are correlated to the modulus of the core material and the geometry of the core. Advantageous geometries like the honeycomb cores have lower compression and shear modulus when compared to higher density foams but have a significantly lower weight.

Foam cores are isotropic meaning that the strength and stiffness does not change based on the loading direction, but honeycomb cores are anisotropic meaning that the strength and stiffness of the core is dependent on the loading direction. Honeycomb cores have two configurations, the ribbon configuration and the "W" configuration. The ribbon configuration is parallel to the adhesive that bonds the honeycomb cells to one another while the "W" configuration is perpendicular to the ribbon configuration.

Foam cores have varying densities just like honeycomb cores, but foam cores have a wider range of density. Foam cores can range from a low density, i.e. 10% to as high as 100% and the stiffness and strength of the sandwich structure is proportional to this change in density. The differences in physical and mechanical properties between a common PVC foam core and different honeycomb cores is shown Figure 15.

Edge closures are used to provide local reinforcement and protect the core from local impacts and environmental damage. Closing out the edges of sandwich panels is necessary for the longevity of the sandwich core. Different edge closures are shown in Figure 16. Edge closure can be used for fastening the sandwich structure. Hard points are features incorporated into the sandwich structure that are used to fasten the sandwich structure to other parts. Hard points have to be sufficient in size to distribute the load to the sandwich panel.

More emphasis has been placed on the strength/stiffness to weight ratio of sandwich panel core materials to reduce the weight of composite structures. Continuous fiber reinforced truss core sandwich panels have begun to be researched due to the potential for an increase in the strength/stiffness to weight ratio [35].

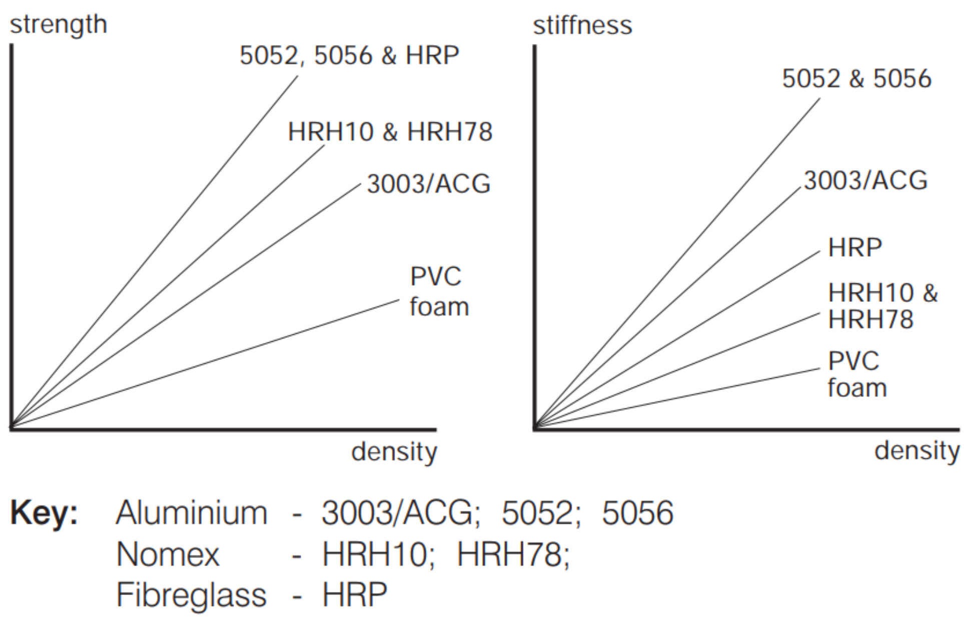

Figure 15: Stiffness of Different Types of Honeycomb Structures Compared to PVC Foam [33]

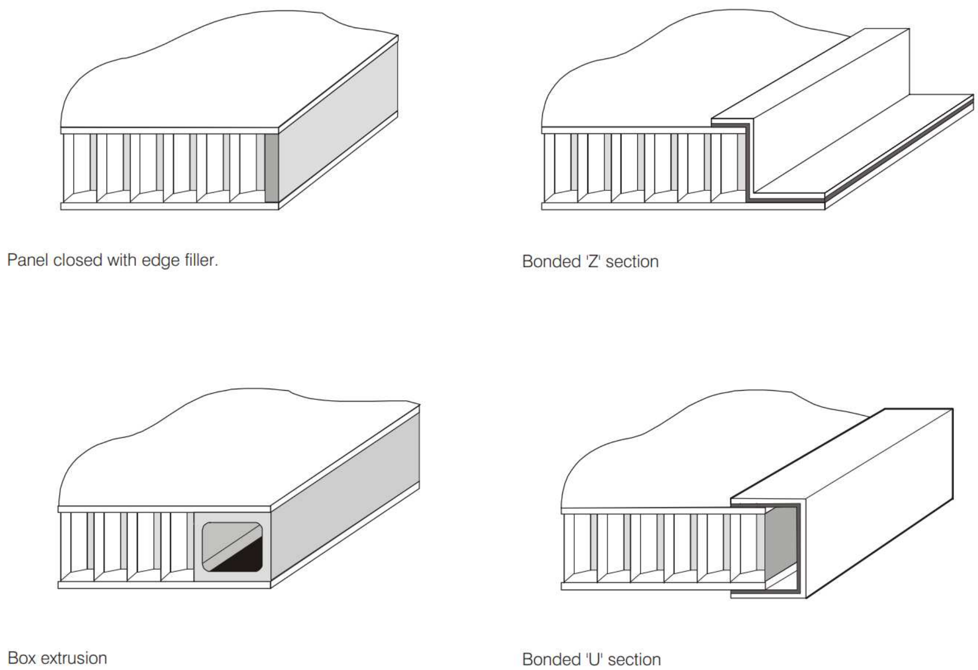

Figure 16: Four different types of edge closure designs [33]

TRUSS CORE SANDWICH PANELS

Lattice core structures have an advantage of a reduced material weight with a strength and stiffness comparable to many foam and honeycomb cores. Therefore, lattice core structures offer the potential for a reduced weight of a sandwich panel, while still maintaining a high strength and stiffness [36]. A lattice core used in a sandwich panel replaces the typical honeycomb or foam core, but the lattice structure has a more advantageous geometry. Placing continuous fiber reinforcement within the lattice of the core has demonstrated an increase in strength with a decrease in weight of the sandwich panels. Lattice cores have predefined shapes, for instance, tetrahedral, Figure 17 (a) [37], kagome, Figure 17 (b) [38], pyramidal, Figure 17 (c) [39, 40], and Navtruss, Figure 17 (d) [41].

The pyramidal shape has been manufactured with a 3D printer using continuous carbon fiber reinforcement [30], waterjet cut and then manually assembled [42], and compression molded with a complex set of tooling [43]. Two methods have been used to bond the core to the facings, a mechanical interlocking method called buried node joining [44, 40], and adhesive bonding [39, 45]. Sandwich panels manufactured with the buried node techniques performed better than panels made with just adhesive bonded joints due to a stronger joint at the truss core/facesheet interface but are more difficult to manufacture. The bondable surface area to bond the core to the facings for pyramidal truss cores is relatively small, by increasing the bond area shear transfer between the facings increases. Thus, increasing the strength of the sandwich structure. A Navtruss core was compared to a buried node pyramidal truss core in compression strength and the results are shown in Figure 18. Bi-directional Navtruss core structures shown in Figure 19, have been manufactured with complex tooling then cut, woven and bonded to the facings [35]. The core shown has 4 Navtruss struts per unit cell and is made from carbon fiber prepreg.

Truss core sandwich panels have significant increases in strength vs. weight and stiffness vs. weight for sandwich plates designed to carry moment and transverse forces. The truss core has an advantage at low core densities, when compared to honeycomb or foam cores but the systems are closely competing [46]. Construction cost becomes the driving force for the decision between honeycomb, foam, or truss cores, with honeycomb and foam cores being currently significantly cheaper to manufacture. Reducing the manufacturing cost of truss core sandwich panels could greatly impact all aspects of the composites industry by reducing the weight and cost of sandwich panel structures.

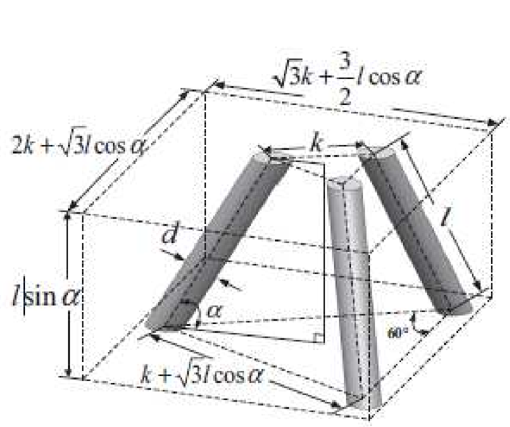

(a) Schematic of a Tetrahedral Truss Core [37]

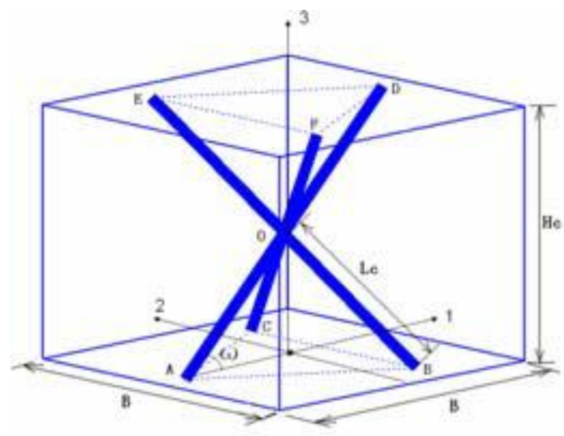

(b) Schematic for Kagome Truss Core [38]

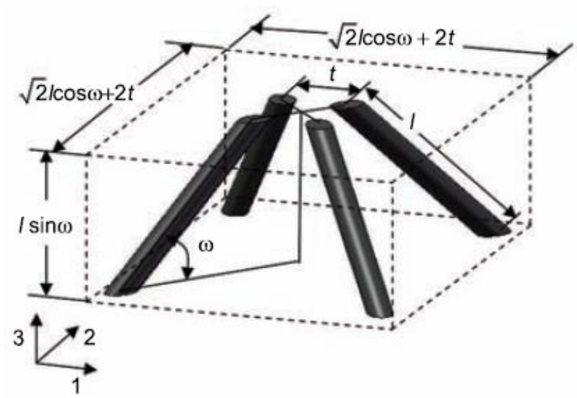

(c) Schematic for Pyramidal Truss Core [43]

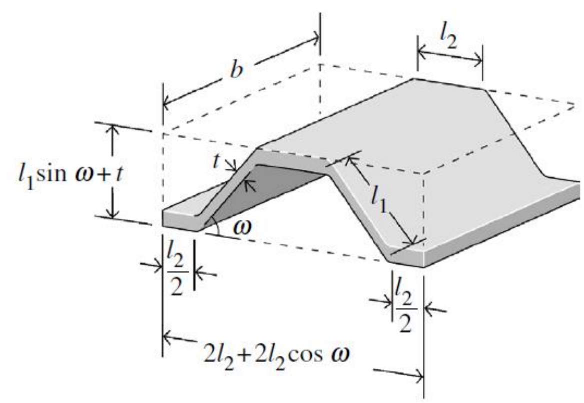

(d) Schematic for Navtruss Corrugation [41]

Figure 17: Schematics for four types of Truss Structures

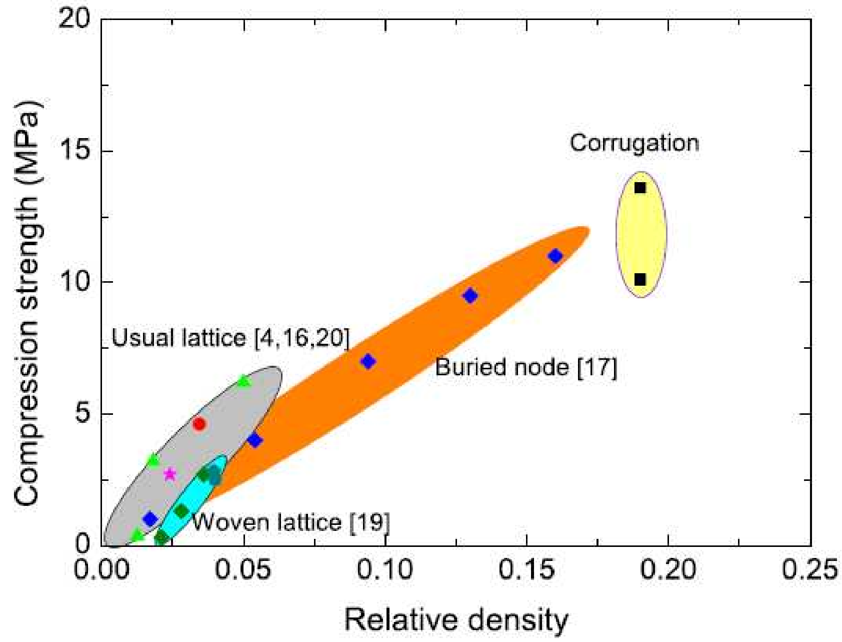

Figure 18: Compression strength of Navtruss Corrugation vs Different Truss Structures [35]

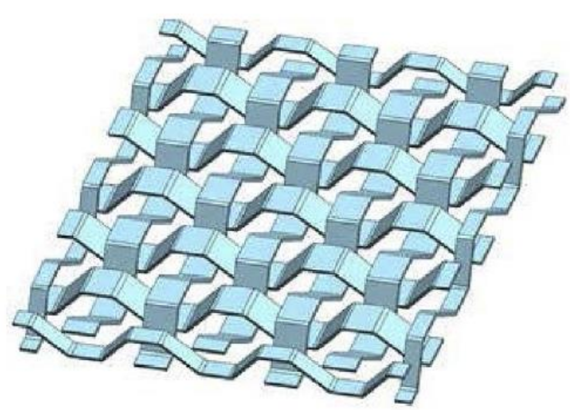

Figure 19: 4 Struts per Cell Woven Bidirectional Navtruss Core [35]

REASON FOR FURTHER INVESTIGATION

Continuous fiber reinforced thermoplastic composites (CFRTC) bring recyclability to the use of composite material structures but the manufacturing cost of CFRTC are still substantial for the realization of recyclable composite parts. Multiple CFRTC manufacturing methods have been investigated but all current manufacturing techniques require the use of complex tooling for the realization of continuous fiber reinforced composite structures. By combining pultrusion, Automated Tape Placement and Fused Deposition Modeling techniques, CFRTC could be manufactured either on existing tooling or in free space, reducing the need for tooling. Utilizing the Modular Additive Generation of Intricate Composites (MAGIC) system developed in the Composite Materials, Manufacture and Structures Laboratory a methodology could be created to eliminate the need for tooling of complex thermoplastic continuous fiber reinforced composite structures. Truss core sandwich panels are a prime example of structures that show mechanical benefits, but are not currently producible because of manufacturing costs, specifically significant tooling costs. Methodologies could be created to be able to redesign existing composite structures, in the case of this work truss core sandwich panels, to make manufacturing of the structures have significantly reduced, if not eliminated, tooling requirements for CFRTC parts.

As the MAGIC system is developed the resolution of parts manufactured will increase and the relative quality of composite structures manufactured will increase. The use of commingled feedstock gives the MAGIC system the ability to manufacture high volume fraction fiber reinforced thermoplastic composites, while keeping the ability to place fiber with tow shearing techniques. Eliminating the need for tooling from composite structures prospects the idea that multiple design iterations can be tested at a quickened pace. Tooling is often a considerable cost in terms of dollars and time for composite structures that have low production volumes. Thus, eliminating the tooling entirely would greatly reduce the cost to produce these composite parts and enable rapid evaluation of the designs.

CHAPTER 3: MAGIC SYSTEM DEVELOPMENT

The Modular Additive Generation of Intricate Composites (MAGIC) system is a combination of methodologies developed to produce high volume fraction composite structures with radically reduced tooling. A large-scale dual gantry 3D printer, shown in Figure 20, was developed to place Continuous Fiber Reinforced Thermoplastic Composite (CFRTC) structures using a commingled roving feedstock and neat thermoplastic using commonly found 3D printing filaments and parts manufactured for fiber placement techniques. Using both the continuous fiber commingled roving and the filament printer in parallel created a unique environment where tooling or support structures could be placed with neat thermoplastic and continuous fiber composites could be manufactured atop the tooling and supported wherever needed.

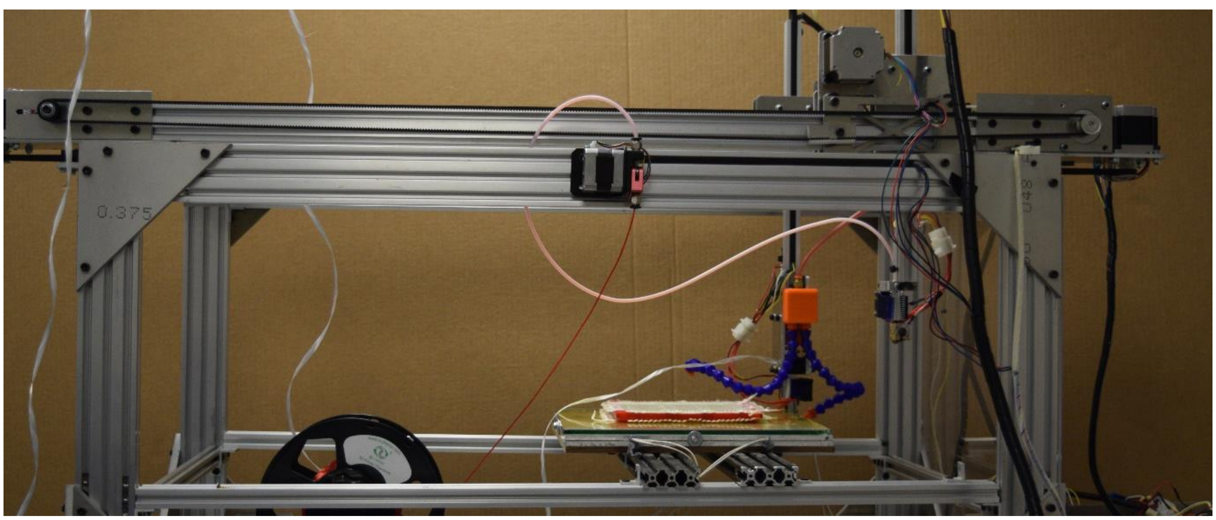

Figure 20: Hardware for the MAGIC system

The anatomy of the MAGIC system includes 3 major parts; (1) hardware used to place materials, (2) firmware used to control the hardware, and (3) software used to generate G-code for the firmware. The nomenclature for the hardware is derived from nomenclature for 3D printing hardware and composite manufacturing. Firmware and software nomenclatures were determined based other manufacturing systems.

During the development of the MAGIC system it was discovered that hardware development was necessary to increase the composite quality. By changing the geometry of the nozzle, the placement head could consolidate intricately placed CFRTC strands. The cooling system was discovered to be necessary when changing the direction of placed CFRTC strands [28] and reduced flash [31]. A computer controlled cooling system was implemented to only use cooling on movements that require it rather than applying the cooling at all times as introduced by Warlick [28]. Increasing the temperature capability of the placement head increased the quality of the placed composite. All of the hardware changes required changing the firmware and the software to produce quality composite structures.

NOMENCLATURE

Important components of the placement system can be found in Figure 21.

Bandwidth – The width of an as placed strand, either a CFRTC strand or a thermoplastic strand.

Build Volume – The smallest volume that both the Composite Placement Head and the Thermoplastic Placement Head can place material.

Composite Placement End Effector – The placement system responsible for CFRTC placement both in free space and consolidating the CFRTC on a substrate.

Composite Placement head – A hot end redesigned to place CFRTC strands using a commingled feedstock, consisting of the nozzle, heater block, heat break and heat sink.

Composite Strand – Commingled roving processed by the composite placement head into a continuous fiber reinforced thermoplastic strand.

Consolidation Spring – Spring used to by the composite placement end effector to apply force to the tip of the nozzle consolidating newly placed composite strands.

Control Temperature – The heater block temperature controlled by the firmware and specified by the G-code.

Controller Firmware – Code written to control the hardware of the 3D printing system. This is currently a heavily modified version of the 2015 Marlin firmware.

Cooling Manifold – Movable outlets for compressed air to locally cool newly placed composite strands.

Fiber Path - The point to point instructions send to the fiber placement head to place fiber between the two points.

Global Coordinate System – The coordinate system used by the firmware to determine the location of both the Composite Placement Head and the Thermoplastic Placement Head while within the build volume.

Heat Sink – A set of fins used to dissipate heat restricting heat to the heater block and nozzle.

Heater Block – The hottest part of the placement head, supplies heat to the nozzle melting the thermoplastic material.

Nozzle – A cylindrical shaft that places material in desired locations.

Nozzle Outlet Temperature – The temperature at the tip of the nozzle.

Repetier Host – Software used to send G-code to the Firmware and displays paths generated with G-code, hot end temperature, and has a user interface to manually manipulate the gantries.

Thermoplastic Placement Head – A hot end used to place neat thermoplastic using traditional FDM 3D printing methods.

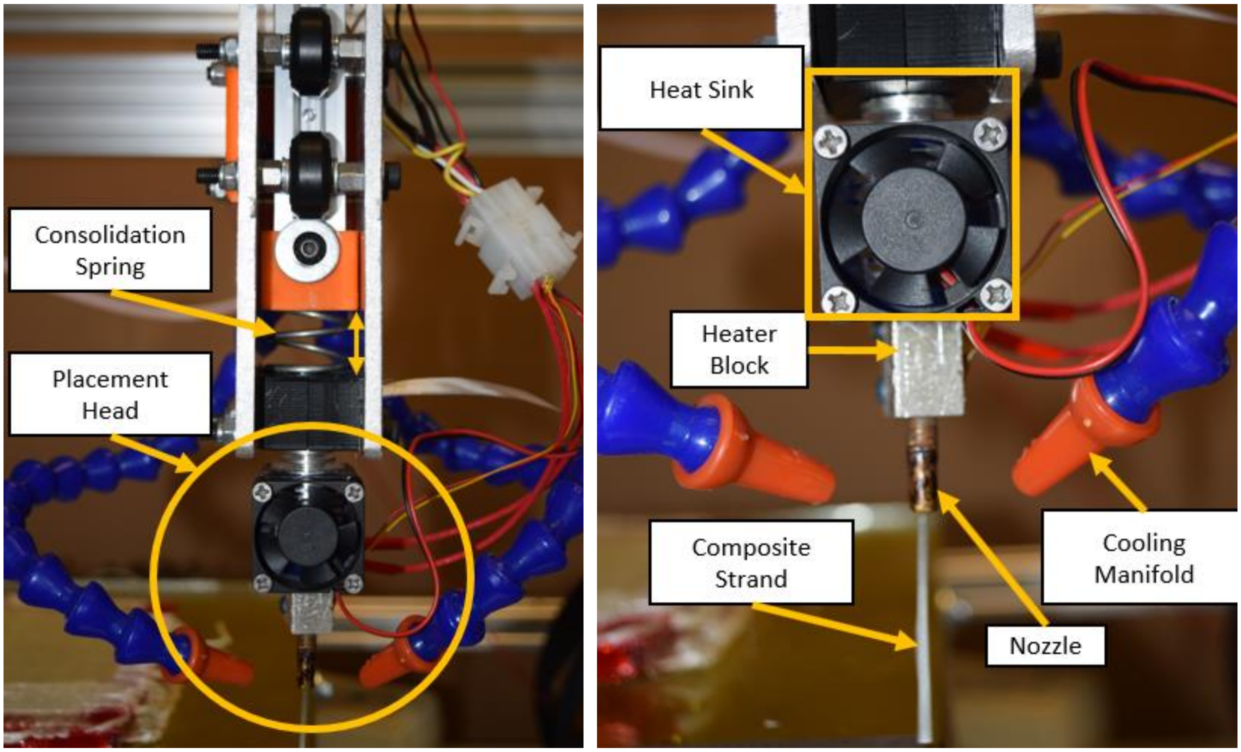

(a) Composite placement End effector (b) Placement Head Components

Figure 21: Composite Placement System Anatomy

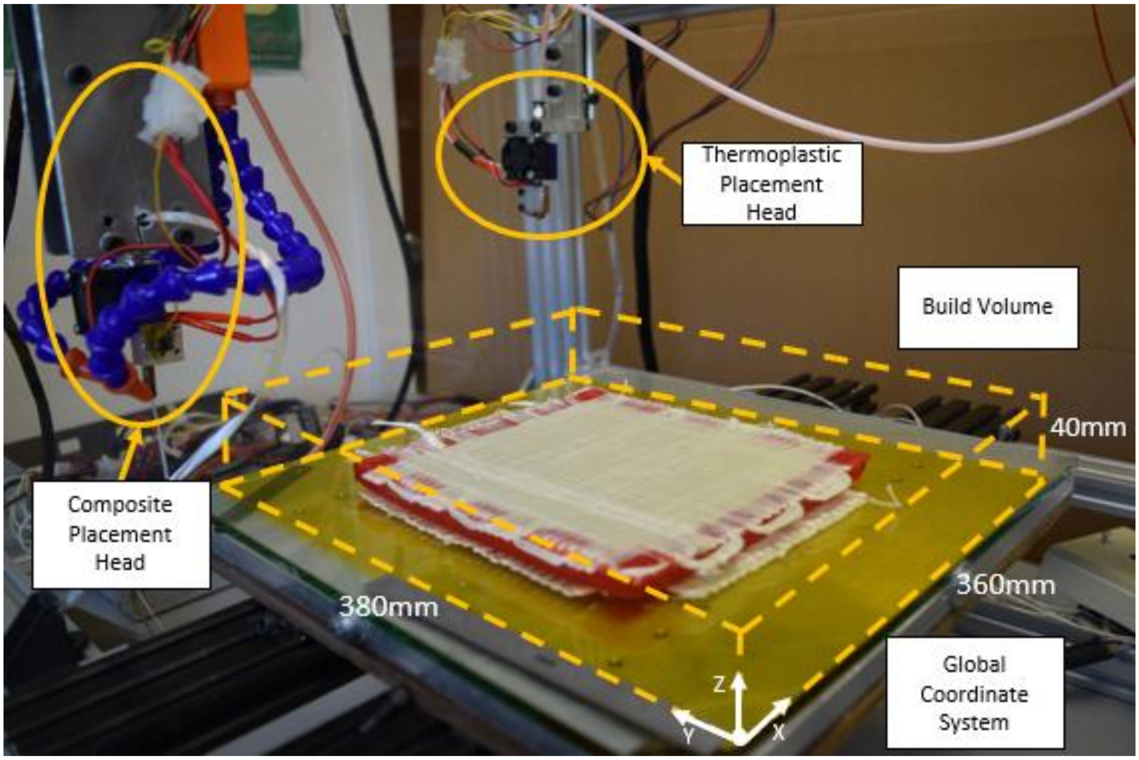

Figure 22: Hardware, Coordinate System, and Build Volume of the MAGIC System

MAGIC SYSTEM DEVELOPMENT

NOZZLE

The nozzle was the first improvement made to the hardware of the composite placement head. The original geometry of the nozzle shown in Figure 23 (a) was compact with a large flat region used to consolidate the composite strand as it was being placed on a substrate. This large flat region worked well for consolidation, but kept the newly placed CFRTC hot. The hot CFRTC would be less advantageous for creating non-geodesic fiber orientations, thus, design changes needed to be made.

An improved composite nozzle was designed and manufactured, shown in Figure 23 (b). By increasing the length of the nozzle and doubling the length of the threaded area that connects to the heater block, the commingled roving would be at the control temperature for a longer period of time. Increasing the amount of time that the thermoplastic matrix material is at the control temperature would increase wet out of the composite strand because the thermoplastic would have more time to flow around the reinforcement. Intricate shapes might also require the composite placement head to move into tight locations, like the edge of a part, and increasing the length while simultaneously decreasing the radius would allow for the nozzle to reach into tighter areas.

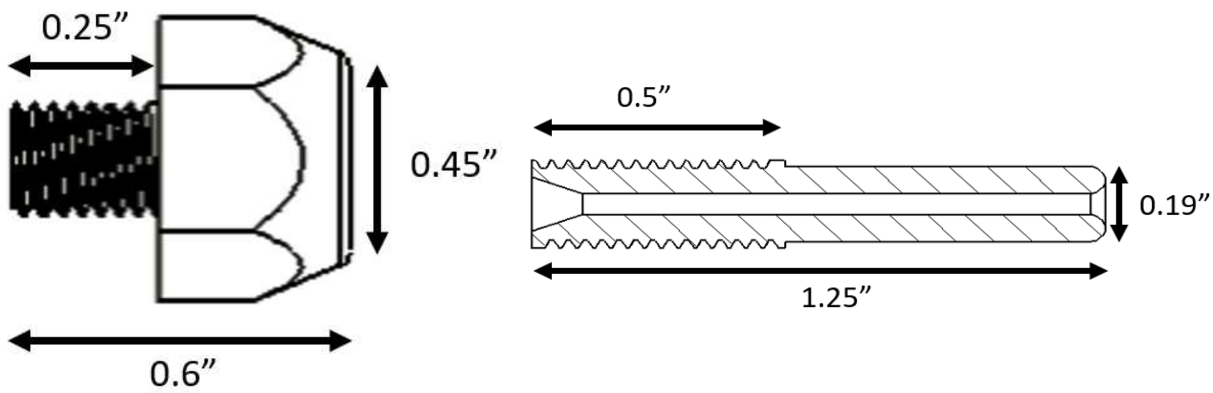

(a) Original Composite Nozzle Design (b) Improved Composite Nozzle Design

Figure 23: Nozzle Designs for the Composite Placement Head

Changing the design did have some negative effects on the composite placement process. The thick walls of the original placement nozzle served as a greater thermal mass and thus, the decrease in nozzle outlet temperature was less than with the new composite placement nozzle which had more surface area and less thermal mass. Decreasing the consolidation area also made the nozzle more sensitive to changes consolidation forces.

FIRMWARE CONTROLLED COOLING SYSTEM

A cooling system to cool newly placed composite strands would be advantageous because positional fidelity increases with tow shearing techniques [28], and thermoplastic flash decreases. Continuous cooling with the new nozzle design showed a decrease in the outlet nozzle temperature decreasing the quality of the CFRTC strand being placed. Having firmware-controlled cooling changed how cooling was used in the system. When the composite placement head is moving in a straight line cooling is not needed and therefore turned off, and a higher quality composite is placed. When creating non-geodesic fiber paths, the cooling is turned on and positional fidelity increases due to the ability to rigidize the filament more rapidly. Development of a placement system that does not decrease the nozzle outlet temperature when cooling is applied to recently placed CFRTC strands will greatly increase the capabilities of the MAGIC system.

THERMAL CAPABILITIES

Increasing the temperature capabilities of the composite placement head from a maximum of 300°C to a maximum of 450° was essential for creating better quality CFRTC strands, and help offset effects of the cooling system on the nozzle outlet temperature, as demonstrated later in this work. When the temperature increases the thermoplastic decreases in viscosity and flows more readily making wet out of the fiber reinforcement more favorable. The previous limit of 300°C was shown, in this work, to be insufficient for good wet out of the CFRTC strands when placed in unsupported space.

CHAPTER 4: PRELIMINARY EXPERIMENTS

Manufacturing parts with the continuous fiber placement system developed is known as Modular Additive Generation of Intricate Composites (MAGIC). As improvements to the MAGIC system have been ongoing it is important to understand the current state of the MAGIC system. Experiments in this section were designed to test the understanding of the mechanisms that govern the placement of continuous fiber reinforced thermoplastic composite (CFRTC) structures. Traditionally CFRTC structures take on complex shapes and curvatures with the use of tooling designed alongside the manufacturing process, therefore the manufacturing process should be chosen that accompanies the desired shape.

Autonomously placing fiber on very complex structures requires the placement mechanism to have additional degrees of freedom, when compared to a traditional FDM 3D printer. A gantry-based dual head continuous fiber placement system was designed with a single automated wrist to place fiber over complex contours mounted to one gantry while a traditional FDM 3D printing thermoplastic placement head on the second gantry was utilized to create 3D printed tooling. The output geometry of placed CFRTC strands on a build surface was determined based on the placement angle. Increasing the placement angle changed the shape of the CFRTC and it was determined that the relative composite placement head angle was important in realizing the shape of the placed CFRTC strand.

Two different techniques were used to generate the points used for programing complex contour curves into a G-code or point to point format, Mesh Grid Projection and Pictured Point Projection. Both techniques were considered for producing G-code for complex curvatures by comparing the differences between the two techniques.

MATERIALS

The commingled feedstock used for these experiments is a continuous E-glass fiber/amorphous PET commingled roving. The commingled roving has a glass fiber weight fraction of 70%. The Tex of the roving is 2700 grams per 1000 meters. Stiffness information for the two constituents can be found in Table 1. Amorphous PET has a glass transition temperature of 78 °C. A neat amorphous PET thermoplastic filament was used to manufacture tooling.

Table 1: Commingled Constituents Material Properties

Property	Amorphous PET [47]	Glass Fiber [48]
Elastic Modulus	410 ksi (2.83 GPa)	10500 Ksi (72.4 GPa)
Flexural Modulus	290 ksi (1.98 GPa)	4350 Ksi (30.0 GPa)
Density	0.734oz/in^3 (1.27 g/cm^3)	1.474 oz/in^3 (2.55 g/cm^3)

5-AXIS COMPOSITE PLACEMENT SYSTEM

Upgrading the hardware and firmware for a 5-axis composite placement system was done to place continuous fiber over complex contours, but still allow for consolidation on the surface of the tool using pressure created from the tip of the nozzle. To apply consolidation pressure on a tool surface the composite placement head needs to be perpendicular to the surface. More degrees of freedom than the typical 3 used in FDM 3D printing would be required to apply consolidation on a sloped surface. A motor on top of the Z axis adds a rotation, the ϕ axis, to the capabilities of a traditional 3D printer and an additional motor attached to a shaft of the initial ϕ axis adds another degree of freedom, the θ axis, to the system making it a 5-axis system. A schematic of the 5-axis composite placement head is shown in Figure 24. The MAGIC system with the 5-axis placement system installed is shown in Figure 25. A 6-axis system is necessary for any position and orientation, but 5-axis increases the capabilities of the 3D printer and allows for research on simple contours and different fiber orientations.

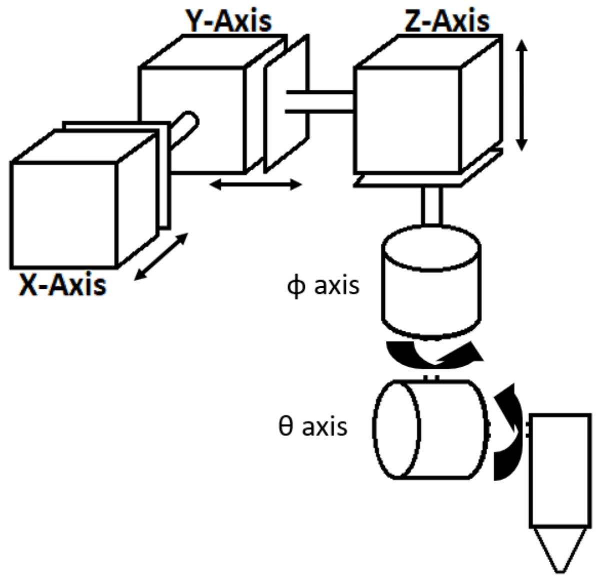

Figure 24: Schematic of the 5-Axis Composite Placement System

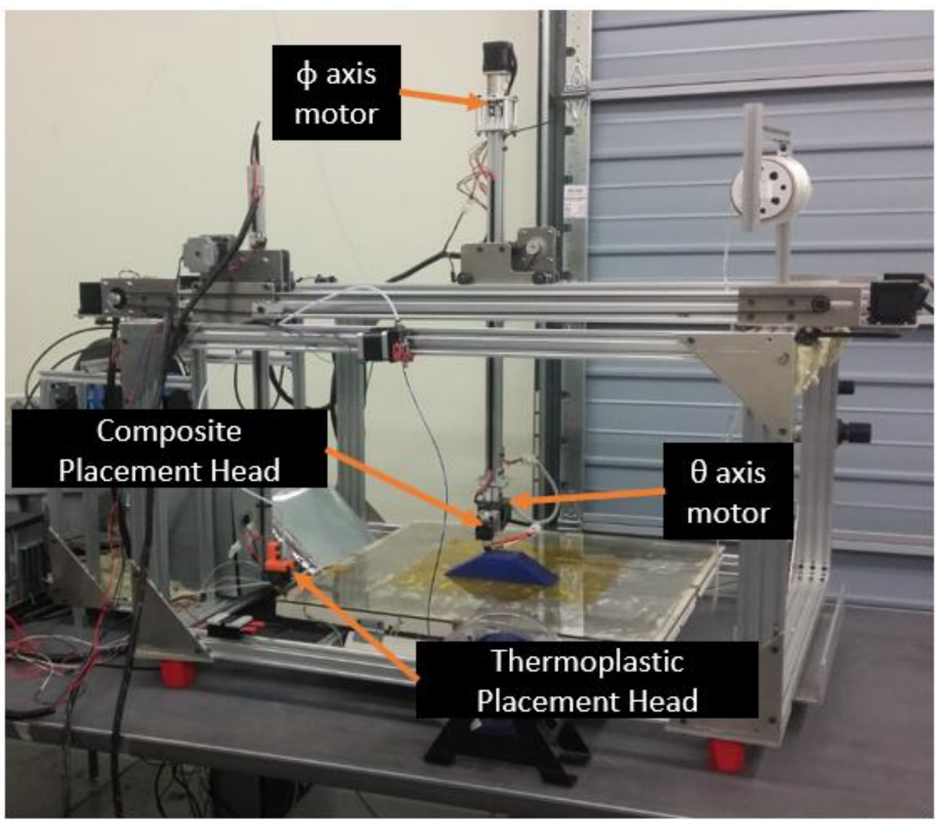

Figure 25: The MAGIC System Utilizing the 5-axis Composite Placement Head

TOW SPREADING

Another benefit to using the 5-axis system is the ability to address tow spreading. Increasing the bandwidth by rotating the composite placement head compared to perpendicular to the placement plane will decrease the thickness of the strand creating thinner, but wider, composite strands. In theory, as a bundle, or tow, of fiber moves over a surface, either cylindrical or round, the individual fiber strand will want to contact the surface and will orient themselves to do so, spreading the tow in proportion to the distance the fiber travels on the surface, as shown in Figure 26 [49]. Composites with spread tows can exhibit better fiber packing, lower void contents and improved mechanical properties [50]. With the additional axes of motion, the placement head can increase its relative angle θ to the tool surface, increasing the distance the fibers travel on the round tip of the nozzle, thus increasing the bandwidth. Conservation of volume would indicate that the total CFRTC strand thickness will also decrease in a controllable manner.

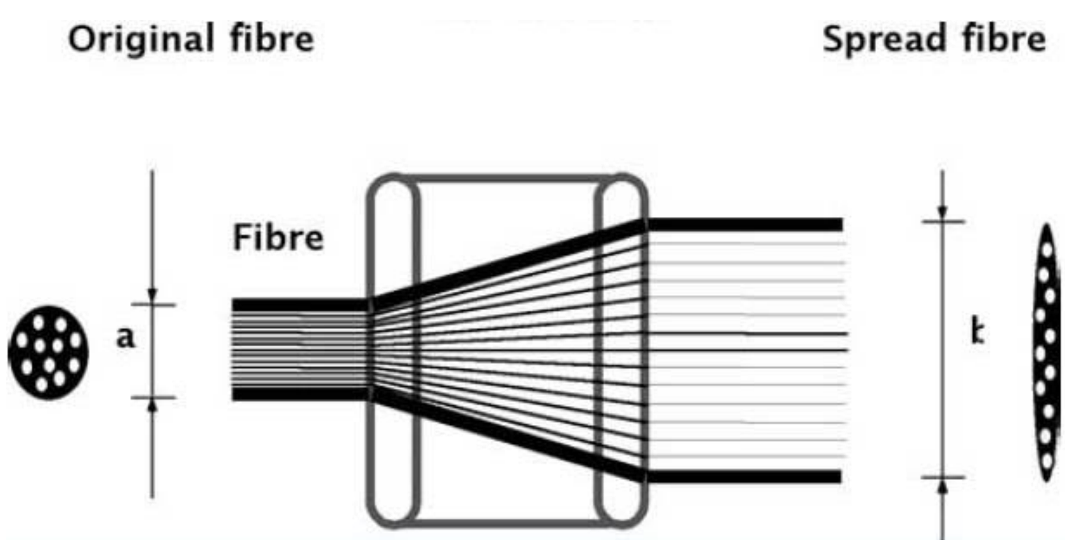

Figure 26: Tow Spreading Around a Curved Surface [51]

Tow spreading occurs regardless of the consolidation of the composite during placement but could help wet out the fibers [51]. An experiment was designed to test how much a CFRTC strand would spread based on composite head placement angle, θ. The direction of travel was in the positive Y-direction with respect to the Global Coordinate System (GCS) and the rotation was done around the point the nozzle would contact the newly placed composite strand, or Consolidation Contact Point (CCP), shown in Figure 27 (a). θ, in Figure 27 (a), is the angle that is being changed for the experiment because the rotation is about the CCP, the height of the nozzle does not change as the angle increases, as it would if the rotation was in the center of the nozzle.

A placement head angle, θ, of 0°, 5°, 10°, 15°, 20°, and 30° was used to determine the amount of tow spreading that occurred when placing fiber on a stiff surface. Four layers of CFRTC strands were placed at each head angle to give a more measurable difference between the resulting CFRTC specimens. 5 points along each strand were measured for the maximum thickness, middle thickness and width, each shown in Figure 27 (b). After measurements were taken specimens were mounted for microscopy to check the wet out of each CFRTC specimens, 3 cross sections were examined for their relative goodness.

Figure 28 shows the change in CFRTC strand width, total thickness, and middle thickness as the angle of placement changes. The layer height was 0.016 in (0.4 mm), indicating the theoretical thickness of the composite is 0.063 in (1.6 mm) without accounting for consolidation effects. The first layer has a programmed Z-offset of 0.008 in (0.2 mm) which is less than the 0.016 in (0.4 mm) layer thickness, which forces the Z-motor to press the tip of the nozzle, and the tow, against the stiff substrate to facilitating consolidation. Note that the consolidation spring was not used for this experiment and consolidation relied only on the machine stiffness. The resulting measured layer thickness is greater than 0.008 in (0.2mm) due to the spring constant of the machine. It was observed that the width of the specimens increased as the placement head angle, θ, increased. The relationship between placement head angle and the tow width is linear in the tested region. The total thickness did not change significantly across all the specimens, but the center thickness decreased taking on the form of the nozzle. The middle thickness decreased as the angle increased due to the shape of the nozzle, consolidation force and the distance the fibers traveled along the surface of the nozzle. The standard deviation for all found values is small, with the highest standard deviation being the width of the 30° head angle sample, having a standard deviation of 0.006 in (0.016 mm).

Consolidation pressure was unknown, so the amount of consolidation was found by evaluating micrographs of the cross section of each specimen. Within the composite beam the layers maintain a uniform thickness except for the first layer, because it was placed onto the substrate which is much more rigid than the previous tow is during subsequent tow placement. Figure 29 shows a cross section view of the composite strand placed with a placement head angle of 20°. The curved shape created by the nozzle geometry can be seen in Figure 29. Each layer has a thickness within the center of the strand that expands toward the edges of the sample. A roller would allow for more uniform consolidation through the width of the composite strand and remove the curvature created by the nozzle generating a flatter composite.

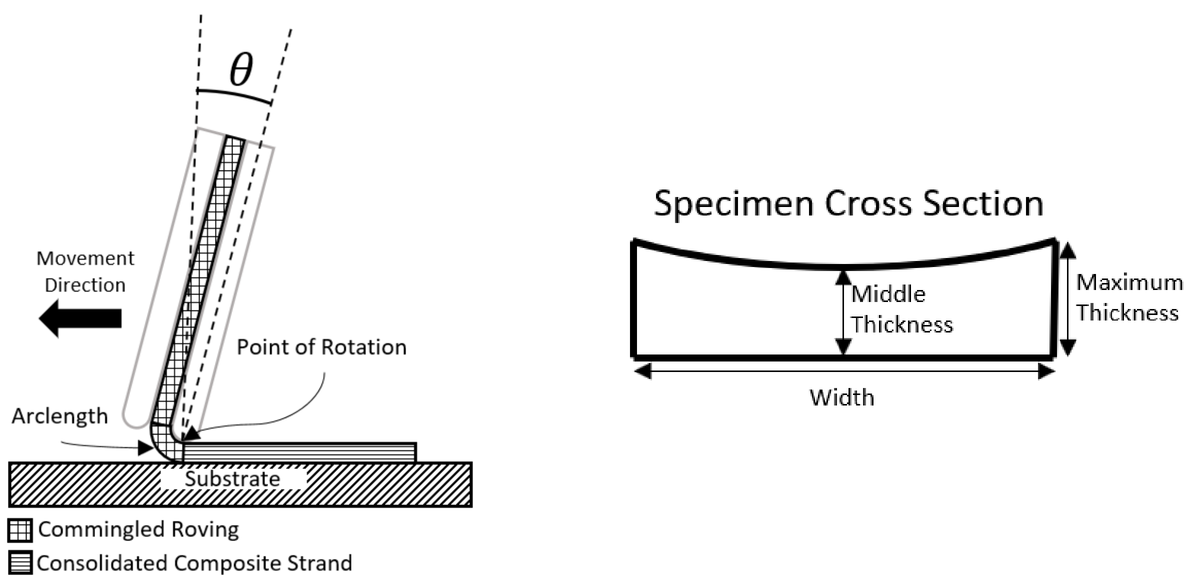

(a) Placement Setup

(b) Measurement Locations

Figure 27: Tow Spreading Test Setup

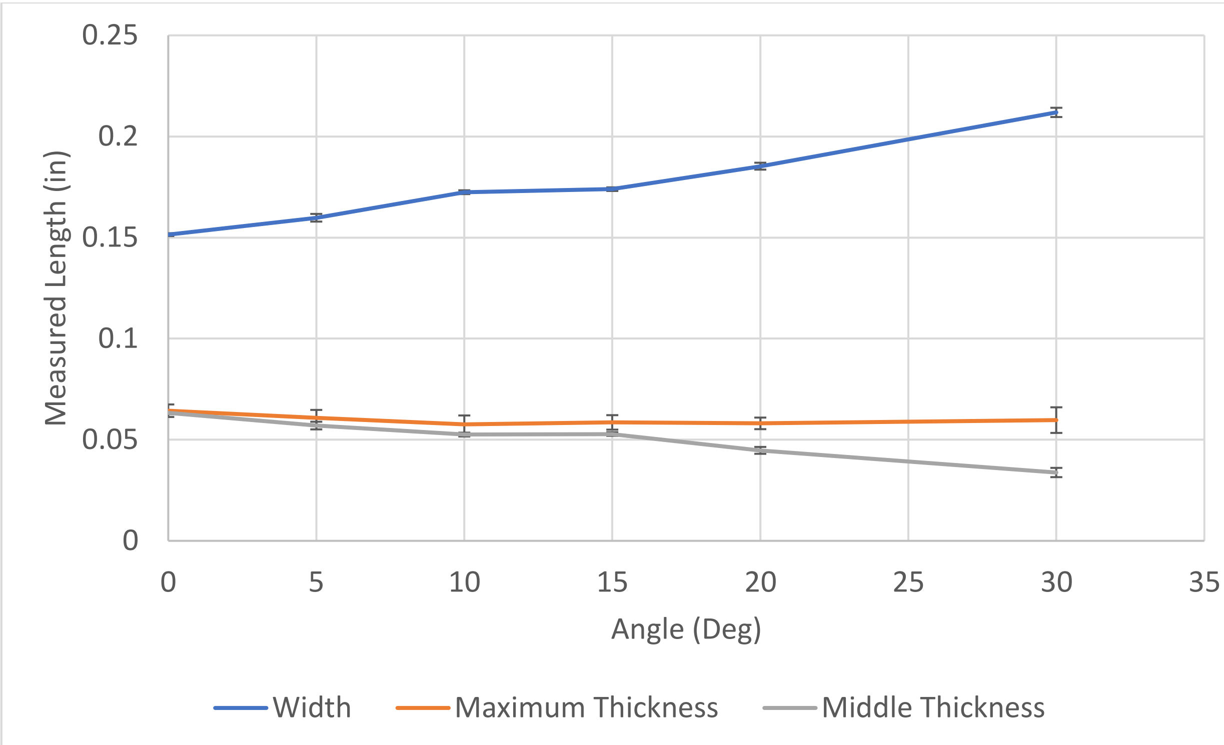

Figure 28: Change in thickness and Width as Placement Angle Changes

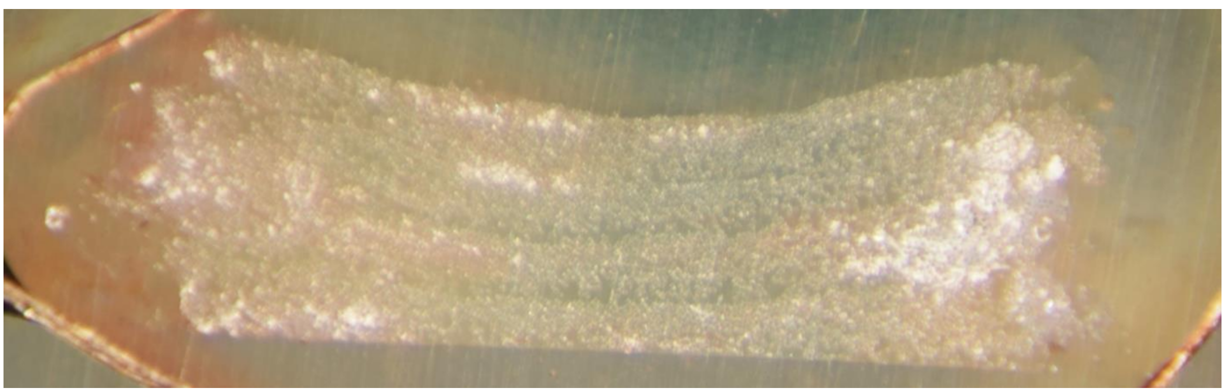

Figure 29: 20° Placement Head Angle Composite Beam

PATH GENERATION TECHNIQUES

Robotic control firmware is limited to the robot and is proprietary for most applications. 3D printing and CNC firmware has become open source and therefore cheaper and easier to modify. A way to generate G-code for CFRTC placement over complex contours was needed. Keeping the composite placement head perpendicular to the surface will eliminate tow spreading. 3D printing firmware and CNC control use G-code formatting to dictate where the machine should go and how fast it should get there. Two different techniques were looked at for generating G-code for complex contours, Mesh Grid Projection and Pictured Point Projection. A computer simulation and physical test was done to show the difference between the two projection methods.

MESH GRID PROJECTION

Mesh Grid Projection (MGP) is forming a mesh grid, two arrays of data points creating a grid of X and Y points, and then projecting this grid on to a contour to get the Z points. To get different fiber orientations the grid is rotated then projected on to the desired shape. Generating different fiber angles for a given shape is as simple as rotating the grid but the angle on the surface is different than the desired fiber angle. The fiber angle would look like the desired angle from above, Figure 30 (a), but when looking perpendicular to the surface of the object the fiber placement angle would be at a higher or lower angle depending on the steepness of the curve at any given location, shown in Figure 30 (c). As the steepness and complexity of the curve increases the difference between the desired fiber path and the programmable path changes greatly. MGP is ideal for relatively simple Euclidean geometries that don't have large surface radial changes. Figure 30 shows both the top view and side view of both Mesh Grid Projection and Pictured Point Projection (PPP) point generation methods over a simple semi-cylindrical geometry.

A semi-cylinder was chosen to emphasize the difference between the two methods in the simplest terms because a more complex geometry, like a semi-sphere, requires more advanced algorithms to produce a fiber path because the fiber path would be non-Euclidean, and a constant fiber angle is not obtainable without fiber build up or large gaps within the layers. Euclidean geometries are the only objects that either MGP or PPP are capable of generating a fiber path over.

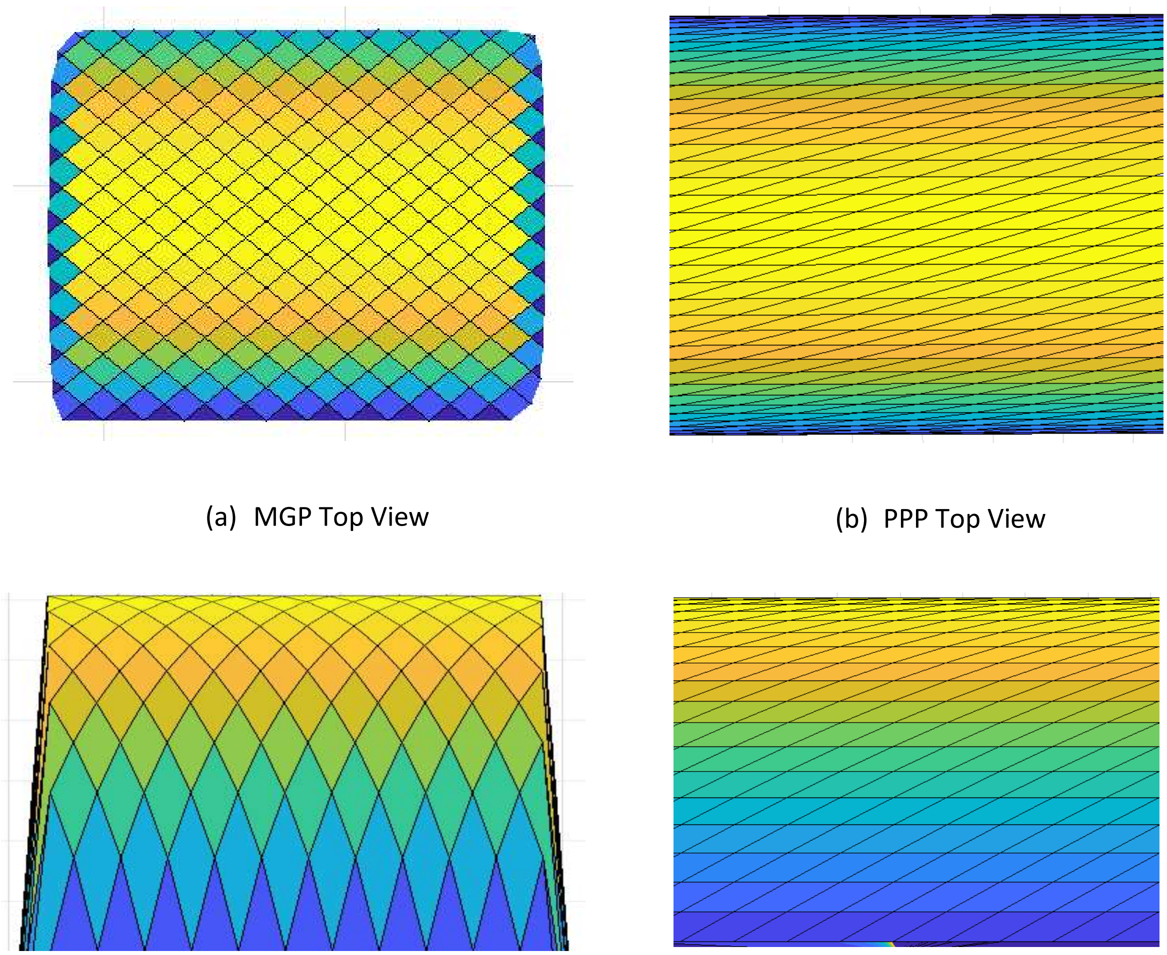

(a) MGP Top View

(b) PPP Top View

(c) MGP Side View

(d) PPP Side View

Figure 30: A Semi-Cylinder with 45° fibers paths of both MGP and PPP

PICTURED POINT PROJECTION

Generating the surface of the part then placing points evenly over the surface is Pictured Point Projection (PPP), the surface is generated with points that are a known arc length from one another on the surface of an object, Figure 30 (b) and (d), and these points are then projected on to a 2D array of points that can be ordered, based on the desired fiber path. PPP is more computationally intensive and requires a 3D model with the points, or a representative formula that these points can be extracted from while MGP only requires a formula that represents the shape. Another way to extract these points is to manufacture a scale version of the part and adhere a net to the part where every node on the net is a point, then take an overhead picture and extract the points from the picture. Although this has some error because the projection goes to a focal point the method can still be more accurate for fiber placement than MGP. A method to start and stop fiber placement is also necessary to manufacture unique shapes using this method, while MGP is better equipped for a continuous fiber path.

Both the MGP and PPP path generation techniques require a tool to be manufactured on to which the fiber is placed, and with advanced algorithms a program could be written to utilize tow spreading within the programmed path to remove gaps that occur when joining together two different geometries. This approach could reduce the error in manufacturing objects with non-Euclidian geometries. Manufacturing of conventional composite structures requires tooling to define the geometry, but with the MAGIC system it is possible to manufacture composites with dramatically reduced tooling by manufacturing the object in space with no supporting structures underneath the sections of composite that are straight.

Placing CFRTC strands over complex contours like a semi-cylinder, and generating consolidation pressure, with the 5-axis system configuration becomes increasingly more difficult due to the stiffness requirements of the rotational systems that allow for surface perpendicularity becomes more critical to the quality of the placed composite.

SMALLEST TACKING DISTANCE

By moving the print head off the substrate, or tool, after the CFRTC strand is sufficiently tacked, the CFRTC strand can be placed with no supporting structures. This is free space placement. Free space placement is facilitated by the cooling induced rigidization of the thermoplastic matrix. Understanding the fundamentals of how the fiber is placed on the substrate and what is happening to the composite as it is being placed will give a better understanding of how to place fiber without support. For programming the fiber path and designing a part it is important to know the resolution capabilities of the manufacturing method. The MAGIC system requires tacking the fiber to the substrate and, if CFRTC strands is to be placed autonomously, this tacking distance resolution must be known.

Resolution in 3D printing is what controls the smallest features that can be created. For composite 3D printing there are 3 different resolution factors, two of which are common in FDM 3D Printing and the 3rd is controlled by the tacking distance. The first is the band width, the second is layer height. The third is the smallest possible band length required to pull the composite from the nozzle, also known as tacking distance, illustrated in Figure 31. Tacking down the CFRTC strand is difficult because it requires precise control of time, temperature, and pressure to control the forces involved in placing the CFRTC strand.

Theoretically, the shear strength between two materials controls the tacking distance. When the shear strength between the composite and the substrate is enough to pull the commingled roving through the nozzle the composite is sufficiently tacked down. Mean shear strength of the adhesive joint is given by the equation:

$$\tau = \frac{P}{l * BW} \qquad \textbf{(2)}$$

Where $\boldsymbol{\tau}$ is the mean shear strength, P is the force required to pull the commingled roving through the nozzle, L is the length of placed composite, and BW, is the bandwidth of the placed composite strand. As the composite strand length increases the average shear stress in the strand decreases. Once the shear stress is below the max shear strength of the bond, between the substrate and the material, the composite strand will be considered sufficiently tacked in place. Controlling the tacking length and the force required to pull the composite through the nozzle will dictate the resolution of the system.

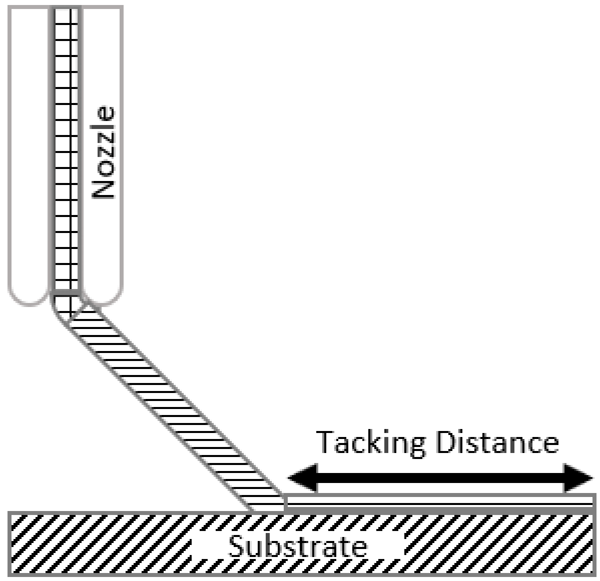

Figure 31: Tacking Distance for a Pultrusion Based System

NOZZLE FRICTION FORCE

An experiment was designed to find the force required to pull the commingled roving through the nozzle. The nozzle-composite tow friction force, P, was found by pulling the fiber through the nozzle at different speeds and temperatures and measuring the resistance with a load cell. The testing was done by attaching the composite strand to a load cell as shown in Figure 32, and moving the composite placement head at a known speed. Three factors were tested, Print Speed, Heater Block Temperature and if active cooling was on or off. The composite strand was attached to a cantilever load cell in the same position for every test and the path that the nozzle took was the same for every test.

Based on the force to pull the composite from the nozzle a higher temperature and lower print speed with no cooling would be the lowest loading conditions while the highest loading conditions are fast speeds, low temperatures and with active cooling turned on. The lower temperature bound is when the force required to pull the fiber from the nozzle exceeds the torque that the stepper motors can handle causing the machine to stall, which is 8.8 lbf (0.04 kN). When cooling is turned on the lower temperature bound is a control temperature of 464 °F (240 °C). When cooling is turned off the lower temperature bound is a control temperature of 428 °F (220 °C). As the force required to pull the composite from the nozzle is reduced the tacking distance is reduced, increasing the resolution for the printing processes.

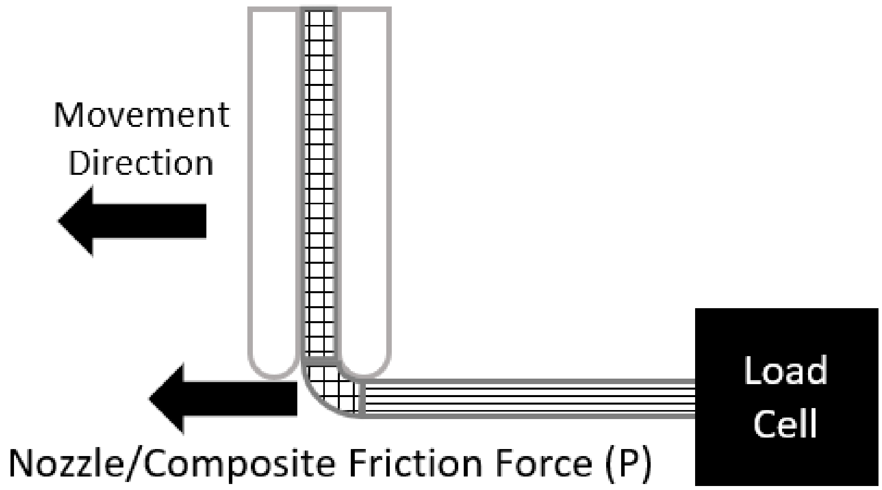

Figure 32: Pulling Force Testing Setup

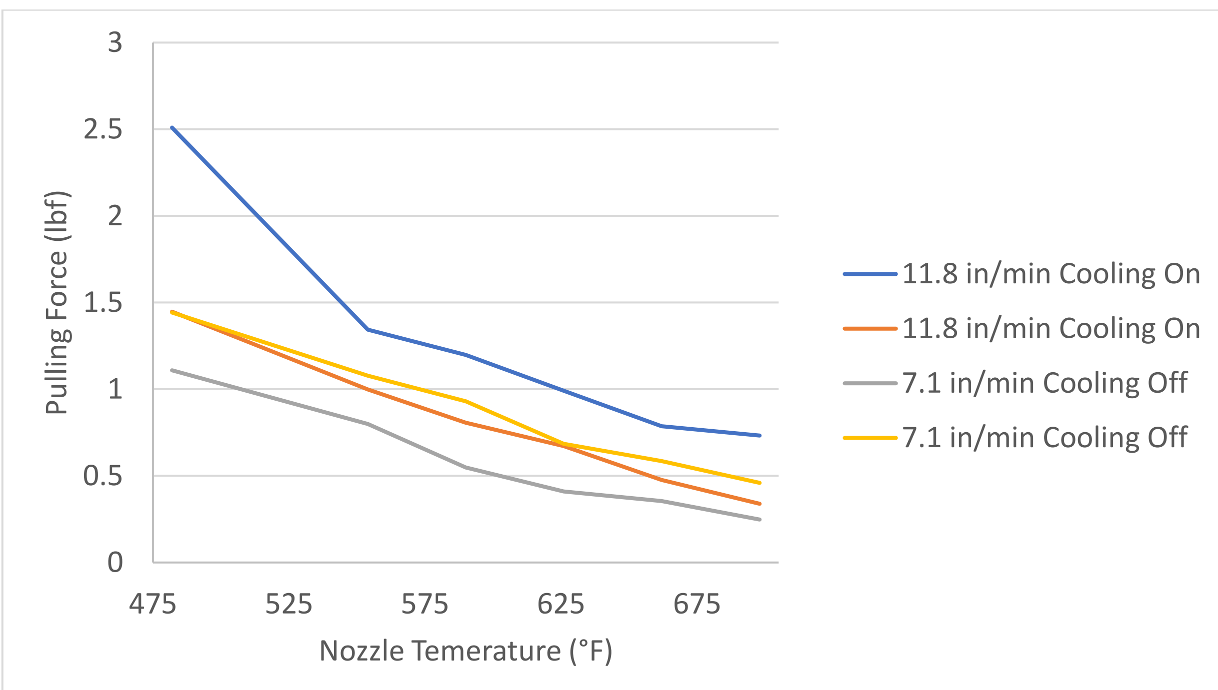

Figure 33: Force of Placing Composite Strands

SHEAR FORCE

Now that the force required to pull the commingled roving through the nozzle has been found the maximum shear force that the bond between the materials can withstand is the only unknown in equation 2 that needs to be found.

$$l = \frac{P}{\tau * BW} \tag{3}$$

Rearranging equation 2 to get equation 3 shows that as the force, P, increases the placement length, l, also increases. Increasing either the shear strength between the two materials, $\boldsymbol{\tau}$, or increasing the bandwidth, BW, will decrease the minimum placement length. To decrease the placement length the shear strength between the composite and the substrate must be increased. Carefully controlling the temperature and pressure in this region is required to increase the maximum shear strength between the composite and substrate.

The maximum shear stress that the material system can resist depends on the matrix of the composite, the material of the substrate, the temperature of the bonded area and the consolidation force. Assuming the force to pull the composite from the nozzle is constant, then the two factors that affect the maximum shear strength in this system are the temperature and the material of the substrate. There are two different substrate materials in the tested system. The first is Kapton, when placing composite strands on the print bed. The second is PETG, when placing composite strands onto a previously placed composite layer. Both the temperature of the composite and the temperature of the substrate is controlled with the firmware. For thermoplastics, as the temperature increases above the T_g of the material the maximum shear stress that the material can withstand decreases. When manufacturing continuous fiber reinforced thermoplastic composites, the reinforcement tows should remain in the same position as when placed.

As the placement temperature increases, newly placed tow can shear until the matrix temperature decreases to a point where the matrix can withstand the shearing effect. For the Kapton system the highest shear strength between the matrix and the substrate is slightly above the T_g of PETG. While with the PETG system the highest shear strength increases as the temperature decreases until the T_g of the matrix has been reached.

The CFRTC strand starts out well above the glass transition temperature of the matrix and as the CFRTC strand cools the matrix becomes rigid. PETG, as a matrix material, is unique because it adheres to Kapton and forms a good bond when both the PETG and the Kapton are above the glass transition temperature of the PETG. The goodness of this bond decreases as the temperature decreases to room temperature. When the PETG is at placement temperature it is malleable and is suitable for wetting out the reinforcement and does not hold a desired shape. Cooling the CFRTC strand increases the matrix viscosity and the strand can withstand the shear force without deforming. If the Kapton is cooled to room temperature the adhesive strength decreases, allowing for part removal, but room temperature is not good for tacking the PETG. To keep the Kapton tape hot enough to allow for good adhesion the bed is heated to above the T_g of the PETG, regardless of how the placed CFRTC is cooled. Having a heated substrate has the added benefit of reducing the warping of the composite related to the shrinkage of the matrix material.

CONSOLIDATION FORCE

When the placement head applies consolidation pressure to the CFRTC strand, voids are removed, and the strand takes on a semi rectangular shape. The free body diagram for CFRTC strand placement if the strand is not already tacked to the substrate is shown in Figure 34. The equations to find the Nozzle/Composite Friction (P) and the composite/substrate friction (F) before any tacking to the bed occurs are as follows:

$$P = P_{nozzle} + N * \mu_c \tag{4}$$

$$F = N * \mu_s \tag{5}$$

Where μ_c is the coefficient of friction between the composite and the nozzle, μ_s is the coefficient of friction between the composite and the substrate, and P_{nozzle} is the force required to place a composite strand. Equations 4 and 5 both have the consolidation force, N, so they both will change proportionately to magnitude of the consolidation force.

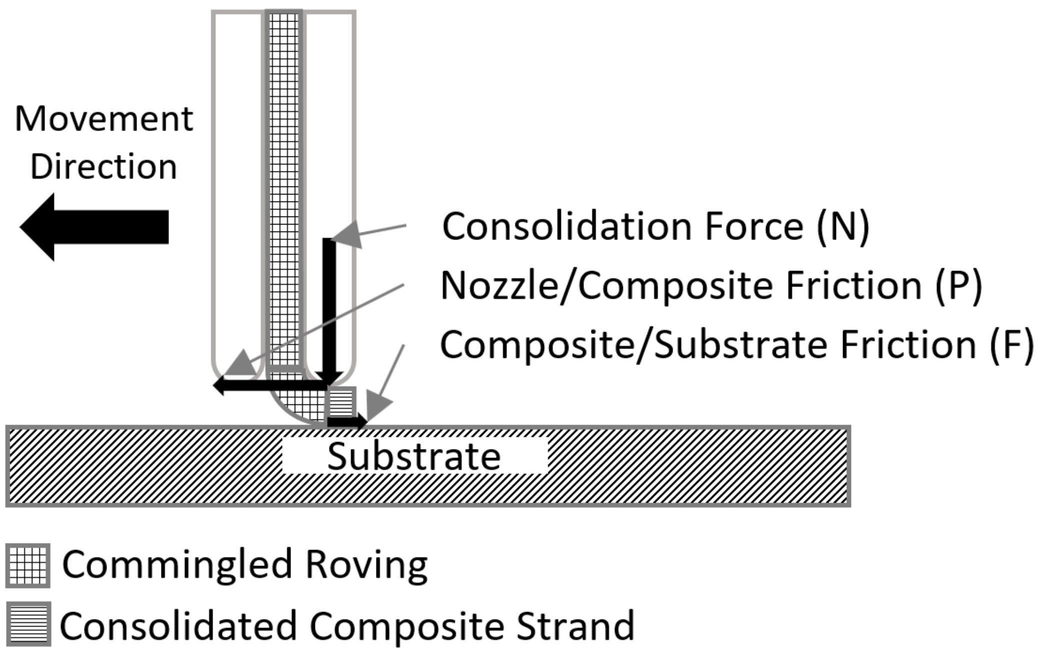

Figure 34: Forces Involved in Fiber Placement

After the composite has been tacked down, equation 5 changes to add the force due to the adhesive bond between the composite strand and the bed.

$$F = N * \mu_s + \tau * BW * l \tag{6}$$

If the force of pulling the fiber out of the nozzle, P, is greater than the maximum force needed to tack the fiber, F, than the composite strand pulls off of the substrate. A few different cases using equation 4 and 6 should be analyzed.

SYSTEM RESPONSE

The first case is when μ_c is greater than μ_s, shown in Figure 35(a). P and F diverge, and F will never be larger than P indicating that the fiber will never be able to tack on its own. When μ_c is less than μ_s, Figure 35 (b). P and F converge and at a certain consolidation force, N, the tow will tack down, but with the current composite placement system the friction between the composite and the nozzle is always greater than the friction between the composite and the substrate.

Both of these cases assume that no tacking has been done. The third case is when the tacking distance is sufficient to hold the CFRTC strand in place, and μ_c is greater than μ_s, Figure 35(c). When the consolidation force, N, is low P will be smaller than F meaning that the tow will continue to be tacked to the substrate, but at large consolidation forces F increases more than P and the composite strand will become detached from the substrate.

A final scenario will be considered, when an extruder is used to push the CFRTC strand through the nozzle, meaning the P_{nozzle} becomes negative, μ_c is greater than μ_s, and the composite has yet to be tacked down, Figure 35(d). In this case a sufficient consolidation force can be used to tack the composite to the substrate, but too much consolidation force will stop tacking from occurring altogether because the friction force between the composite and the nozzle has increased due to the normal force. Using equations 4 and 5, any tacking scenario can be analyzed based on the placement mechanism and any variable can be isolated depending on the situation.

In summary, the smallest tacking distance is the smallest distance that is sufficient to stop the composite and substrate from breaking apart. Decreasing the temperature of the composite to the glass transition temperature of the matrix material, controlling the nozzle temperature and carefully controlling the consolidation force, N, will then produce the smallest tacking distance for the given substrate and composite material.

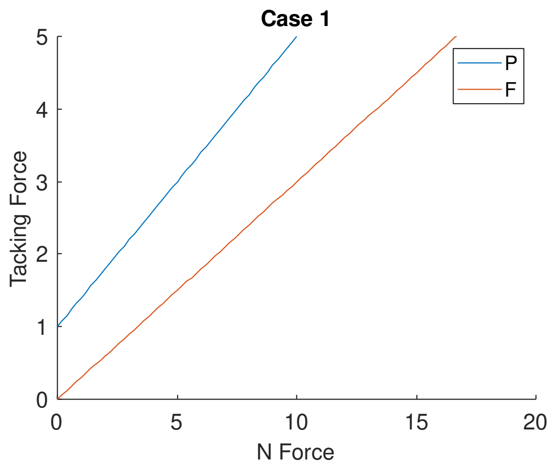

(a) $\mu_c > \mu_s, \tau = 0, P_{nozzle} > 0$

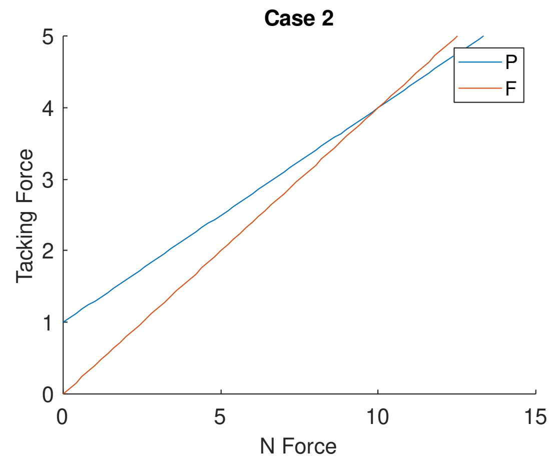

(b) $\mu_c < \mu_s, \tau = 0, P_{nozzle} > 0$

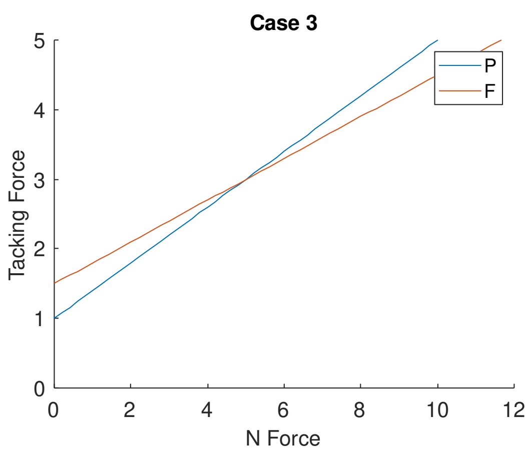

(c) $\mu_c > \mu_s, \tau > 0, P_{nozzle} > 0$

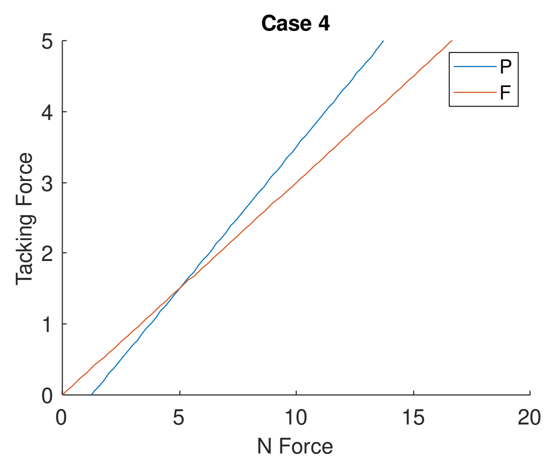

(d) $\mu_c > \mu_s, \tau = 0, P_{nozzle} < 0$

Figure 35: Forces Involved When Placing Composite Strands

180° TURNING

When manufacturing with a single continuous fiber reinforced thermoplastic composite (CFRTC) strand at a time there are two ways to build up a composite lamina. By cutting the CFRTC strand at the end of each pass and then restarting it, as shown in Figure 36 (a), or by turning 180° at the end of each pass and placing a new CFRTC strand directly next to the previously placed CFRTC strand during the return pass, as shown in Figure 36 (b). In theory, turning 180° requires advanced temperature control at the tip of the nozzle [28]. As shown earlier in this section, cooling the nozzle increases the force required to pull the CFRTC strand from the nozzle, but it also helps solidify the newly placed material increasing the shear strength between the CFRTC strand and the substrate.

(a) Composite Placement Head Path With Implemented Cutting System

(b) 180° Turn Composite Placement Head Path

Figure 36: Side by Side Placement of CFRTC strands

After numerous unsuccessful attempts to automate the tow cutting process, an experiment was designed to determine if turning the CFRTC strand 180° was possible. A thermal imaging camera was used to measure the temperature of the CFRTC strand as it is being placed. The distance between the nozzle outlet and the location were the CFRTC strand is the same temperature as the bed would have to be small enough to facilitate turning. At just above `76 °F (80 °C), the glass transition temperature of the matrix, the composite strand is stiff but still adheres to Kapton. 176 °F (80 °C) will be the fully solidified temperature that will be used to determine if turning 180° is possible.

The distance from the nozzle to when the CFRTC strand is at 176 °F (80 °C) is between 0.787 inches (20 mm) to 1.181 inches (30 mm), as determined from Figure 37 (a). With cooling being directed at the tip of the nozzle this distance decreases to between 0.0788 inches (2 mm) and 0.118 inches (3 mm), as determined from Figure 37 (b). The nozzle is moving at 180 mm/min so the time to cool is 8-10 seconds with no extra cooling and 1 second with air passing over the newly placed CFRTC strand. With no cooling the composite placement head would have to stop for 10 seconds every time there was a change in the placement path. With cooling turned on the length between the tip of the nozzle and where the CFRTC strand is 176 °F (80 °C) is 0.118 inches (3 mm), indicating that no stopping would be needed to turn 180°.

When executing a 180° turn cooling is required, the CFRTC strand needs to be strong and stiff enough to resist the placement forces of the next composite strand. At elevated temperature the composite strand will not be rigid enough to withstand the pulling force within the nozzle and the CFRTC strand will unbind from the Kapton substrate, with controlled cooling turning 180° is possible while maintaining the nozzle outlet temperature.

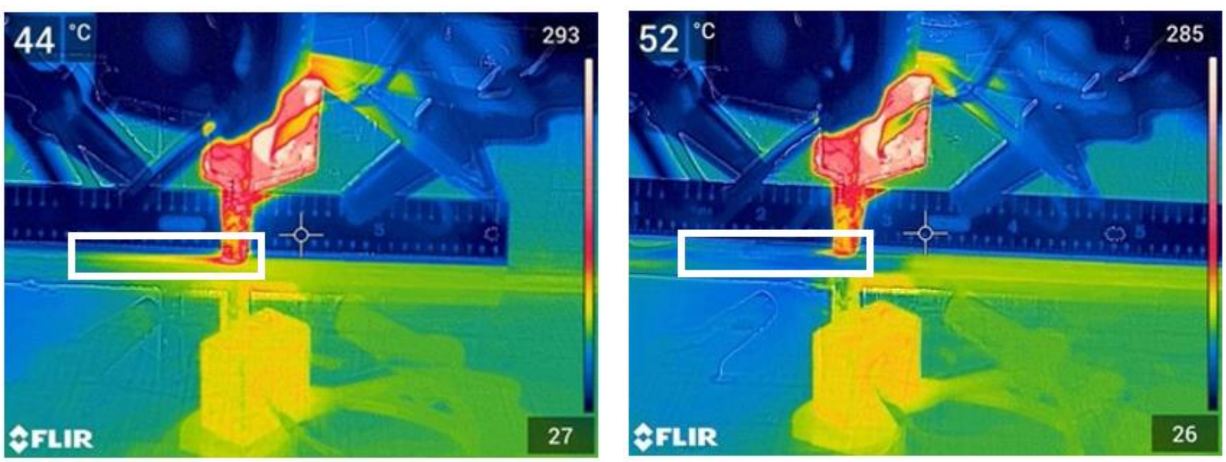

(a) Cooling Length with Cooling off

(b) Cooling Length with Cooling on

Figure 37: Tacking Length vs. Cooling Mode

CHAPTER 5: MAIN EXPERIMENTS

The main experiments were designed to test the mechanical properties of continuous fiber reinforced thermoplastic composite (CFRTC) strands placed with the MAGIC system. Knowledge gained in the preliminary experiments was applied to fully automate the manufacturing of CFRTC structures that are difficult to manufacture using compression molding or other thermoplastic composite manufacturing techniques. The MAGIC system was developed to place CFRTC with dramatically reduced tooling, resulting in a need to place CFRTC strands in unsupported space. Experiments were designed and performed to test the quality of composites manufactured with different methodologies, utilizing the MAGIC system. Laminate quality was evaluated with lap shear testing and void content evaluation based on the number of laminae placed with the MAGIC system. Nozzle temperatures were manipulated during the placement of CFRTC strand and these strands were tested for their bending stiffness. Sandwich panels with Navtruss corrugated cores were manufactured with the MAGIC system utilizing the different manufacturing techniques that were developed. Compression and shear tests were then performed on these sandwich panels to compare the structural stiffnesses to similar panels manufactured via compression molding, a traditional thermoplastic composite manufacturing process. This section will cover both manufacturing processes, in detail, and the geometry of the specimens that were manufactured.

MATERIALS

Three different precursor materials were used in the experiments proposed in this section, a commingled feedstock material, fully consolidated CFRTC sheets and a neat thermoplastic used for edge closures and supportive scaffolding. The neat thermoplastic was an amorphous Polyethylene Terephthalate (PET) polymer commonly found within the commercial 3D printing industry.

COMMINGLED ROVING

The feedstock material that the MAGIC system uses is a commingled roving. The commingled roving used for all these experiments consists of PET as the matrix material and continuous fiber E-glass as the reinforcement, but any commingled roving could, in concept, be used with the MAGIC system. The specific commingled roving used has a Tex, grams per 1000 meters, designated by Jushi the manufacture, of 2700 and an E-glass fiber weight fraction of 70% (55% fiber volume fraction). The PET filaments are amorphous and have a glass transition temperature of 172 °F (78 °C) [31].

THERMOPLASTIC PRE-IMPREGNATED SHEETS

The material used for the compression molded truss core sandwich panels is a semi-crystalline glass fiber reinforced PET unidirectional prepreg with an E-glass fiber weight fraction of 60% (47% fiber volume fraction). The PET/E-glass prepreg has a glass transition temperature of 172.4 °F (78°C), and a melt temperature of 464 °F (240 °C). These values were determined using Differential Scanning Calorimetry (DSC). Three DSC heating cycles were completed at 68 °F (20°C) per minute. The thickness of the prepreg tape is 0.01 inches (0.25 mm).

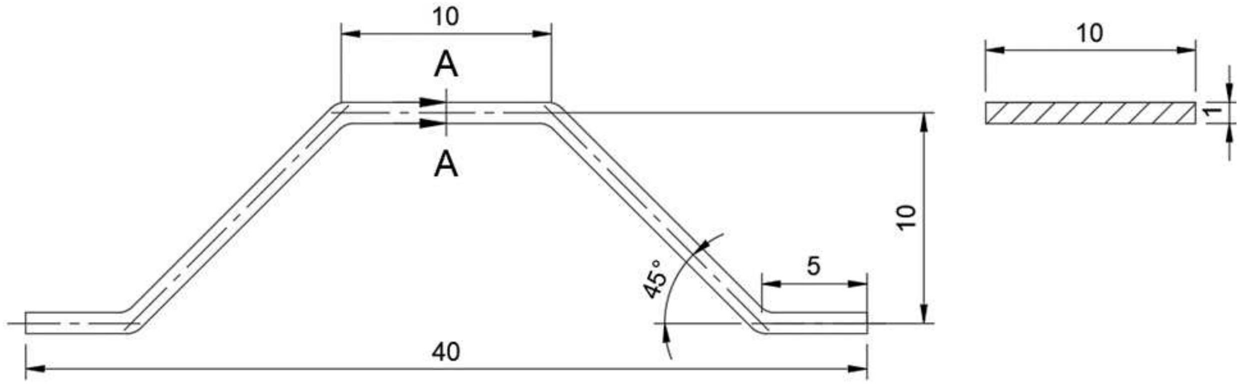

Figure 38: Navtruss Core Strutt Geometry

The Navtruss geometry was used for the majority of the experiments performed. One cell of the desired Navtruss core is made up of two struts, a single strut is shown in Figure 38 and has a cross section of 10 mm x 1mm. The total height of a single strut is 12 mm, thus, the as-designed core thickness is nominally 12 mm (0.47 in). The current form of the MAGIC system limits the number of struts to two in a single cell, as shown in Figure 39 (a). The maximum possible for the Navtruss core is 4 struts in a single cell, Figure 39 (c), and the maximum possible for the MAGIC system is 3 struts in a single cell of the core, Figure 38 (b), but this research is limited to 2 struts because of factors discussed later in this work. Core density is the volume of all the material in a cell divided by the total volume of the cell, a 2-strut core with the geometry shown in Figure 38 has a theoretical volumetric core density, volume of the material over the volume of a cell, of 3.02%, the total volume of a cell is 32,000 mm^3, and the total volume of material in the 2-strut core is 966 mm^3.

A 2-strut core is the simplest to manufacture with the current MAGIC system. With the 2-strut core the bonding areas between the core and the facesheet are rotated 90° between the bottom face sheet and the top face sheet making the bending response different based on how and where the panel is loaded. The baseline used for a comparison is a specimen geometry made by compression molding the core and then bonding the molded core to prefabricated, compression molded, facesheets.

To manufacture truss core sandwich panels with CFTRC strands the MAGIC system has to be able to place tensioned CFRTC strands out of the build plane. A preliminary investigation into how to place CFRTC strands was done using a simpler pyramidal truss core geometry.

(a) 2 Strut Core (b) 3 Strut Core (c) 4 strut Core

Figure 39: Multiple Strut Cores

TOOL REDUCTION USING UNSUPPORTED MANUFACTURING

When placing CFRTC strands with no supporting structures or extrusion system, the strand makes a straight line between the tip of the nozzle and last known good tacking position. The tension in the CFRTC strand pulls the CFRTC strand through the nozzle and straightens the strand. A supporting structure placed to carry the load required to pull the fiber from the nozzle acts as an inflection point that allows the composite to change directions even though the length of the composite is unsupported, this is called Point-to-Point manufacturing.

An initial geometry was chosen to determine if point to point manufacturing could be used to manufacture CFRTC sandwich panels. Truss cored sandwich panels are a good choice for point to point manufacturing because the core geometry is relatively complex and conventional manufacturing requires a significant amount of tooling and post processing procedures. However, with point to point manufacturing; the entire sandwich panel could be made without tooling, leading to great cost savings for low production volume truss core composite structures. A pyramidal core structure was chosen because of the complexity of the core, as well as the relatively simple composite path that would need to be implemented.

For a pyramidal truss core, CFRTC strands are placed between two sides of the outer edge closure, in an intercrossing pattern, that can be seen in Figure 40. Each point that two paths cross is a node point where the peak of a pyramidal structure will be placed. The two paths adhere at node points increasing the stiffness of the intercrossing CFRTC strands. Manufacturing the outer edge closures with the neat thermoplastic placement head, then placing tensioned CFRTC strands atop, eliminating the need for supporting structures to be made inside the core. The supporting CFRTC strands are non-removable because the core structure bonds to the support as the core is being placed but they become an integral portion of the structure.

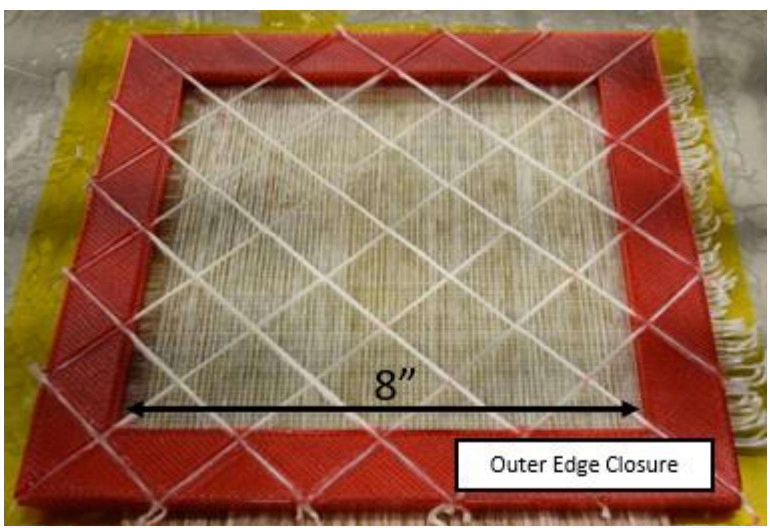

Figure 40: Pyramidal Truss Core Scaffolding

For the MAGIC system the CCP is the location where consolidation of the CFRTC is performed for this reason the Cutter Contact (CC) is more accurately represented as the Consolidation Contact

Point (CCP) for the MAGIC system. The CL and CCP for the MAGIC system is shown in Figure 41, the CL is the generated path that CAM software generates to send to the firmware that runs the hardware system and the CCP is the path that the CFRTC strand will take when being placed. A tool path, shown in Figure 42 (a), shows the CL path for half of a pyramidal structure. For the pyramidal truss core, the CL moves according to the following steps:

1. Initiate pultrusion at the start point.
2. Move upward to a point that is 0.049 inches (1mm) above the intercrossing support to account for variances in the composite scaffolding.
3. Move down to have composite strand contact the pultruded composite scaffolding.
4. Move across the scaffolding until the nozzle is no longer above scaffolding.
5. Move down to Pause Point. As the placement head moves downward the composite strand is spread around the nozzle.
6. Pause for 2 second while cold air is passed over the composite strand, quickly bonding the strand to the face sheet.
7. Move to the start point at the next node.
8. Repeat steps 1 through 7 until the core is complete. Cutting at the ends of the outer edge of the scaffolding.

The Navtruss core used later in this work was manufactured with a CL path shown in Figure 42 (b). The only difference between the pyramidal truss path and the trapezoidal truss path is the distance the end effector travels before it starts going toward the bed. For the pyramidal truss core the end effector travels 8 mm on step 4 but with the Navtruss truss core the end effector travels an extra 0.394 inches

(10 mm), for a total of 0.708 inches (18 mm). This extra length requires more CFRTC scaffolding, but allows for a better bond between the core and the top facing. Locations where the manufactured shape was different than the desired shape were analyzed and methods to improve the geometric stability were implemented in the MAGIC system. After manufacturing a pyramidal truss core, it was determined that the bond area between the core and the facings would need to increase for an acceptable quality CFRTC sandwich panel.

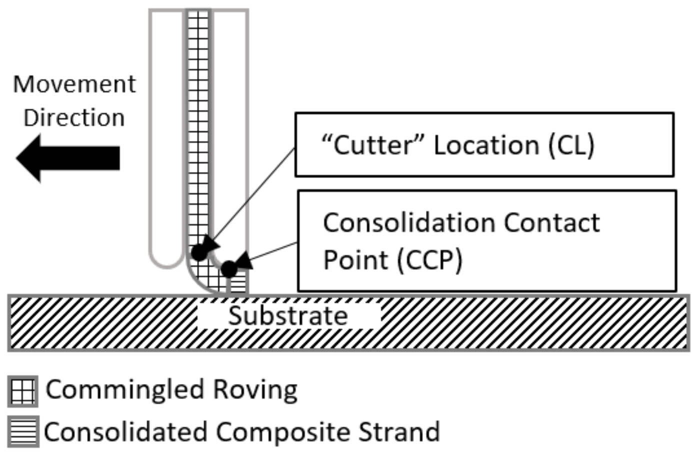

Figure 41: Cutter Location and Consolidation Contact Point Location Relative to the Nozzle

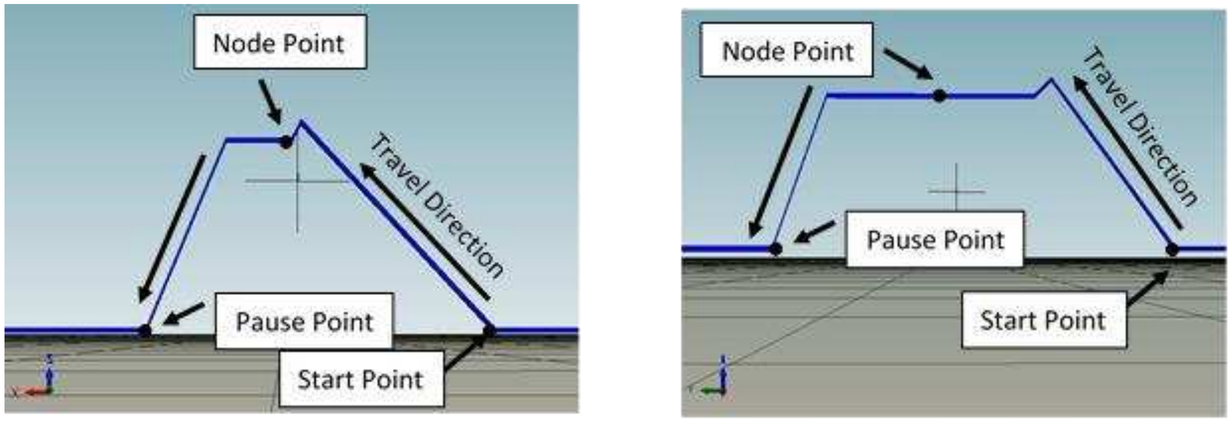

(a) Pyramidal CL Path (b) Navtruss CL Path

Figure 42:Programmed Placement Path

COMPOSITE QUALITY

A reduction in stiffness of a CFRTC Navtruss core sandwich panel, manufactured with the MAGIC system, will be most likely to occur in one or more of 3 different areas, the core, the core/facesheet interface, or in facesheet buckling, as shown in Figure 43. An investigation was done to better understand the quality of the CFRTC in each of these regions and find methods to improve the quality of the CFRTC laminates in these regions.

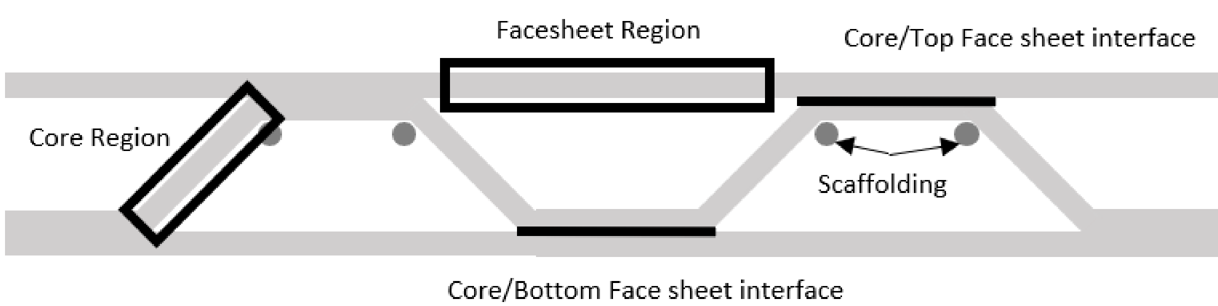

Figure 43: Sandwich Panel Stiffness Limiting Regions

CONSOLIDATION OF MULTIPLE COMPOSITE LAMINAE

As CFRTC laminae are being placed the laminate itself becomes stiffer creating a better structure for consolidation of later laminae. This experiment was designed to find the relative goodness of CFRTC laminate within the facesheet region, shown in Figure 43, based on the void content in the composite after manufacturing the laminate on a substrate and with no supporting structure under the span of the laminate. A total of 18 samples were manufactured and 2 specimens were cut from every sample. There were 3 samples per subgroup, and a total of 10 subgroups. 5 subgroups were manufactured onto a stiff substrate while the other 5 were manufactured with no supporting structure. Void fractions of the laminates were found following ASTM D792 [52] for determining the composite density and ASTM D3171 [53] for determining fiber and matrix fractions. An acrylic coating was used to keep water from seeping into any open porosity of the composite specimen surface, changing the equations needed to compute the void content. The equations that were used to find the volume fraction are as follows:

$$V_i = \frac{m_i}{\rho_i} \tag{7}$$

$$V_{void} = 1 - V_f - V_m - V_p \tag{8}$$

$$V_s = \frac{m_{sw}}{\rho_{water}} \tag{9}$$

$$m_{sw} = m_{air} - m_{water} \tag{10}$$

$$\%_{void} = \frac{V_{void}}{V_{specimen}} \tag{11}$$

The subscripts are defined as; fiber (f), matrix (m), acrylic polish coating (p), specimen in water (sw). V is volume, m is mass, ρ is density. The mass of all constituents was found using the burn out method. The volume fraction of each constituent was found, using the reported density of each constituent, and subtracted from 1 to get the void fraction within the laminates.

3D PRINTED LAP SHEAR

An experiment was designed, based on ASTM D5868, Lap Shear Adhesion for Fiber Reinforced Plastic Bonding [54]. By testing the shear strength between lamina placed on a stiff substrate and lamina placed with no supporting structure the quality of the bond between lamina in a laminate (facesheet region) can be examined as well as the bond between the facings and the core (Core/Top facesheet interface). The experiment used lap shear coupons that were manufactured in a fashion similar to how the top and bottom face sheets would be manufactured. The simulated bottom face sheet was manufactured on a warm substrate. The simulated top face sheet was placed on to CFRTC scaffolding. For this lap shear test the scaffolding span and thickness were designed so the specimen would represent two areas; the core and top facesheet bond of a Navtruss sandwich panel, and the inter laminate bond between unsupported regions of the facings. A perfect representation is not possible, but this test gives a general idea of the strength between core and the facesheets, and the interlaminar strength within the facesheets. The better the bond in this region the more shear stress the sandwich panel will be able to withstand due to the stiffness of the facesheets.

The configuration in which these specimens were manufactured is shown in Figure 44, where supports, CFRTC scaffolding, and the representative facesheets were placed. Two layers of composite strands were placed to make the flanges for the tension grips. The “adhesive area” is between the flanges or between the flange and a 90° layer of composite strand that was placed in this region to simulate the adhesion at a transverse fiber. The core is placed in two different directions; a 0° and a 90° orientation so both conditions need to be tested.

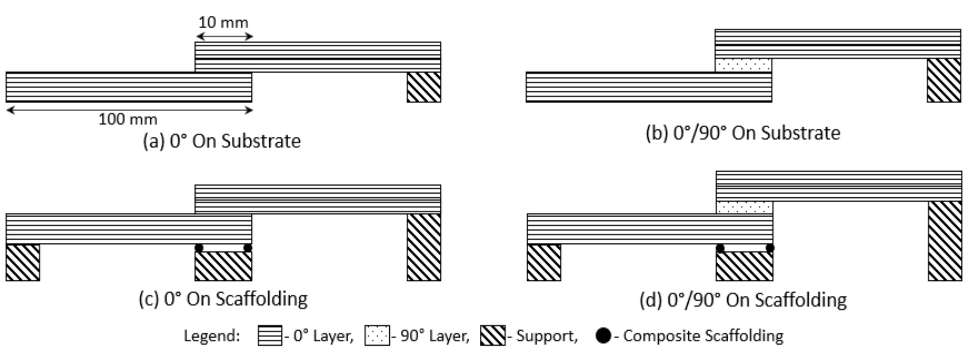

Figure 44: Lap Shear Specimen Configurations

Sample (a) represents the bond between the bottom face sheet and the core that was placed in the same fiber direction. Sample (b) represents the bottom face sheet and parts of the core that will be placed with the core fiber direction perpendicular to the bottom face sheet fiber direction. Sample (c) represents the bond between the top face sheet and the core with the bottom layer of the top facesheet fiber direction being parallel to the fiber direction of the core. Sample (d) represents the bond between the top face sheet and the core with the bottom layer of the top face sheet having a fiber direction perpendicular to the fiber direction of the core. The samples manufactured on the scaffolding did not have support directly under the sample. The support was only attached to the scaffolding at the edges, similar to the scaffolding on the composite Navtruss core sandwich panels, and the scaffolding position is shown in both Figure 43 (representative scaffolding) and Figure 44 (c & d).

Testing of the lap shear specimens was done by aligning a specimen in the tension grips, shown in Figure 45, using a laser guide to ensure proper alignment of the specimen within the jaws. The testing speed was 0.5 in/min (12.7 mm/min) as recommended by ASTM D5868 and the environment for the test was at 74 °F (26 °C). Specimens had a nominal width of 0.39 inches (10mm).

Figure 45: Practice Lap Shear Testing Specimen Placed in Tension Grips

To measure the bond area the specimens were painted in the bond region after bonding, so the bond area was a noticeably different color after failure and an area was found using quantitative optical analysis with IMAGEJ. A specimen, after lap shear failure occurs, is shown in Figure 46. The non-painted area was the bond area and was easily traceable within IMAGEJ, and the ruler was to scale IMAGEJ areal calculations. Five specimens were manufactured for each sample for statistical purposes.

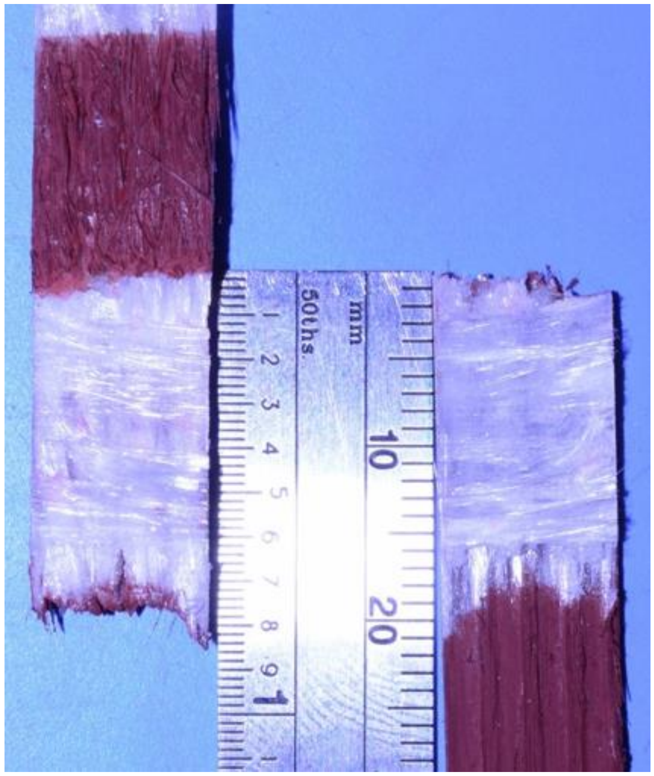

Figure 46: Painted [0/0/90/0/0]T Lap Shear Specimen to Measure Bond Area

The average shear strength for each specimen was calculated using equation 7, shown below, and the peak load was determined by failing the specimen in tension and finding the peak load from the loading curve. An example of a loading curve for the lap shear test is shown in Figure 47.

$$\tau = \frac{F_{peak}}{A} \tag{12}$$

Where τ is the apparent shear strength of the lap shear joint, F_{peak} is the peak load found through experimentation, and A is the bond area of the lap shear joint.

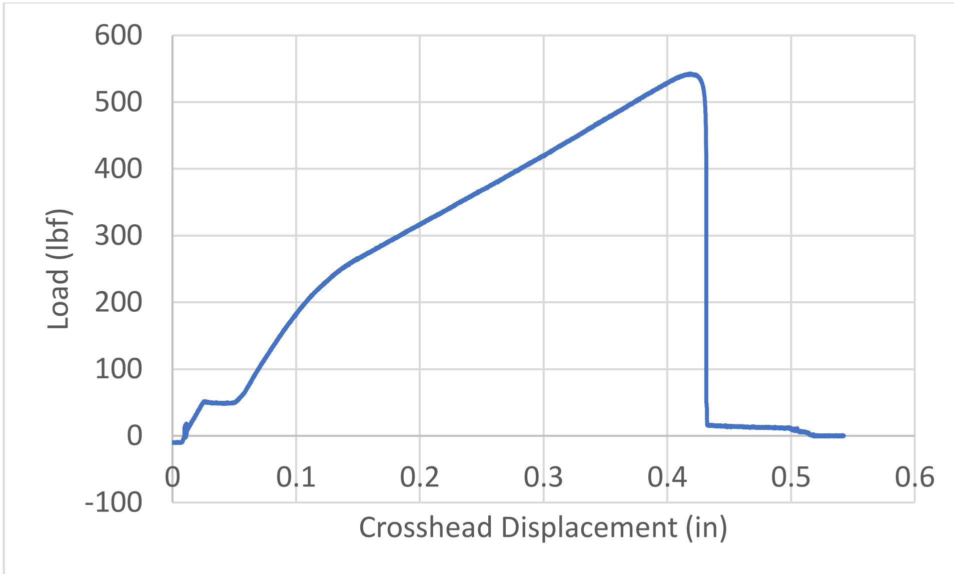

Figure 47: Lap Shear Test Specimen Loading Curve

STIFFNESS OF A STRAND

In theory, when placing a single CFRTC strand the temperature of the heating block is a factor in the resulting stiffness of the composite due to a decrease in matrix viscosity resulting in better wet out of the reinforcement. After increasing the thermal capabilities of the MAGIC system to be able to handle increased placement temperature a test was designed to determine the effects of increasing the placement temperature on placed composite strands. Single CFRTC strands were placed by tacking the strand to the substrate then the placement head moved off the substrate at a 45° angle at 3.94 in/min (100 mm/min). Five CFRTC strands were manufactured at three different placement temperatures, 518 °F (270 °C), 554 °F (290 °C) and 590 °F (310 °C) for a total of 15 strands. Cooling was used when placing the CFRTC strands on the substrate just as it would be used when manufacturing the core of the Navtruss sandwich panels. A diagram of the placement path is shown in Figure 48.

The unsupported section of the CFRTC strand was tested in 3 point bending with a span of 1.2 inches (30.5 mm). The loading rate was 0.1 in/min (2.54 mm/min) and the diameter of the specimens had a range from 0.05 inches (1.30 mm) to 0.08 inches (2.03 mm) in the tested region. The loading pins had a diameter of 0.125 inches (3.175 mm), and the center pin had a diameter of 0.25 inches (6.35 mm).

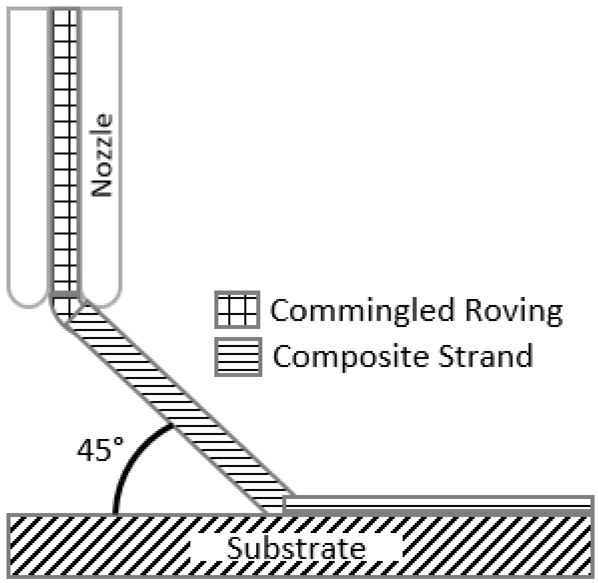

Figure 48: Temperature Stiffness Specimen Manufacturing Path

Each Specimen was loaded until the drop in the load was stagnant or there was a significant drop in the load. The load displacement curve was used to find the specimens stiffness factor EI, for each specimen and used is equation 13. The section of the load displacement curve used was the first linear region of the curve for each specimen. Figure 49 shows the load displacement curve of all the specimens tested for the control temperature of 518 °F (270 °C) and the representative slope of the sections used for the stiffness calculations.

$$EI = \frac{dP}{du} * \frac{L^3}{48} \tag{13}$$

Where $\frac{dP}{du}$ is the slope of the load displacement curve, L is the span of the 3-point bend test, and EI is the stiffness factor of the specimen and includes geometric and material factors.

When finding the stiffness factor of a CFRTC strand, geometric factors were not removed because the geometry contributes a significant amount to the stiffness of the composite strand [55]. The amount of fibers and matrix in any given cross section was constant but the geometry along the length of each specimen differed because of variances in drag within the nozzle. These variations along the length cannot be accounted for in the calculations. Variations in tested specimens are expected to represent variation within the Navtruss core.

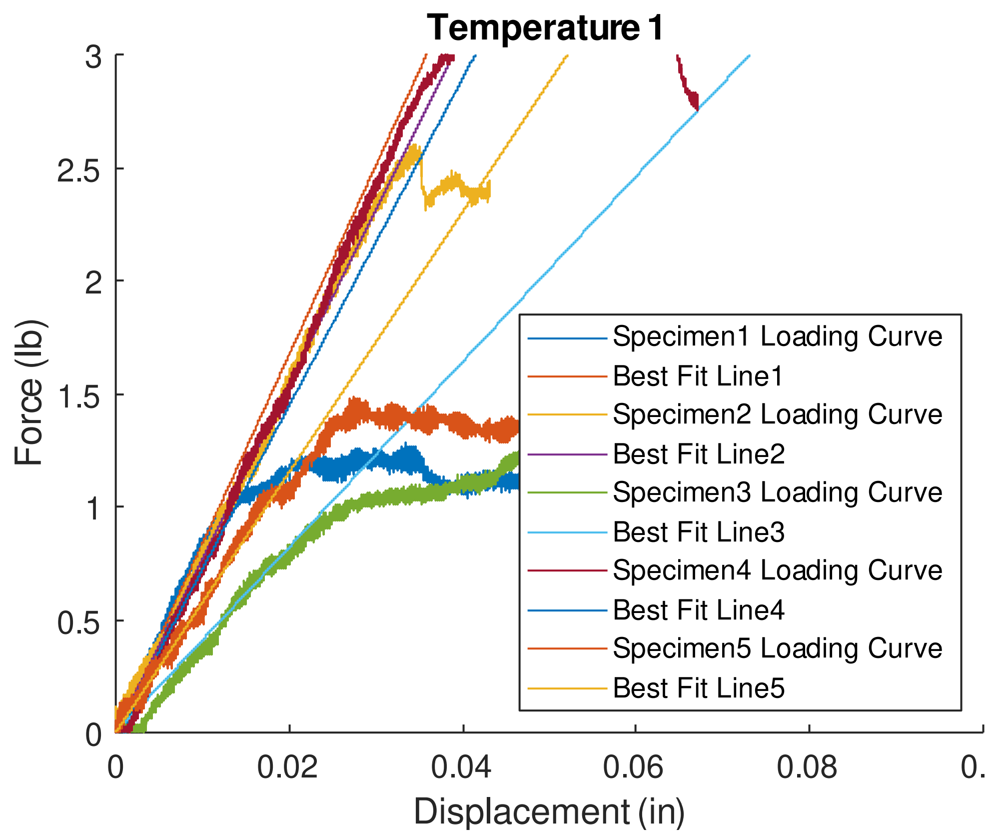

Figure 49: Load Displacement Curve of Temperature Test Specimens

COMPRESSION MOLDING AND HEAT FUSION BONDING

To generate a baseline for a CFRTC Navtruss panel it was decided that a set of panels would be produced by a technique common in the literature [35]. The Navtruss core struts were manufactured using compression molding in matched aluminum molds and then the top and bottom flat surfaces of these compression molded trusses were heat fusion bonded to the facesheets. The compression molding was done using a custom compression molding machine with a platen size of 8”x8” and a hydraulic press that consolidates 7 plies of the unidirectional thermoplastic prepreg into a unidirectional laminate.

Figure 50: Left: Top Half of Compression Mold, Right: Bottom Half of Compression Mold

Chemlease 41-90EZ was applied to the molds to ensure proper release of the PET. The UD prepreg was cut into 3”x6” strips with the fiber parallel to the long direction of the strip. Seven prepreg strips were placed on top of each other on the center of the mold and pressed until the alignment pins engaged the alignment holes, shown in Figure 50. The platens where heated to 554 °F (290 °C), measured with a K-type thermocouple, and when the composite reached 554 °F (290 °C), 140 lb (0.62 kN) of press force was applied to the mold. Once the plies were fused together the mold and platens were slowly cooled under pressure. When the composite temperature dropped below 158 °F (70 °C) the pressure was removed, and further cooling took place until a safe handling temperature was reached.

After the compression molding process the parts had any flash removed. These 3” (76.2 mm) x 6” (152 mm) pressed laminates were then cut to a nominal width of 0.393 inches (10 mm) using a high-speed saw cooled with water to create the truss core struts. The edges of the struts were wet sanded to remove defects induced by the cutting process and the struts were then dried for one hour at 131 °F (55 °C). After drying the struts were ready to bond to the facings. These compression molded struts have a nominal fiber volume fraction of 45%, and a void content of 3%, found by finding the composite specific gravity, ASTM D792, and finding the composite constituent content, ASTM D3171.

The top and bottom face sheets were cut from a prefabricated E-glass/PET $[0/90/0/90/0]_T$ laminate with a nominal thickness of 0.05 inches (1.2 mm). The face sheets were cut to 6" (152 mm) x 6" (152 mm) to prepare them for bonding to the core. The facesheets had a nominal fiber volume fraction of 45%, and a void content below 3%.

Bonding the core to the facesheets is non-trivial because the PET matrix material does not bond to many of the conventional adhesives, including epoxies. Therefore, the core needed to be fusion bonded to the facings with heat and a small amount of pressure. The core was bonded to the facings one at a time by first placing the core onto a facing, Figure 51(a), then heating the entire facesheet and core bond area and applying slight pressure. The applied pressure was sufficient to push the core into the hot facesheet without crushing the core, Figure 51(b). Once the facesheet and core bond areas have reached a sufficient bonding temperature the entire panel is cooled to a handling temperature, Figure 51(c). The cooled half of the sandwich panel is then flipped over to bond the other facesheet to the core, the heating process is repeated to bond the other facesheet to the core. Half of the structure must be at a low temperature otherwise the core would become malleable along with the facesheets, having this temperature gradient keeps the core stiff enough to support a minimal load while the bonding areas of the core are hot enough to bond sufficiently to the facesheets. Once the facesheets are bonded the sandwich panel is trimmed to its final size with a high-speed water-cooled saw and dried at 131 °F (55 °C) for one hour, Figure 51(d).

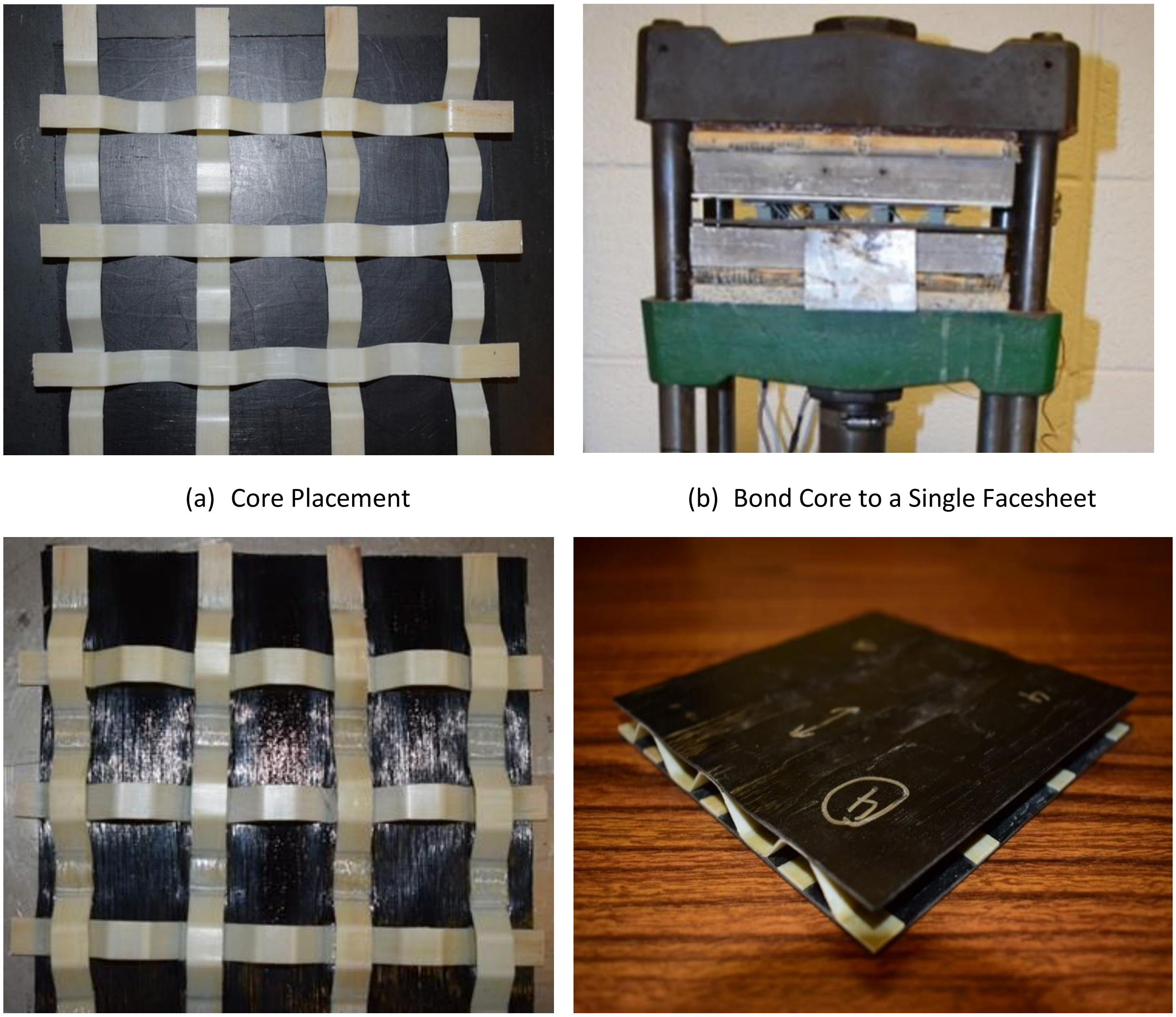

(a) Core Placement

(b) Bond Core to a Single Facesheet

(c) Bonded Core to Facesheet

(d) Completed Navtruss Core Sandwich Panel

Figure 51: Bonding Sequence for Compression Molded Specimens

3D PRINTED COMPOSITE MANUFACTURING

The MAGIC system builds up the Navtruss core composite sandwich panel one CFRTC strand at a time, starting with the bottom face sheet. An outer edge closure is placed which also serves as the CFRTC scaffolding and eliminates the tooling requirements. CFRTC scaffolding is placed with the core and then the top facesheet is placed to complete the manufacturing of a CFRTC Navtruss core sandwich panel.

BOTTOM FACESHEET MANUFACTURING

The bottom facesheet is started by tacking down the tow to the bed by hand, once the composite strand is properly adhered to the substrate tacking is complete and holding the composite strand is no longer required. The composite placement head then moves at 7.08 in/min (180 mm/min) across the substrate placing the CFRTC strand as it moves. Once the placement head moves into the cooling zone, just off the edge of the area that will be used as a facesheet, as shown in Figure 52 (a), the pressurized air turns on, cooling the nozzle for the 180° turn described in more detail in Chapter 2. The placement head then moves back and forth repeating the process until the bottom facesheet is completed. When a single lamina is complete the composite placement head starts placing the next lamina in a similar fashion but with a different fiber orientation. During the placement of the second lamina, and the third lamina of the composite facesheet, the composite strands are being placed directly onto the previous continuous fiber reinforced/PET layer. The thermoplastic adheres to the previous layer quickly and when cooled the bond is strong enough to withstand the tensioning force within the nozzle and can double back on itself, at the end of each pass, with adequate temperature control. The bottom face sheet has a ply sequence of $[0/90/0]_T$.

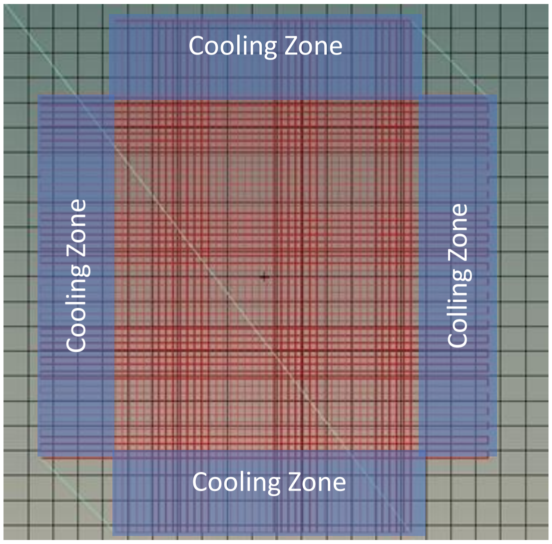

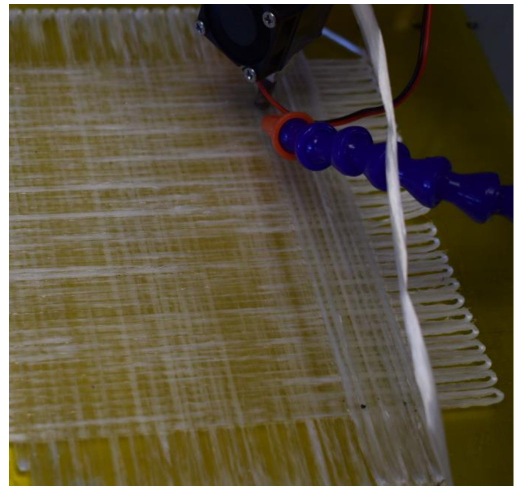

G-code with Cooling Zones

Manufactured Facesheet Panel

Figure 52: Manufacturing of Bottom Facesheet

OUTER EDGE CLOSURE MANUFACTURING

When the bottom face sheet is completed the fiber placement nozzle moves to a safe location and the neat thermoplastic placement head begins to print the outer edge closure. The outer edge closure is manufactured using a traditional FDM additive manufacturing system, being built up layer by layer with the G-code shown in Figure 53 (b). The design of the outer edge closure accommodates the CFRTC scaffolding for the core, shown in Figure 53 (a & b). Ridges are designed into the outer edge closure, giving room for the composite placement nozzle to be below the height of the top facesheet, stopping unwanted material build up from occurring in these areas.

After the neat thermoplastic PET outer scaffolding is manufactured, Figure 53 (c), the bed is cooled to room temperature and the neat thermoplastic gantry is moved to a safe location for the remainder of the time that the sandwich panel is being manufactured. The composite placement gantry is activated and starts placing the Navtruss core. The outer edge closure is removed for mechanical testing of the completed Navtruss sandwich panel, but would not need to be removed for an actual part.

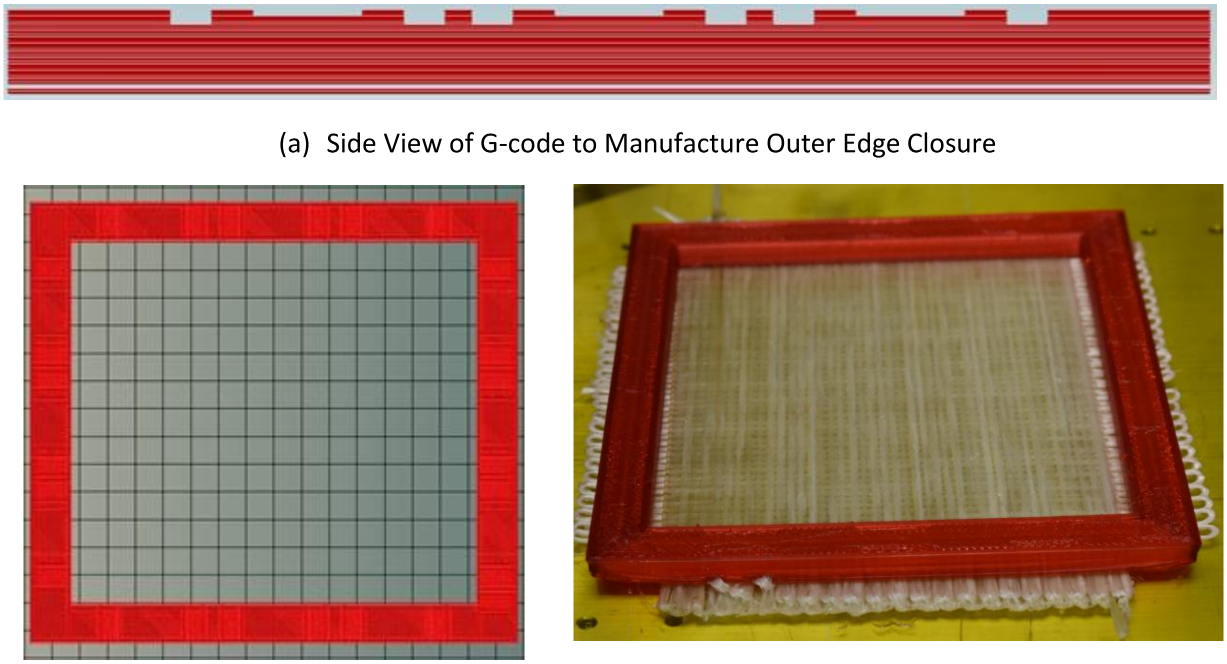

(a) Side View of G-code to Manufacture Outer Edge Closure

(b) Top View of G-code for Outer Edge Closure

(c) Manufactured Outer Edge Closure

Figure 53: Outer Edge Closure Manufacturing

CONTINUOUS FIBER REINFORCED THERMOPLASTIC NAVTRUSS CORE MANUFACTURING

The core requires Point to Point manufacturing, discussed in detail in earlier in this chapter, and the points are the top corners of the struts. CFRTC strands are placed in a way to facilitate the cores shape and not get in the way of the placement head during other manufacturing steps. The placement of the core can be broken down into 4 steps, continuous fiber reinforced scaffolding in the Y direction, truss core in the X direction, scaffolding in the X direction then truss core in the Y direction.

Steps 1 and 3, shown in Figure 54, have similar placement mechanisms but a different number of layers to have enough stiffness to hold the core as it is being placed. The scaffolding in step 1, the Y direction, has 4 composite strands placed atop one another to increase bending stiffness, while the scaffolding in step 3, the X direction, only has 2 strands placed atop one another because the span distance between supports is 1.18 inches (30 mm) for step 3 while the span for step 1 is 4.725 inches (120 mm). A thicker CFRTC scaffolding deflects less when placing the core because of the increase in bending stiffness due to an increase in the moment of inertia. Another way to increase the scaffolding stiffness is to include neat thermoplastic 3D printed pylons directly into the core that would be structural. These pylons, which could remain or be dissolved out in a post-processing step, would reduce the span of the strands and can be placed discreetly based on the size of the sandwich panel being manufactured.

Steps 2 and 4, shown in Figure 54, are the placement of the Navtruss core. Figure 55 shows the G-code path for the placement and the cooling zone used to manufacture the core. The two critical areas for manufacturing a single strut are when the CFRTC strand is being placed onto the facesheet, the pause point in Figure 55, and when the CFRTC strand is being pulled of the bottom facesheet, the lifting point in Figure 55. The composite placement head moves down from over the CFRTC scaffolding until it reaches the pause point. At the pause point cooling is turned on and the placement head pauses in place for two seconds allowing the CFRTC strand to cool and adhere to the facesheet. Because the strand has already been tacked the CFRTC strand can be tacked in new locations, but cooling needs to be applied to this area otherwise proper bonding will not be achieved and the CFRTC strand will peel off of the facesheet. The placement head moves across the cooling zone and starts to move upward off the composite facesheet. The tension tries to pull the newly placed CFRTC strand off the build plate, but because cooling was applied, the length of malleable composite in the newly placed tow is roughly 0.039 inches (1 mm) and this distance can be accommodated in the code generation. As the placement head moves upward, the relative head angle changes from 90° to 45°, and the geometry of the CFRTC strand changes as it becomes a rigid rod. When the placement head moves over the composite scaffolding a weak bond is formed between the scaffolding and the CFRTC strand. After reaching an adequate height to go over the scaffolding the head, again at a head angle of 90°, moves across the scaffolding and then downward to the pause point. When the composite moves over and downward the relative head angle changes between the placed tow and the nozzle, from 90° to 135°, spreading the tow out, which decreases the center thickness and increases the width of the CFRTC strand, as described in chapter 2. The CFRTC strand forms a bond between the previously placed upward strand because of the increase in strand width.

Step 1) Composite Scaffolding in Y Direction

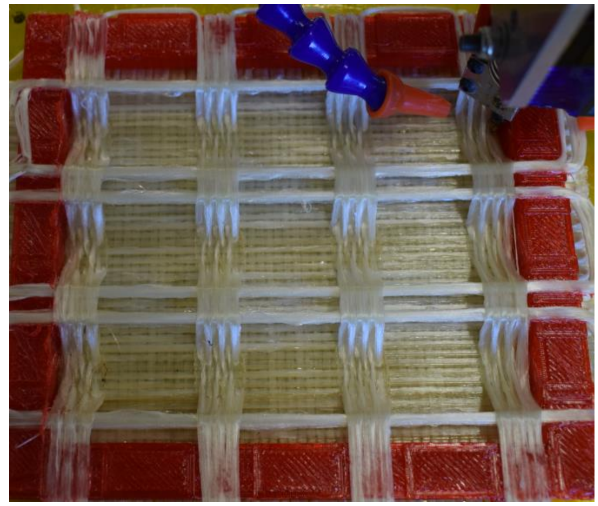

Step 2) Composite Core in X Direction

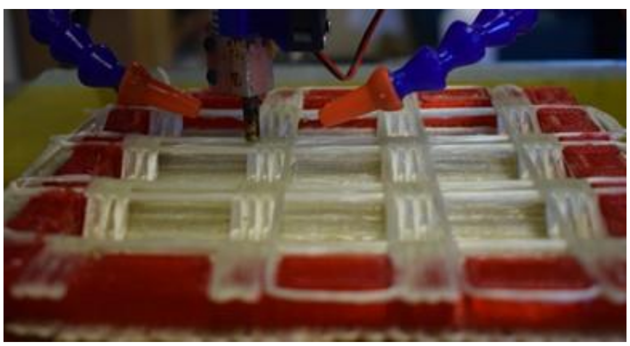

Step 3) Composite Scaffolding in X Direction

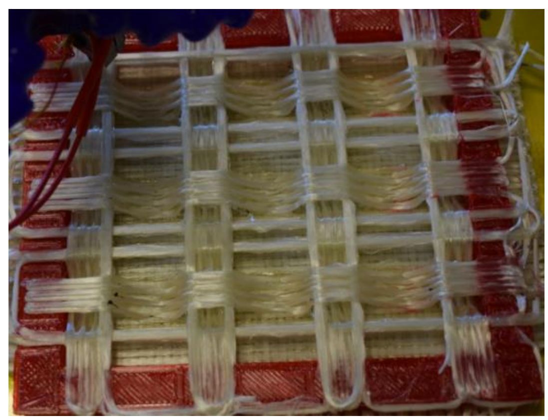

Step 4) Composite Core in Y Direction

Figure 54: Manufacturing Steps of a 3D Printed Navtruss Core

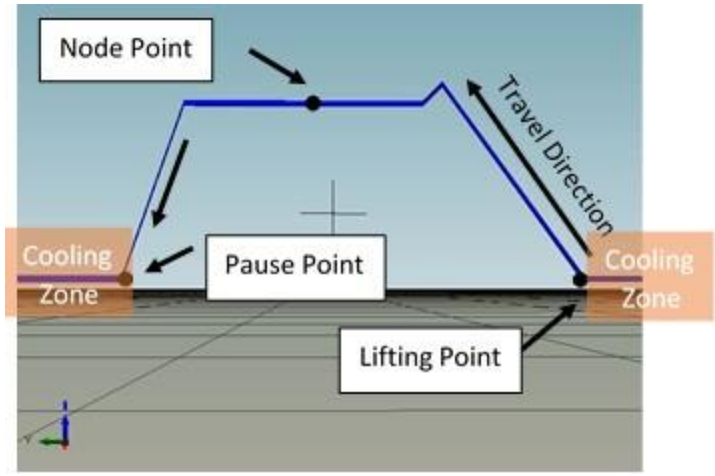

Figure 55: Placement Path for Navtruss Strut

TOP FACESHEET

Placing the top facesheet requires the same code as the bottom facesheet, but the Z height is adjusted for the thickness of the panel, as shown in Figure 56. The second layer [90°] is placed at the same height utilizing the consolidation spring to allow the head to move up and down and follow the undulations of the first layer. This improves the ability to consolidate the lamina and decreases fluctuations in placement force while placing composite strands of the top facesheet. The stiffness of the first layer of the facesheet is a function of the distance between supports. The distance between supports is 30mm in most locations and 140 mm in the others. The second layer is consolidated onto the first and the third layer is consolidated onto the combination of the first and second. A completed 3D printed specimen with the outer edge closure removed is shown in Figure 58, the edge closure was removed for core quality testing.

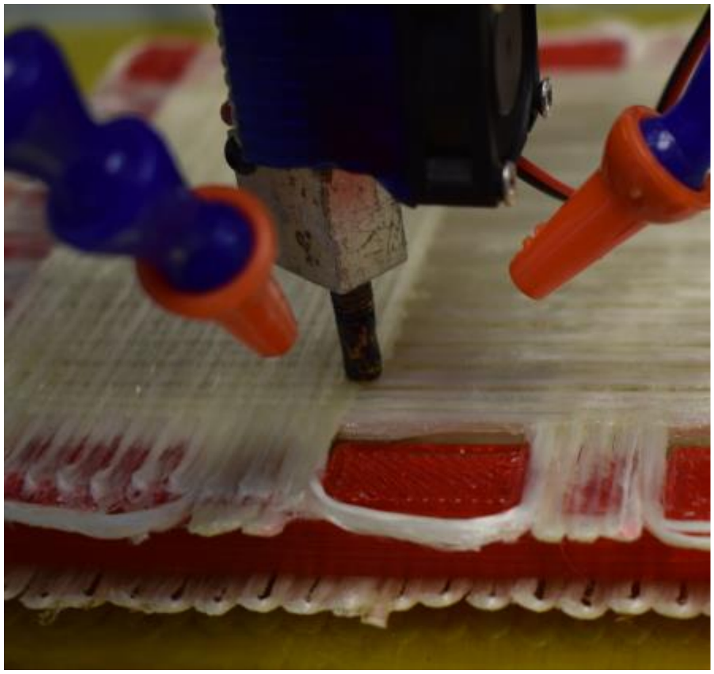

Figure 56: Placement of Top Facing onto Core

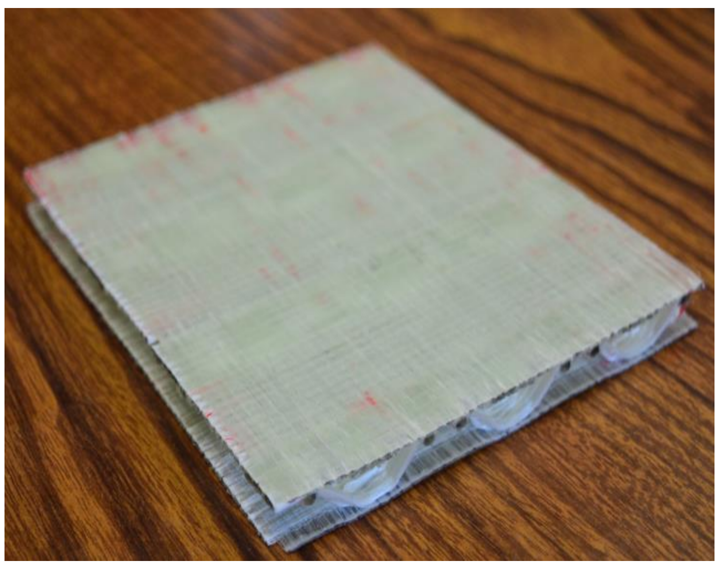

Figure 57: Finished 3D Printed Navtruss Sandwich Panel

MODULUS EXPERIMENTS

STIFFNESS

Flexural stiffness of a composite structure is controlled by fiber direction, fiber volume fraction, the reinforcement modulus, and the geometry of the structure. The matrix material is used to transfer stress into the reinforcement and hold the designed shape. If the matrix material does not fully wet the fibers, then there is not adequate stress transfer and the stiffness of the structure will decrease significantly. With the MAGIC method there is no consolidation pressure wetting out the fiber when placing CFRTC strand in free space, only the consolidation that occurs within the nozzle. Testing for stiffness of the core will show stiffness differences between the MAGIC method and compression molding manufacturing method indicating differences in fiber wetting. The MAGIC method is still in development, so the first major milestone is matching the stiffness between the two manufacturing methods, after which, work toward increasing the strength can be undertaken.

COMPRESSION MODULUS

ASTM C365 [56] is the experimental procedure to calculate a sandwich panels core compressive modulus and core compressive strength. Core compressive modulus translates to the stiffness of the core, while compressive strength shows the maximum stress within the core before failure occurs. Getting stiffness from the sandwich panel structure requires recording the load applied through the thickness and the corresponding displacement. Stiffness is the focus of this study because the required loading is in the linear region of the mechanical response curve and all strains are, for the most part, recoverable and the specimen is not damaged during testing. To measure the deflection as the panel is crushed, two aluminum plates were designed to have points for a clip-gage extensometer to attach. The aluminum plates sandwich the sandwich panel during the test, accomplishing two things, the first is providing enough area for the entire sandwich panel to be pressed and the second is providing a non-fixed surface to record deflection of the sandwich panels during loading. Figure 58 shows the testing setup with a compression molded specimen placed in the compression testing apparatus.

The procedure for testing and calculations that were done are based on ASTM C365. A single cell size of the core is large compared to a honeycomb structure, so a larger area is used rather than the ASTM recommendation because a total of 9 cells are specified for this test, which for the Navtruss configuration, requires a 5.5” (140mm) x 5.5” (140mm) panel. The loading rate was 0.02 in/min (0.51 mm/min) up to a total load of 1000 lbf (4.45 kN), then the specimens were unloaded. Each specimen was loaded 5 times for test for repeatability. The equation used for finding the compression modulus is as follows, and the variables with respect to the sandwich panel can be found in Figure 59:

$$\mathrm{E}_z = \frac{\Delta P * t}{\Delta u * L * b} \tag{14}$$

Where:

E_Z = Core flatwise compressive chord modulus (psi),

ΔP = change in force between the displacement Δu (lbf),

Δu = recorded displacement between two loads (in),

t = measured core thickness prior to loading (in),

L = Length of the specimen (in), and

b= width of the specimen (in).

By plotting P vs Δ, from Figure 60, a linear region can be found where $\frac{\delta P}{\delta \Delta}$ is the slope of the plot. This slope is multiplied by t/A to determine the core modulus in this load region. The ASTM recommends finding a load region between 25% and 50% of the load at failure of the specimen. For these specimens the maximum load found through experiment was nominally 2000 lbf. The linear region of the graph used was between 600 lbf (2.66 kN) and 800 lbf (3.56 kN) because the specimens seemed to settle after ~500 lbf (2.24 kN). The core thickness and cross-sectional area were measured with calipers that have an accuracy of 0.0005 inches (0.001 mm) by taking 5 different measurement in different areas for a single specimen and averaging them.

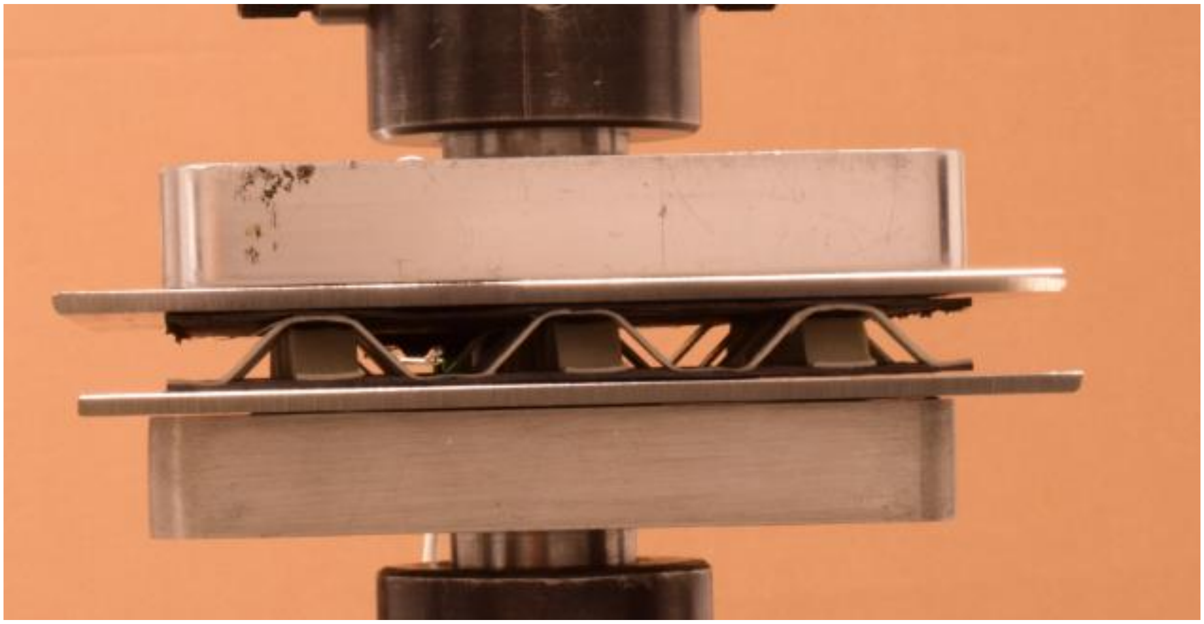

Figure 58: Compression Modulus Testing Setup

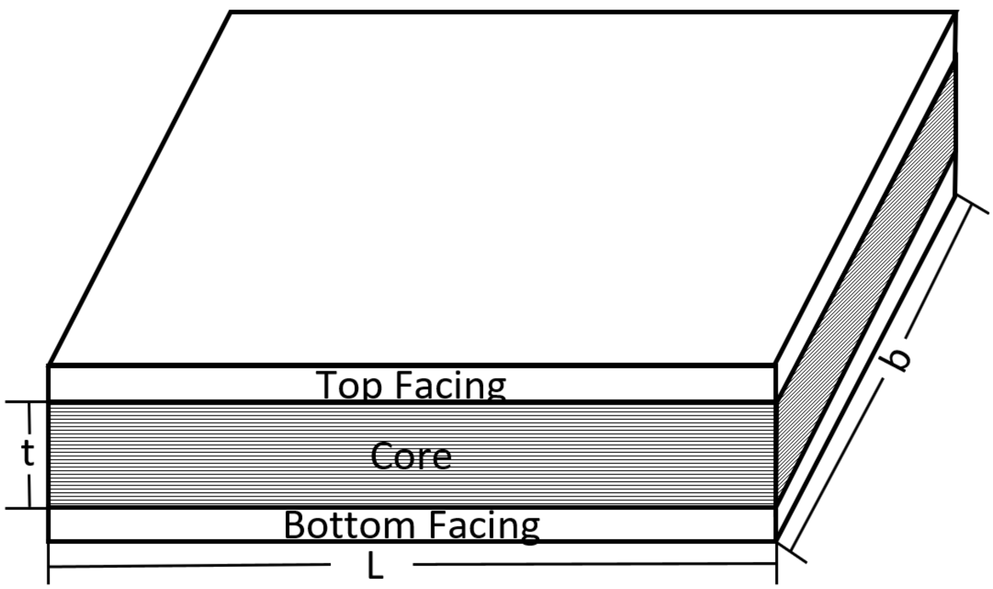

Figure 59: Sandwich Panel Dimensions

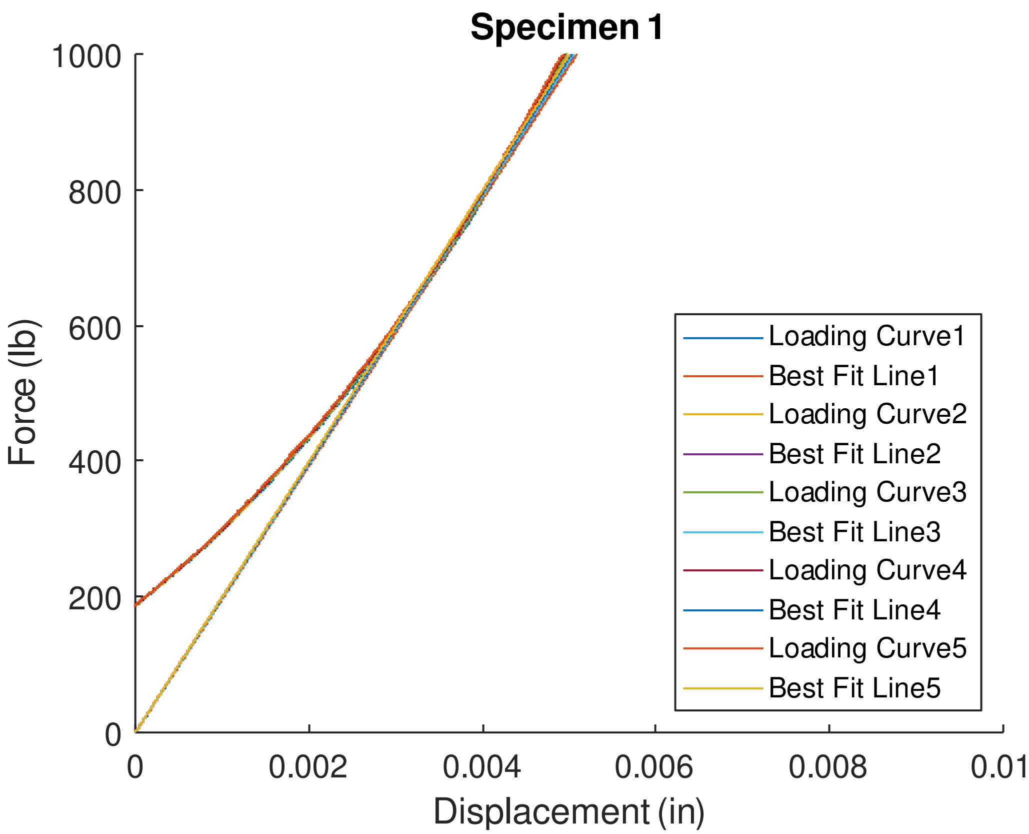

Figure 60: Load vs. Displacement of a Representative 3D Printed Navtruss Specimen

SANDWICH SHEAR

Core shear modulus can be found using procedures found in ASTM C273 Shear Properties of Sandwich Core Materials [57]. For a core shear strength to be found failure needs to occur within the core and not at the core to facing bond. Core shear modulus can be found, using the linear region of the load vs. displacement curve. The core shear modulus experiment requires the sandwich panel specimens be bonded to relatively stiff plates, and these plates are subsequently loaded in shear to test the core. After doing initial trials it was determined that large aluminum or steel plates would be needed to accurately measure the displacement between these panels. In the interest of saving cost, and maintaining the specimens after testing, thinner plates were used. The displacement was based on the crosshead displacement.

The sandwich panel specimens where bonded to 1/8" (3.18 mm) thick aluminum plates using an epoxy adhesive, Loctite EA9394. The Loctite was cured at 75 °F (24 °C) for 24 hours and then post cured at 140 °F (60 °C) for one hour. The sample alignment between the plates was important because variations in plate alignment with the testing rig would result in an uneven application of pressure during the tests. A pin was used to rotate the lower fitting with the specimen reducing the effect of variations in the alignment of the loading plates after the bonding process. Specimens 1 and 2 were bonded to 3/32" (2.38 mm) plates to test the bonding and loading procedure and will not be used in the comparison due to variances in loading plate stiffness.

The shear tests were done with a crosshead displacement speed of 0.02 in/min (0.51 mm/min) and unloaded after a load of 600 lbf (2.67 kN) to keep the specimens intact for retesting. Each specimen was tested 5 times to generate statistical information. Figure 61 shows the testing setup with the two loading plates being placed into the upper and lower fittings. The equation to find core shear modulus, using the procedure within ASTM C273, is as follows:

$$G = \frac{\Delta P * t}{\Delta u * L * b} \tag{15}$$

Where:

G = core shear modulus (psi),

ΔP = change in force between the displacement Δu (lbf),

Δu = recorded displacement between two loads (in),

t = measured core thickness prior to loading (in),

L = length of the specimen (in), and

b = width of the specimen (in).

The length, width and core thickness were found prior to bonding the specimens to the aluminum loading plates. Using crosshead displacement as a measure of strain is not a perfect representation of the shear displacement and an accurate core shear modulus cannot be calculated using this method. However, all of the specimens tested were subject to this same inaccuracy and, thus, comparisons between the different cores can be made, with the exception of specimens 1 and 2 which showed increased compliance due to thinner loading plates. The experiment can be modeled as a series of springs, as the loading plates increase in thickness, and stiffness, the result of the tests is driven to the core shear modulus. When the stiffness of the loading plates is not significantly greater than the stiffness of the core the plates have a greater role in determining the stiffness of the specimen being tested, as is the case with specimen 1 and 2.

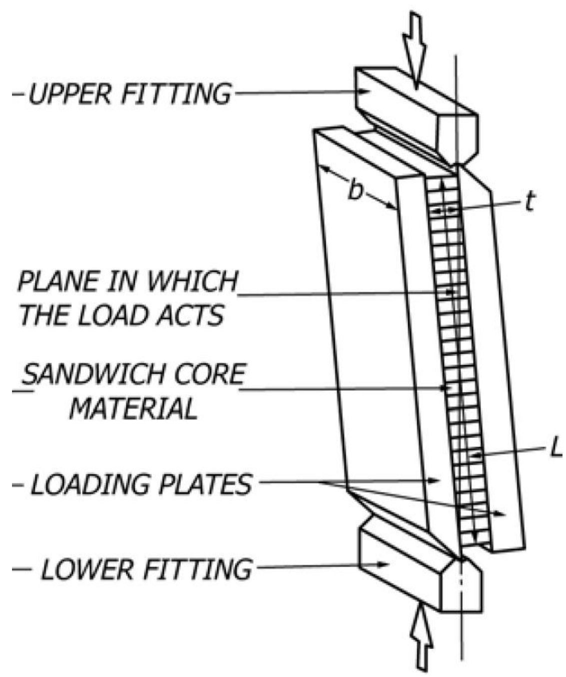

Figure 61: ASTM C273 Sandwich Shear Modulus Testing Setup [57]

SPECIMEN DEVELOPMENT

Two sets of specimens were manufactured for the compression modulus and shear modulus experiments. Compression Molded specimens are referenced directly with the reference tag CM#, where the number relates to the specimen number. 3D printed specimens manufactured with the MAGIC system are referenced with 3D#. Therefore, specimens CM1-5 have compression molded cores and 3D1-5 were 3D printed with the MAGIC system

COMPRESSION MOLDED SPECIMENS

The facing thickness of the 3D printed specimens are different between 3D1-3 and 3D4-5. In theory the facing thickness will not affect the core compressive modulus or shear modulus. To test if the facing thickness effects the core modulus specimen CM1 was manufactured with facings twice as thick as specimens CM2-4 to determine if there is a difference in core compression modulus based on the thickness of the facings.

The 3D printed specimens 3D1-3 and 3D4-5 have different fiber orientations within the facings and the interface compliance between the core and the facings could change the stiffness of the core. CM2, CM3 and CM5 were manufactured to determine if the fiber orientation of the lamina that interfaces with the core effects the core compressive or core shear modulus.

Specimen CM2 and CM4 were manufactured to check consistency of the compression modulus between the compression molded core specimens.

3D PRINTED SPECIMENS

Specimen 3D1 was manufactured before the development of the 180° turning method and cooling was used to place the entirety of the core. The facings were limited to two laminae because the manufacturing time of a single lamina was between 2 and 3 hours as a lab technician was required to be present to manually cut and tack the CFRTC strand after every pass.

Specimen 3D2 was manufactured utilizing the 180° turn and cooling was used for the entirety of the sandwich panel manufacturing process. The as-manufactured core geometry changed to its final form during this step, because the composite placement head could move from one end of the build area to the other end without cutting and restarting the CFRTC strand. The core was no longer placed in single direction and instead was manufactured by the placement head placing a single CFRTC strand of the core in one direction and then turning back on itself and placing the following strand directly next to the previously placed CFRTC strand.

Specimen 3D3 utilized the firmware-controlled cooling mechanism and cooling was only used in locations where it would be beneficial. The controlled cooling mechanism allowed for the automated on/off control of the cooling airflow at specified points in the manufacturing sequence. Cooling zones were implemented for this specimen and all remaining 3D printed specimens.

Specimen 3D4 was manufactured with facings that had a ply sequence of $[0/90/0]_T$ because automation of the MAGIC system decreased the manufacturing time of a single lamina from 2-3 hours to just 1.5 hours. This allowed a 3 ply laminate, which is less susceptible to warping during cooling, to be produced in less time than a 2 ply laminate had previously taken.

Specimen 3D5 was manufactured using the same G-code as 3D4, but at a control temperature of 590 °F (310 °C). With specimens 3D1-4 the maximum temperature that the hot end could achieve was 572 °F (300 °C)

CHAPTER 6: RESULTS AND DISCUSSION

The goal of this work is to show the current state of manufacturing with the MAGIC, Modular Additive Generation of Intricate Composites, system. The MAGIC system is the process of selectively placing continuous fiber reinforced thermoplastic composite (CFRTC) structures in and out of the build plane to manufacture complex geometries. In the current engineering culture, the term 3D printing is used for similar processes and the specimens could be referred to as being 3D printed with the MAGIC system. Specimens manufactured with the MAGIC system were evaluated for composite quality.

Composite pyramidal truss structures were manufactured during the development of the MAGIC system to amplify issues with the point to point, unsupported fiber placement techniques. A Navtruss corrugated core was selected as a better demonstration article because the unsupported core and facings could be manufactured without tooling showing the capabilities of the system. As the facings are manufactured sections will be unsupported and as the laminates are built up with the MAGIC system the quality of the laminate increase. The void fraction and lap shear strength of CFRTC lamina placed with the MAGIC system, both on and off a substrate, were evaluated for their relative goodness. Different temperatures were used to manufacture individual CFRTC strands placed out-of-plane and each strand was tested for bending stiffness to determine the composite quality.

Compression molding was also used to manufacture Navtruss core panels, to allow a comparison between 3D printing with the MAGIC system and a more conventional approach. Inaccuracies specific to the thermoplastic manufacturing methods were analyzed. The Navtruss core sandwich panel specimens were tested for their stiffness in compression and shear demonstrating the capabilities of the MAGIC system in comparison to compression molding. This work is the result of developing the MAGIC system to automate both in and out-of-plane fiber placement. Sandwich panels were manufactured utilizing the different automation techniques to demonstrate how improvements have not only increased the part quality, but also increased the functionality of the MAGIC system. Core stiffness testing was done to find out the differences between a fully consolidated core using compression molding and a core made with the MAGIC system.

UNSUPPORTED MANUFACTURING

RESULTS

CFRTC strands were placed to make a pyramidal truss core structure, as shown in Figure 62. The distance required to tack the CFRTC strand to the bottom facing was nominally 1.2 inches (30 mm). The designed height of the pyramidal structure was 0.39 inches (10 mm). The manufactured core pyramidal structure was 0.32 inches (8.13 mm), a difference of 0.07 inches (1.78 mm). The height of the core placed near the center was the lowest, with a placed height of 0.27 inches (6.86 mm) and was the highest close to the outer edge closure, with a height of 0.302 inches (7.67 mm). The gap between the as-placed facing and the pyramidal core was largest near the center, with a separation distance of 0.05 inch (1.27 mm).

DISCUSSION

The areas of interest identified to contribute to the quality of the pyramidal truss core sandwich panel was the bond between the top facing and the core. Multiple pyramidal truss structures in the middle of the panel deflected more than 0.0394 inches (1 mm) when being placed and therefore were too low to bond to the top facing. The top facing was placed just above the top of the pyramidal structure, as shown in Figure 63. Increasing the stiffness of the CFRTC scaffolding would decrease the deflection when placing the core.

There are a few ways to increase the stiffness of the CFRTC scaffolding. Increasing the thickness of the CFRTC scaffolding by placing multiple strands atop one another will increase the relative stiffness of the scaffolding. Decreasing the span between scaffolding supports will also help reduce deflection. With the pyramidal panel the supporting span for the scaffolding was 9.44 inches (240 mm). Large spans increase the deflection of the scaffolding due to bending stresses caused by the force required to pull the CFRTC strands from the nozzle. Placing structural pylons within the core that would support the scaffolding and add to the structure of the sandwich panel would increase the CFRTC scaffolding stiffness and increase the positional accuracy of CFRTC core placement but would add additional weight to the composite sandwich panel.

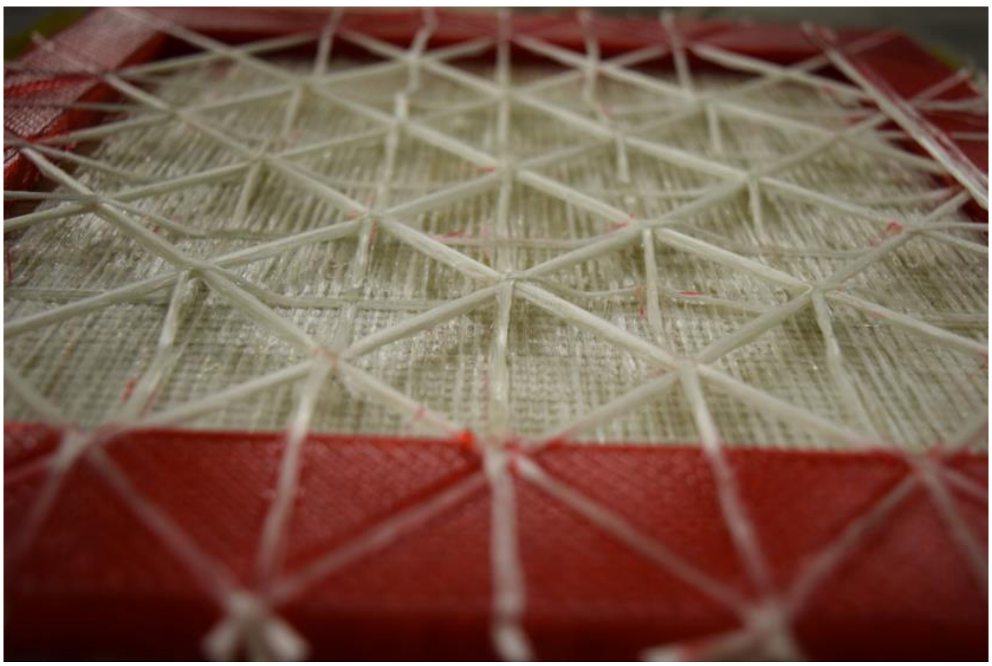

Figure 62: Continuous Fiber Reinforced Thermoplastic Composite Pyramidal Truss

Figure 63: Gap Between Pyramidal Core and Facing

CONSOLIDATION OF MULTIPLE LAMINAE COMPOSITES

RESULTS

The average void content for CFRTC laminate specimens with different numbers of lamina are displayed in Figure 64. Specimens manufactured on the bed are represented in orange. Specimens manufactured in unsupported space are represented in gray. The average and standard deviation are reported for each specimen group, and represented by the error bars. A CFRTC lamina placed directly on the substrate has an initial void content of 3.1% and a standard deviation of 1.5% and the void content of the laminate stays below 5%, except for layer 4 which was abnormally high at 8.3%, as the laminate is built up from 1 lamina to a total of 5 laminae.

A laminate with a single CFRTC lamina placed with no supporting structure has an average void content of 22.1% with a standard deviation of 2.0% and as the laminate is built up the average void content of the laminate decreases to 10.6% with a standard deviation of 1.6%. Each lamina placed after the first lamina has a substantial decrease in void content when no initial supporting structure is used. The void content of the laminate as the number of laminae placed increases is an asymptotic relationship and converges on a void content of 10%.

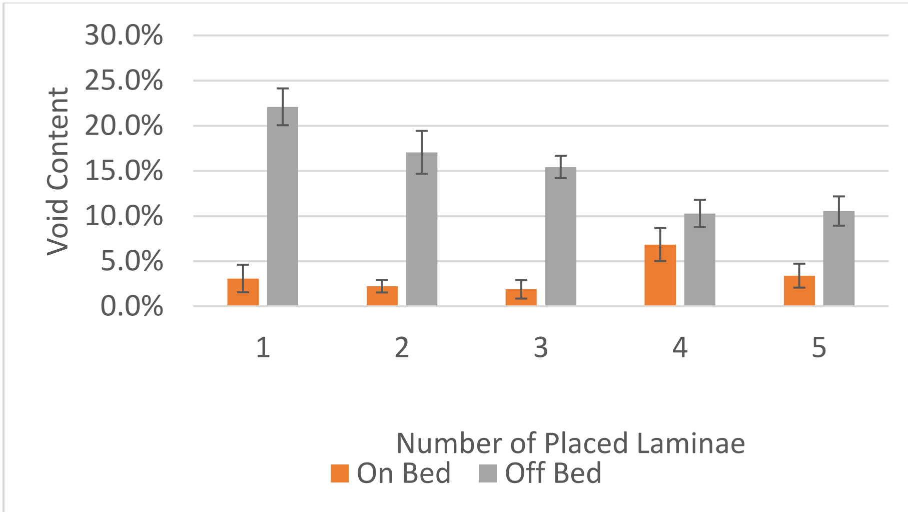

Figure 64: Void Content of Laminates Placed on a Substrate and No Support

DISCUSSION

An increased standard deviation occurs for the first CFRTC layer placed on the substrate because of variations of the topology of the substrate. Laminae 2 through 5 are placed on previously placed laminae and not directly on the stiffer substrate. As the nozzle moves across the previously placed plies, heat and pressure are being applied to not only the lamina being placed but also to the previously placed lamina, helping to improve the previous ply consolidation and thus, slightly decreasing the void content within the laminate.

Differences in machine compliance for the direction of placement can affect the void content of the layer that is being placed. The MAGIC system is currently more compliant when placing fiber in the X-direction than in the Y-direction and this increased compliance led to a higher void content in sample group 4, which was placed on the substrate. For the 3 laminae specimen only one CFRTC lamina was placed in the X-direction and was reconsolidated when the 3rd lamina was placed atop of the 2nd layer. For the 4th specimen two CFRTC laminae were placed in the X-direction without a lamina being placed in the Y-direction between the two laminae. The reduced machine compliance can lead to a decrease in bandwidth because less force is being applied to the CFRTC strand, increasing the distance between two placed strands creating a gap that increases the void content. When a layer is between the two laminae placed in the X-direction, the 5 laminae specimens, the void content was significantly lower and maintained a standard deviation similar to the single lamina laminate.

The quality of the composite CFRTC laminates, placed in space, is related to the length of the unsupported span. When a force is applied to the strands of the first layer by the nozzle placing the next lamina, consolidation of the newly placed composite lamina will change based on the amount of deflection that occurs in the previously placed laminae. As discussed earlier, increasing the span will increase the amount of deflection within the laminae for a given placement force, decreasing the composite quality. A span of 40mm was chosen because this is a common span that occurs within Navtruss core sandwich panels discussed in the literature and could easily be cut into specimens. For the 40mm span the number of CFRTC laminae that needed to be placed to reach the asymptotic void content is 4 laminae because the 4 laminae composite facesheet had statistically the same void content as the 5-lamina laminate.

LAP SHEAR

RESULTS

The shear strength and standard deviation of four different lap shear strength CFRTC samples is shown Figure 65. The shear samples with a 0° interface, that were manufactured on a substrate, had an average shear strength of 1580 psi (10.89 MPa) with a standard deviation of 92 psi (0.63 MPa). The CFRTC samples with a 0° interface, manufactured on the scaffolding, had an average shear strength of 1440 psi (9.93 MPa) with a standard deviation of 168 psi (1.16 MPa). The lap shear samples with a 90° interface manufactured on the substrate had an average shear strength of 911 psi (9.28 MPa) with a standard deviation of 63 psi (0.43 MPa). The lap shear samples with a 90° interface manufactured on the scaffolding had an average shear strength of 618 psi (4.26 MPa) with a standard deviation of 157 psi (1.08 MPa).

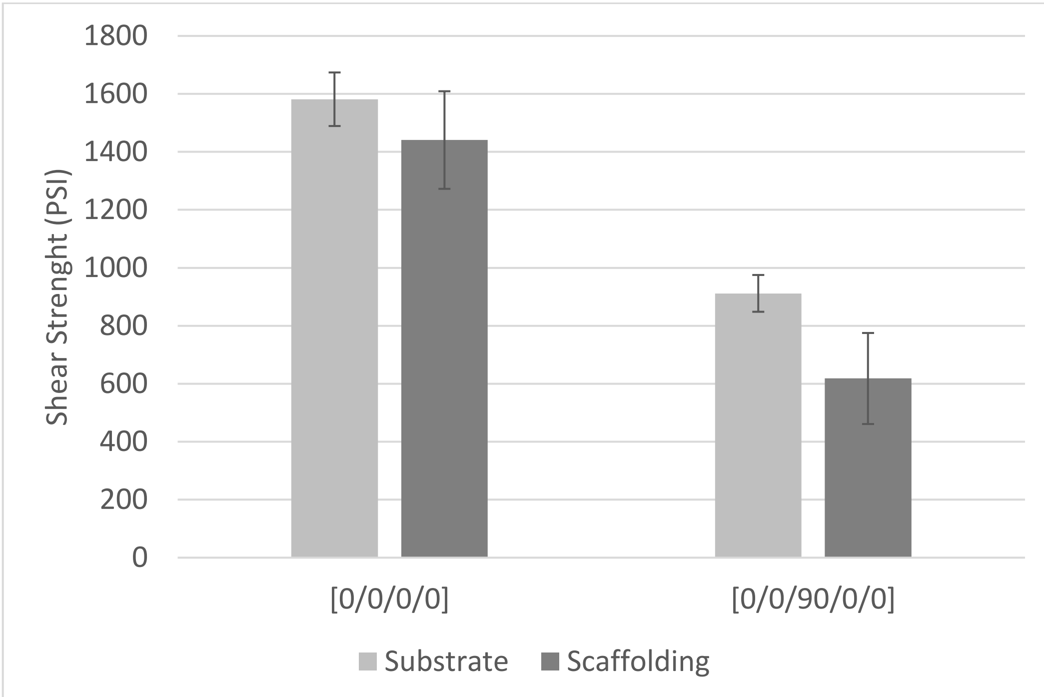

Figure 65: Lap Shear 3D Printed Samples

DISCUSSION

Variations in this data can be attributed to the repeatability of the two different placement techniques. When manufacturing samples on the substrate the supporting stiffness was the same for every sample, decreasing the variation between specimens. Manufacturing the samples on the CFRTC scaffolding resulted in a large deviation between samples because the stiffness of the supporting structure varied along the length depending on the stiffness of the CFRTC scaffolding. The quality of the specimen being placed decreased toward the center of the CFRTC scaffolding. Earlier it was shown that when placing CFRTC strands with no support the quality of the composite increases as the number of placed laminae increase. By the 3rd laminae there is still a high void content that is reduced by the 5th laminae. The increased void content in the 1st layer can account for some of the variability because the stiffness of a

CFRTC strand is dependent on the geometry of the strand, a concept that is discuss in detail in the next section. The reported shear strength values in this work are expected to be lower than the shear strength for PETG because the shear area of specimens manufactured was smaller than the ASTM recommendation for minimum shear area.

STIFFNESS OF A STRAND

RESULTS

The stiffness factors of CFRTC strands placed at control temperatures of 518 °F (270 °C), 554 °F (290 °C), and 590 °F (310 °C) are shown in Table 2. The stiffness factor, EI, of the CFRTC strands is the modulus of the material multiplied by the area moment of inertia of the specimen. Both the material stiffness and the geometric stiffness have a role in determining the stiffness factor. Each specimen has the same amount of the two constituents and are different only in cross sectional geometry and fiber wet out along the length of each CFRTC specimen. The stiffness factor of the specimens manufactured at 518 °F (270 °C) and 554 °F (290 °C) are statistically the same and fall entirely in the lower half the 590 °F (310 °C) specimens. The CFRTC strand specimens all have the similar lower bound stiffness factor but the upper bound of the 310 °C specimen is significantly higher with a stiffness factor of 4.33 lb-in^2. The majority of the specimens manufactured with a control temperature of 310 °C had a higher stiffness factor than any of the specimens manufactured with the other two control temperatures.

Table 2: Single Composite Strand Stiffness

Temperature	Highest Stiffness Factor	Average Stiffness Factor
518 °F (270 °C)	3.01 lb-in^2	2.39 lb-in^2
554 °F (290 °C)	2.87 lb-in^2	2.35 lb-in^2
590 °F (310 °C)	4.33 lb-in^2	3.10 lb-in^2

DISCUSSION

As the control temperature increases the matrix material decreases in viscosity allowing the matrix to move more freely and coat the fibers as the composite passes through the nozzle. When the commingled roving passes though the nozzle the friction changes based on what is happening with the fibers in the nozzle. If the fibers are broken when they enter the nozzle they can start to curl within the nozzle increasing the force required to pull the CFRTC strand from the nozzle. When this happens on a small-scale, sections of the CFRTC strand will see more tension than others and, in some cases, this will pull fibers away from the matrix material causing less wet out within the CFRTC strand. Fiber curling can occur at any temperature and can happen regularly, setting the lower limit of the stiffness factor for all control temperatures used. Since each strand has the same number of glass reinforcing fibers, voids can increase the stiffness of a composite structure [55] by changing the composite geometry to have a larger area moment of inertia. Although, this assumes that all the fibers in the composite are fully wet out and the voids only interact with the matrix material. With the MAGIC system CFRTC strand placement in unsupported space can leave a void that runs the entire length of the CFRTC strand and other voids within the composite that effect the wet out of the reinforcement decreasing the total stiffness of the structure. One of the reasons that a stiffness factor was used instead of finding the material stiffness is the wet out and geometry change constantly with the current placement system and stiffness factor contains both inconsistencies.

COMPRESSION MOLDING VS 3D PRINTING MANUFACTURING METHODS

MANUFACTURING RESULTS

Differences in specimen length width and core thickness have an effect on the calculations for compression and shear modulus. The critical dimensions of each specimen can be found in Table 3.

Table 3: Sandwich Panel Navtruss Core Specimen Information

Specimen tag	C: Core Thickness (in)	t1: Top Facing Thickness (in)	T2: Bottom Facing Thickness (in)	b: Base (in)	W: Width (in)	Total Ply Sequence
CM1	0.2753	0.1072	0.1145	4.8724	4.8483	$[[0/90/0/90/0]_s/core/[0/90/0/90/0]_s]$
CM2	0.3433	0.0539	0.0528	5.37	4.9160	[0/90/0/90/0/core/0/90/0/90/0]
CM3	0.3151	0.0541	0.0526	5.119	5.1302	[90/0/90/0/90/core/90/0/90/0/90]
CM4	0.3525	0.0561	0.0558	5.2273	5.1611	[0/90/0/90/0/core/0/90/0/90/0]
CM5	0.3483	0.0525	0.0542	5.1362	5.2104	[90/0/90/0/90/core/0/90/0/90/0]
3D1	0.3929	0.0572	0.0469	4.9190	5.5824	[0/90/core/90/0]
3D2	0.3669	0.0667	0.0533	4.9391	5.5892	[0/90/core/90/0]
3D3	0.3910	0.0655	0.0496	4.9241	5.5622	[0/90/core/90/0]
3D4	0.3958	0.0731	0.0605	4.8321	5.5849	[0/90/0/core/0/90/0]
3D5	0.3798	0.0762	0.0640	4.8866	5.8540	[0/90/0/core/0/90/0]

The designed core thickness is 0.433 inches (11 mm) for all specimens. Compression molded specimens had the largest thickness variation with an average core thickness of 0.33 inches (8.31 mm). The 3D printed specimens had an average core thickness of 0.39 inches (9.78 mm). Both sets of specimens had a decrease in core thickness when manufactured. The compression molded specimens had the same nominal facing thickness of 0.05 inches (1.27 mm). The 3D printed specimens had a bottom 2 laminae thickness of nominally 0.05 inches (1.27 mm) and a nominal top 2 laminae thickness of 0.06 inches

(1.52 mm). The bottom 3D printed 3 lamina face sheets had a nominal thickness of 0.062 inches (1.58 mm). The top 3D printed 3 lamina face sheets had a nominal thickness of 0.075 inches (1.90 mm).

MANUFACTURING DISCUSSION

When the compression specimens were manufactured the core was bonded to the facings by heat fusion bonding. Heating up the facings and pressing the core into the hot facings would bond the thermoplastic matrix from the facing to the core. By using a force to press the core into the facing the core deforms under the soft facing and a smaller core thickness is observed because the facing intrudes within the upper and lower limits of the Navtruss core struts. Figure 66 is an illustration of the error observed in the core thickness of the compression molded core specimens. The compression molded specimens are better represented by a buried node truss core sandwich panel.

The thickness of the compression molded facings increased after fusing the core to them. When the temperature of the matrix increased melt temperature of the PET the matrix flowed around the fibers and in sections without pressure the consolidation of the facings decreased, resulting in an increase in thickness, as shown in Figure 66.

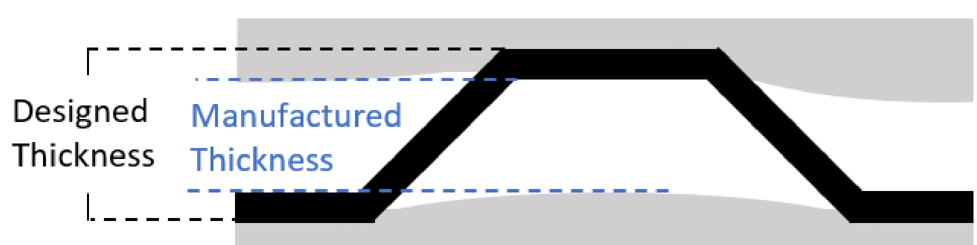

Figure 66: Compression Molded Core Thickness Manufacturing Error

The 3D printed CFRTC sandwich panels had a higher geometric precision than the compression molded specimens, but the accuracy of the MAGIC system is still not producing as-designed parts. Differences in facing thickness are attributed differences in consolidation pressure when placing the top or bottom facings. Differences in core thickness are attributed to variance in consolidation pressure while manufacturing the entire sandwich panel. When designing the Navtruss core structure, it was assumed that the thickness of the CFRTC strand would be between 1 and 2 millimeters in all areas including in small areas were the CFRTC strands will be consolidated, i.e. where the core is fused to the bottom facing. This assumption was correct for the core and the top facing to core interface but not true for the bottom facing to core interfacial region. Another area where a decrease in core thickness would be noticed is the increase in thickness of the first lamina of the top face sheet.

NAVTRUSS CORE GEOMETRIC AND MATERIAL DIFFERENCES

Having a similar total volume of reinforcement in a single strut is equally as important as having similar geometries. Geometric factors have significant influence on the stiffness of a composite structure. As discussed in the "stiffness of a strand" section, the 3D printed CFRTC strands have variable cross-sectional areas. Variation in the cross-sectional area will change the mechanical response of the CFRTC strand. Variances in the 3D printed CFRTC Navtruss core are difficult to account for and a physical comparison between compression molded and 3D printed CFRTC Navtruss cores will not be very accurate. Instead, a difference in volumes can be used to compare the two methods.

MATERIAL DIFFERENCE RESULTS

To have a comparison between the two manufacturing methods the geometries of the two parts must be similar, and the materials the parts are made from must be the same. The mass of the sandwich panel can be calculated, based on the placement distance, and an estimate of the mass of the fiber in any individual section of the 3D printed specimens can be calculated. A summary of this section is presented in Table 5.

A 3D printed CFRTC strut has a placement length of 11.4 inches (289.7 mm), with a Tex of 2700 that works out to a total mass of 0.0279 oz (0.782 g) with a 70% glass fiber weight fraction making for a total of 0.0194 oz (0.550 g) of glass fiber reinforcement in a single strut manufactured with the MAGIC system.

For the compression molded specimens, the continuous fiber moved with the thermoplastic when pressed. The mass of the fiber in any given section was found by burning out the matrix and weighing the fiber for those sections. The density of the compression molded struts was found, and the volume of a single strut is known, so multiplying the density by the volume of a single strut allows the determination of the weight of glass fiber reinforcement within the strut. Given a total weight of 0.888 grams with a 60% weight fraction this translates to a total of 0.0188 oz (0.533 g) of glass fiber and 0.0125 oz (0.355 g) of semi-crystalline PET in a single compression molded strut.

The facesheets of the compression molded specimens have a nominal glass fiber weight fraction of 60%, found with constituent combustion following ASTM D3171 [53], and a density 1.081 oz/in^3 (1.87 g/cm^3), found with ASTM 792 [52]. A volume calculation results in a total volume for a facesheet of 1.375 in^3 (22.532 cm^3). A total weight of 1.486 oz (42.13 g) per facesheet, which is made up of 0.8917 oz (25.28 g) of fiber and 0.5944 oz (16.85 g) of plastic.

The weight of the 3D printed CFRTC facings can be calculated with placement length like before. Using a bandwidth of 0.114 inches (2.9 mm), the number of bands in the 0° direction is 44 bands (43.8 rounded up), and in the 90° direction is 48 (48.17 rounded down) the length in the 0° direction is 5.5 inches (139.7 mm) and the length in the 90° direction is 5 inches (127 mm). The total placement length for a 3-layer facesheet is 724 inches (18.39 m) for a total weight of 1.7513 oz (49.65 g), 1.2258 oz (34.75 g) of fiber and 0.5221 oz (14.8 g) of plastic. For a 2-layer facesheet the placement length is 481.89 inches (12.24 m) for a total weight of 1.1658 oz (33.05 g).

A summary of the above information can be found in Table 5 with the volumetric calculations. The cross section of a strut can be found by dividing the volume of the strut by the length of the strut.

Using equations 7 to find the volume of each constituent within each strut will show geometric differences.

Table 4: Stiffness of Constituents

Property	Semi-Crystalline PET	Amorphous PET	Glass Fiber
Elastic Modulus	455 ksi (3.14 GPa)	410 ksi (2.83 GPa)	10500 Ksi (72.4 GPa)
Flexural Modulus	355 ksi (2.45 GPa)	290 ksi (1.98 GPa)	4350 Ksi (30.0 GPa)
Density	0.797 oz/in^3 (1.38 g/cm^3)	0.734 oz/in^3 (1.27 g/cm^3)	1.474 oz/in^3 (2.55 g/cm^3)

Table 5: Material Differences Between Manufacturing Methods

Single Strut	3D Printed CFRTC Strut	Compression Molded Strut	% Difference
Total Mass (grams)	0.0275 oz (0.782 g)	0.0313 oz (0.888 g)	11.9%
Mass of Fiber (grams)	0.0194 oz (0.550 g)	0.0188 oz (0.533 g)	-3.2%
Mass of Matrix (grams)	0.0082 oz (0.232 g)	0.0125 oz (0.355 g)	34.6%
Volume Fiber	0.1312 in^3 (0.215 cm^3)	0.0128 in^3 (0.209 cm^3)	-3.2%
Volume Matrix	0.0112 in^3 (0.183 cm^3)	0.0157 in^3 (0.257 cm^3)	29.0%
Total Volume	0.0243 in^3 (0.398 cm^3)	0.0284 in^3 (0.466 cm^3)	14.6%
Facings	3D Printed CFRTC Strut (3 Laminae)	Compression Molded Strut	% Difference
Total Mass	1.751 oz (49.65 g)	1.486 oz (42.13 g)	-17.9%
Mass of Fiber	1.225 oz (34.75 g)	0.892 oz (25.28 g)	-37.5%
Mass of Matrix	0.522 oz (14.8 g)	0.594 oz (16.85 g)	12.2%

DISCUSSION1

A perfect comparison cannot be made between the two sample groups because the total volume of a single CFRTC strut is greater in the compression molded specimens, but an estimate of the composite quality that the MAGIC system can produce is still a viable outcome. Differences in shear stiffness are likely due to the difference in the amount of matrix material between the two specimens as well as the structure of the matrix material, because the matrix material carries most of the shear loads. Compression modulus should be comparable because the stiffness will be fiber dominated especially because the fibers are all unidirectional in an orientation advantageous for compression.

MODULUS EXPERIMENT

COMPRESSION MODULUS RESULTS

There are two mechanical properties that can be tested for, strength and stiffness. Strength is dictated by the type and population of defects, the surface finish, and other stress concentrations, when the part is made from the same material. Stiffness is based on geometry of the structure and the modulus of the material. By testing for stiffness instead of strength, composite quality can be observed. When testing for stiffness the parts manufactured can be loaded in the elastic region of the load displacement curve and do not need to be destroyed during testing. The 10 specimens manufactured were tested, for stiffness, in compression and then in shear. Shear testing required bonding the specimens to a thick stiff sheet making this the last test to be performed on the specimens.

The data was manipulated with a MATLAB according to ASTM D3619 [56] to produce the compression modulus, using equation 14 in Chapter 3 and restated below, for all the specimens tested. Each compression test had a settling region and a linear response region. The settling region is when the specimen and the two plates would begin loading and shifting of the plates would take place prior to generating a stable force across the complete surface of the test specimen. Every specimen displayed a linear region between 600 lbf (2.66 kN) and 900 lbf (4.00 kN). The slope of the line in the linear response region was found using the MATLAB function polyfit, a function that finds the best line of fit for a data set with the user selecting what order of polynomial should be used. A linear response is a first order polynomial so two different numbers were output with this function, in simple math terms the output is m, and b in the equation y = mx+b. A settling region correction was done with every data set based on the output of the polyfit function. The x intercept of the first order polynomial can be found by setting y equal to 0 then finding x, making the equation -b/m = x intercept. Then a plot is created with this toe correction to check for accuracy in this linear region, all load vs. displacement curves can be found in Appendix A.

$$\mathrm{E}_z = \frac{\Delta P * t}{\Delta u * L * b} \tag{14}$$

The average and the standard deviation of the apparent core flatwise compressive chord modulus was calculated for each 3D printed specimen and displayed in Table 6.

The compression molded specimen group has an average compression modulus of 2.33 ksi (16.06 MPa), and a standard deviation of 0.07 ksi. The 3D printed specimens have an average compression modulus of 1.81 ksi (12.48 MPa), and a standard deviation of 0.23 ksi (1.58 MPa). The highest compression modulus of the 3D printed specimens was specimen 3D4, with an average compression modulus of 2.08 ksi (14.34 MPa) and a standard deviation of 0.051 ksi (3.51 MPa). The lowest compression modulus for the 3D printed specimens was specimen 3D2, with a compression modulus of 1.48 ksi (10.20 MPa) and a standard deviation of 0.06 ksi (0.41 MPa).

The differences in the averages of the apparent core compression modulus between the compression molded core and the 3D printed core is 0.52 ksi (3.58 MPa), which is 22.4% lower than the compression molded specimens. The difference between the stiffest 3D printed specimen and the average apparent compression modulus is 10.94%. The stiffest 3D printed specimen exhibited an increase in compression modulus of 25% when compared to the least stiff 3D printed specimen.

Table 6: Compression Modulus by Manufacturing Method

	Compression Modulus	Standard Deviation
Compression Molded	2.33 ksi (16.06 MPa)	0.07 ksi (0.48 MPa)
All 3D Printed Specimens	1.79 ksi (12.34 MPa)	0.22 ksi (1.51 MPa)
3D1 Standard	1.76 ksi (12.13 MPa)	0.07 ksi (0.48 MPa)
3D2 New Core	1.48 ksi (10.20 MPa)	0.05 ksi (0.34 MPa)
3D3 System Cooling	1.74 ksi (12.00 MPa)	0.06 ksi (0.41 MPa)
3D4 Thicker Facings	2.02 ksi (13.93 MPa)	0.07 ksi (0.48 MPa)
3D5 Hotter Placement	1.99 ksi (13.72 MPa)	0.06 ksi (0.41 MPa)

SANDWICH SHEAR MODULUS RESULTS

For the sandwich shear tests the specimens needed to be bonded to aluminum loading plates to increase the bending resistance of the facings. Specimens CM1 and CM2 had loading plates with a thickness of 3/32 inches (2.38 mm) instead of the 1/8 inches (3.175 mm) thickness plates used in all other specimens. This difference in plate thickness has an effect on the measured shear properties of the sandwich panel and it is for this reason that CM1 and CM2 were excluded from average and standard deviation calculations used during this section. These plates are not thick enough to determine the absolute shear modulus of the specimens and small differences in loading plate stiffness can have an impact on the measured shear modulus. Specimen configuration would have a significant impact on the shear stiffness. Thus, only a single specimen configuration was included to be able to directly compare the stiffness of the specimens.

A MATLAB script was written to take the raw data from testing and calculate the apparent shear modulus using equation 15 in chapter 5, restated below for convenience. Each specimen was tested 5 times and the average of the 5 tests is the reported shear modulus for that specimen. The settling region was removed to offset the displacement for calculating the shear modulus. The linear response region occurred between 300lbf (1.33 kN) and 600 lbf (2.66 kN) for every specimen. A linear regression was done on the linear region to find the slope and use it in equation 15 to find the apparent shear modulus.

The results of the shear modulus testing can be found in Table 7. The 3 compression molded specimens that can be compared have an average apparent shear modulus of 1.66 ksi (11.44 MPa) with a standard deviation of 0.05 ksi (0.34 MPa). The 3D printed specimens have an average apparent shear modulus of 0.97 ksi (6.69 MPa) with a standard deviation of 0.18 ksi (1.24 MPa). Within the 3D printed specimen group the highest apparent shear modulus is specimen 3D5, the specimen with increased placement temperature, with a modulus of 1.26 ksi (8.69 MPa) and a standard deviation of 0.06 ksi (0.41 MPa), a 24% increase from the specimen that exhibited the lowest apparent shear modulus. The lowest apparent shear modulus is specimen 3D2, the specimen with the back and forth core, with a modulus of 0.79 ksi (5.45 MPa) and a standard deviation of 0.05 ksi (0.35 MPa). The 3D printed average apparent shear modulus is 41.3% lower than the compression molded specimens shear modulus. The 3D printed specimens with the highest apparent modulus has a modulus that is 23.8% lower than the average of the apparent shear modulus of the compression molded specimens.

$$G = \frac{\Delta P * t}{\Delta u * L * b} \tag{15}$$

Table 7: Shear Modulus Testing Results

	Shear Modulus	Standard Deviation
Compression Molded	1.66 ksi (11.44 MPa)	0.06 ksi (0.41 MPa)
3D Printed	0.97 ksi (6.69 MPa)	0.18 ksi (1.24 MPa)
3D1 Standard	0.96 ksi (6.62 MPa)	0.03 ksi (0.20 MPa)
3D2 New Core	0.79 ksi (5.45 MPa)	0.05 ksi (0.34 MPa)
3D3 System Cooling	0.88 ksi (6.07 MPa)	0.08 ksi (0.55 MPa)
3D4 Thicker Facings	0.98 ksi (6.76 MPa)	0.07 ksi (0.48 MPa)
3D5 Hotter Placement	1.26 ksi (8.69 MPa)	0.06 ksi (0.41 MPa)

DISCUSSION OF THE MODULUS EXPERIMENT

Compression

The core compression modulus and core shear modulus show how stiff the manufactured core is in response to either a compressive or shear load respectively. In compression the compression molded specimens, CM1-5, were statistically the same with an average compression modulus of 2.331 ksi (16.07 MPa). The 3D printed specimens, 3D1-5, were less stiff with an average compression modulus of 1.810 ksi (12.48 Mpa). There are statistically significant differences between the average compression modulus of the compression molded specimens and that of the specimens manufactured with the MAGIC system. There were no statistically significant differences between the compression moduli of the individual compression molded specimens; however, there were statistically significant differences between the compression moduli of the 3D printed specimens.

Compression testing deviated from ASTM C365 Flatwise Compressive Properties of Sandwich Cores because of an error when measuring the displacement between the two facings. The tops and bottoms of the sandwich panel specimens were not aligned due to manufacturing errors and would cause the compression plates to rotate until the specimen was settled, which led to displacement measurement errors. Using crosshead displacement eliminated the errors due to specimen and plate rotations and improved the repeatability of the measured specimen loading response.

Shear

In shear testing specimens CM1 and CM2 are a part of a different sub group because the loading plates are thinner than the loading plates bonded to the other specimens. The specimen response to a shear load can be modeled as three springs in series, two of the springs are the loading plates and the third is the core of the sandwich panel. The equation for springs in series is:

$$\frac{1}{K_e} = \frac{1}{K_{p1}} + \frac{1}{K_c} + \frac{1}{K_{p2}} \tag{16}$$

Where K_{pi} is the representative spring constant of the loading plate 1 or 2. and K_c is the modulus of the core. Equation 16 shows that as K_p goes to infinity the equivalent spring constant will be equal to K_c. In this case the loading plates are not infinitely stiff compared to the core and contribute to the equivalent modulus K_e. The thickness of the plates of all specimens is small enough to contribute to the apparent modulus and an absolute modulus for the core cannot be found. An apparent modulus was found and is used when referring to the shear modulus of all specimens. K_p is the same for every panel except for CM1 and CM2 meaning that a comparison can be made between specimens CM3-5 and 3D1-5 for the apparent shear modulus.

There were also a few deviations from ASTM C273 Sandwich Core Shear Modulus and Strength. The first was a roller being used to align the specimen with the upper and lower fittings. Using the roller stopped variations from occurring, based on the orientation of the loading plates, and produced more consistent loading curves. The second deviation was the lack of an extensometer during testing. ASTM C273 requires the use of a device to measure the movement between the two loading plates as testing occurs, but after testing different ways to measure how far the plates move relative to one another it was discovered that an accurate measurement could not be taken for these specimens due to smaller loading plates than required. Cross head displacement was used instead of a measured value, and although this displacement is not the same as the movement between the plates and an absolute modulus cannot be found, a relative modulus could be found if the same procedure is followed for all specimens. The equations used in ASTM C273 were still used but it was known that the relative modulus would be less than absolute because of the displacement measurement error.

Load Response of Core

It is believed that the reason the 3D printed specimens are less stiff is poor wet out within the CFRTC strands that make up the core. When placing CFRTC strands on a substrate the placement head can apply a consolidation pressure removing voids and wetting out the fibers in the process. However, the core is being placed in free space so there is no consolidation force to aid fiber wet out and void reduction can only occur within the nozzle. Work done by Eichenhofer et al. [23] was done to quantify how the nozzle outlet geometry effects the consolidation within the nozzle. Eichenhofer concluded that the void content in a CFRTC strand increased if the nozzles outlet was 15% larger than the total cross section of the CFRTC strand. The MAGIC system uses a nozzle that has an outlet diameter of 0.059 inches (1.5 mm), an estimated diameter of the CFRTC strand was determined to be 0.055 inches (1.4 mm). The nozzle has an outlet that is 7% larger than the CFRTC strand at room temperature. Based on the work done by Eichenhofer, consolidation within the nozzle is at a maximum based on the geometry of the nozzle but temperature and feed rate could affect the consolidation within the nozzle and neither were considered by Eichenhofer and his team.

Void content within a CFRTC strand could contribute to a decrease in stiffness. The void content of specimens CM1-5 is less than 5% within the core while the void content within the core of specimens 3D1-3D5 is nominally 25% based on the single layer facing composite quality tests. A higher void content could indicate that not all of the fibers within the core were fully wet out and would support the theory that the drop-in stiffness is due to a lack of fiber wet out within the core.

The MAGIC system uses a commingled roving with a predetermined fiber weight fraction shifting the major contributing variable that controls stiffness from fiber volume fraction to fiber wet out, and any change in the fiber wet out will change the CFRTC strand stiffness of the composite. When placing fiber in unsupported space the thermoplastic must fully wet out the fibers within the nozzle. The strand stiffness experiment in this work showed that increased control temperatures result in stiffer CFRTC strands.

Individual Specimen Response

The control temperature was set to 554 °F (290 °C) for specimens 3D1-3D4 and increased to 590 °F (310 °C) for specimen 3D5 because of a hardware change. Looking at the apparent compressive and shear modulus data the connection between placement temperature and composite stiffness is clear. Specimen 3D1 had cooling on the entire time the core was placed, but not when the facings were being placed. 3D2 had cooling on during the placement of the entire panel. Leading to the idea that the facings of 3D1 had an increased stiffness, but the core quality is the same for specimens 3D1 and 3D2. Thus, the difference in stiffness within the facings of these two specimens is significant for both compression and shear modulus and explains some of the difference in compression and shear moduli.

Another difference between specimen 3D1 and 3D2 is the core geometry. When the composite placement head moves upward the composite strand forms in to a rod-like shape, but when moving downward the composite strand spreads around the nozzle forming a spread out curved shape. When placing composite strands in a single direction the rod like strands will be on one side of the Navtruss strut while the spread out composite strands will be on the other, as shown in Figure 67 (a). When placing the core back and forth both the rod like composite strands and the spread out composite strands will be placed next to one another as shown in Figure 67 (b). The change in core geometry could lead to a decrease in both core compressive modulus and core shear modulus. The remaining specimens manufactured with the MAGIC system use the same core geometry as specimen 3D2.

The manufacturing difference between specimen 3D2 and 3D3 was software-controlled cooling. By selectively cooling the placed tow the nozzle outlet temperature would be hotter during the manufacturing of the core because the coolant would not be on the entire time. The facings and the CFRTC strands would be wet out more in the core of specimens 3D3-3D5 than in specimens 3D1-3D2, increasing the compression and shear modulus of specimen 3D3. Specimens 3D3 and 3D4 have statistically the same core shear moduli but different compression moduli. Specimens 3D4 and 3D5 have statistically the same compression modulus but different shear moduli. The differences between specimens could be either due to variation in fiber wet out or in geometry. The geometry of the cores is relatively the same, suggesting that differences measured would be related to variations in fiber wet out in selective sections of the core.

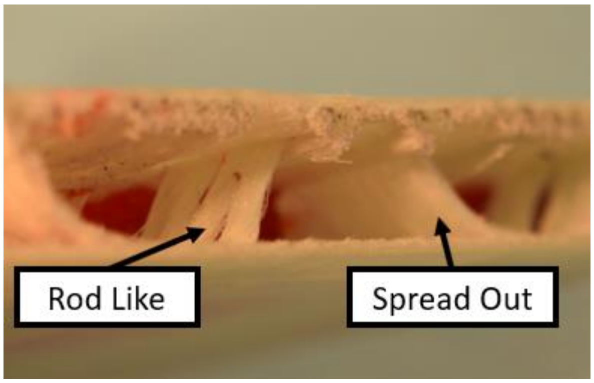

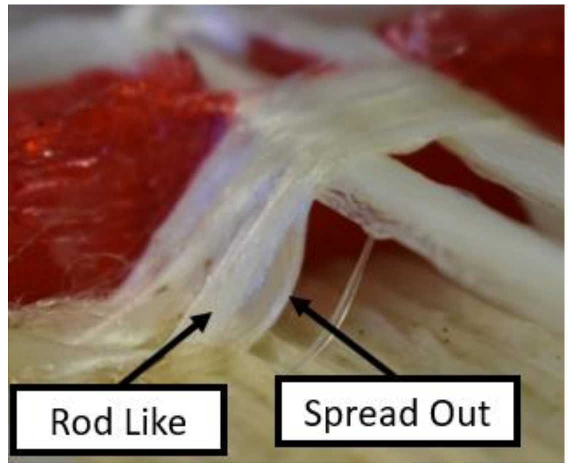

(a) Unidirectionally Placed Core (b) Core with 180° Turning

Figure 67: Differences between 3D1 core and 3D2-5 Core

LOADING CONDITIONS

Understanding the loading conditions and the stresses within the core can help explain measured differences in the stiffness of the core, based on where poor wet out conditions could be, and why these conditions would affect core stiffness. A free body diagram of a single Navtruss strut, loaded in compression, is shown in Figure 68.

There are four different sections of the core that need to be looked at to see how the stiffness of the core would respond if there was not enough load transfer between the matrix and the reinforcement.

In compression the four sections are the two joints, sections 1 and 4, the shear area, section 2, and the arm of the strut, section 3. When loading initially occurs if section 1 is not fully wet out then the facings will deform until the arm is being fully loaded, bypassing the section entirely. This will have a minimal impact on the core compression modulus after the specimen settles. Poor wet out in region 1 occurs because there is no surface to consolidate the tow against and as the placement head makes an angle change in space the fibers want to follow this movement, creating voids in the joint section. This effect is reduced with cooling. Section 4 can have poor wet out because the geometry of the CFRTC strand shifts rapidly from a rectangular cross section to a semi-circular cross section, or vice versa and when changing geometry, the fibers in the CFRTC strand spread in these sections increasing the local void content.

When section 2 has a decrease in fiber wet out the stiffness of the core does not change as long as the matrix bond between the core and the facing is enough to withstand the loads being applied. The fibers in section 2 are not as important to the functioning of the core because the matrix withstands the majority of the shear loading in this section. The facings must be thick enough to not buckle under loading. For the 3D printed specimens with 2 laminae the facings were not thick enough to withstand these loads and therefore the increase in compression modulus is likely due to an increase in composite facing quality when the 3D printed specimens were manufactured with 3 laminae facings.

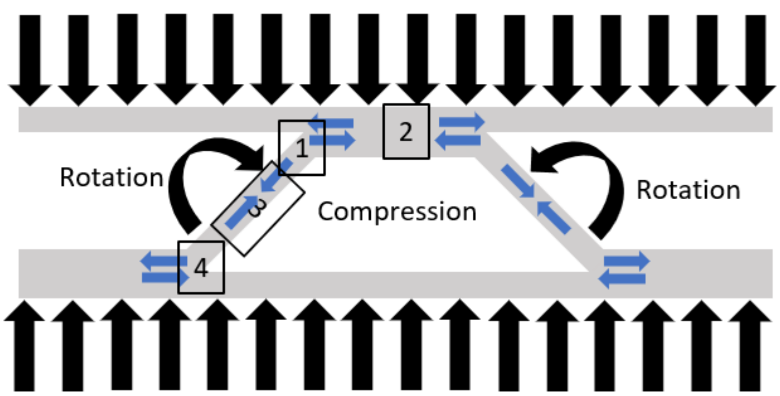

Figure 68: Freebody Diagrams of Compression Loading Mode

Section 3, when loaded in compression, supplies the majority of the core stiffness and any decrease in fiber wet out here will result in a large change in the core modulus because this section is responsible for withstanding the entirety of the compressive load. If the there is an increase in fiber wet out in section 3 then the core compression modulus will increase. Only increases in the composite quality in section 3 are expected to have a significant impact on the composite core compression modulus. This is consistent with the results for specimens 3D4 and 3D5, which have similar compressive moduli but different shear moduli.

SHEAR RESPONSE

The free body diagram for loading the core in mode 1 shear is shown in Figure 69. There is a second shear loading mode, mode 2, where the load is perpendicular to the strut. Mode 2 places the entire strut in shear. When the strut is loaded in mode 1 there are sections of the core in compression and sections in tension. This variation will lead to sections which will have a different effect on the core shear modulus based on their local composite quality.

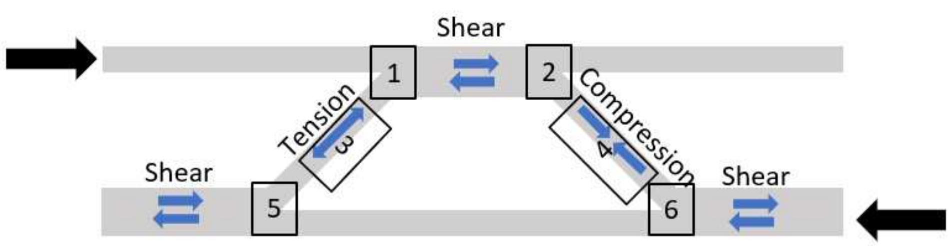

Figure 69: Shear Loading Mode 1 Free Body Diagram

The quality of sections 1 and 5 will have the same effect on the core shear modulus but different response in loading mode 1 and loading mode 2. In loading mode 1, if section 1 and 5 have a decrease in their stiffness then the arm in tension will not be able to load unless there are large deformations, and this will decrease the resultant core stiffness with low deformations but not have a large impact on stiffness with larger deformations. When the core is loaded in mode 2, sections 1 and 5 have a more important role in determining the core shear stiffness because these areas transfer shear to the arm of the strut and need to be stiff enough to do so. However, this stiffness does not rely heavily on the fiber content, but more on the matrix material and shear transfer between CFRTC strands.

Sections 2 and 6 have the same effect on the core stiffness as section 1 and 5 in loading mode 2 but differ in loading mode 1. When loaded in shear mode 1, sections 2 and 6 have an impact on the core stiffness because these areas will transfer the shear stress into the arm of the strut that is in compression and if the reinforcement fibers are not wet out the stiffness of the core will decrease with small displacements. With large displacements sections 2 and 6 are less important to the stiffness of the system, but the loading for shear is more based on small displacements because some of the core is loaded in mode 2.

Section 3 is in tension when loading in mode 1 and in shear when loaded in mode 2. When the strut is loaded in mode 2 the shear stress within the strut is resisted by the matrix material and by the area of the strut because the strut is in an optimal orientation to resist the shear and bending. Fiber wet out is less important and, as long as there is shear transfer between CFRTC strands, an increase in the core shear modulus will occur. When section 3 is in tension the fiber can still be loaded, as long as the majority of the area in section 3 is well wet out, even if individual areas are poorly wet out, resulting in little effect on the core shear modulus.

Section 4 will react the same as section 3 in shear loading mode 2 but differently in loading mode 1. In compression, if the reinforcement fibers are not wet out, the load they can withstand without buckling is very minimal. This suggests that section 4 is one of the most important sections that will contribute to the core shear stiffness. Specimen 3D5 had an increase in shear stiffness because every section of the core was better wet out.

A summary of the information discussed in the loading conditions section of this text can be found in Table 8. Each change in the manufacturing system influenced the compression and shear modulus of the 3D printed specimens. Using all the changes to manufacture a panel produced a panel that was 25% stiffer in compression and 24% stiffer in shear when compared to the 3D printed specimen that exhibited the lowest stiffness.

Table 8: Impact that Changes Had on Sandwich Structure Quality

3D Printed Specimens Change In Manufacturing Variables	Compression Modulus	Shear Modulus
Back and Forth Core Geometry	Decrease	Decrease
Selective Cooling	Increase	Increase
Increasing Facing Thickness	Increase	Increase
Increasing Placement Temperature	Increase	Increase

CHAPTER 7 – CONCLUSIONS

The MAGIC system was developed to investigate the potential to reduce the tooling requirements of complex continuous fiber reinforced composite (CFRTC) components. The 3D printing platform, combined with a CFRTC placement system, was used to produce sandwich panels with structural edge closures designed to aid in the manufacture of truss core sandwich panels and eliminate the need for tooling. Removal of the edge closures was only done to test the sandwich panels and is not needed in final parts. Additionally, hard points could be manufactured into the part with the thermoplastic placement system and could be reinforced with the composite placement system within the designed structure, without any extra manufacturing steps.

Based on the results of tests done in this work the following conclusions can be drawn:

- Placement of CFRTC is possible in unsupported space, but a structure is needed to facilitate any change in direction as the CFRTC strands are placed.
- CFRTC laminates placed without full support of a baseplate increase in quality as the laminate is built up.
- Laminates manufactured without support show a decrease in lap shear strength.
- Increasing the temperature of the placement process significantly improves the CFRTC strand stiffness
- Improvements to the MAGIC system have increased composite quality by 25%, but more work needs to be done to generate CFRTC performance that matches other manufacturing methods

Understanding how the CFRTC strand tacks to the substrate gives valuable information as to what factors need to be controlled to increase the resolution of the manufacturing process and the geometry of placed CFRTC strands. Implementation of system-controlled cooling allowed for the continuous placement of CFRTC, cutting manufacturing times in half. System-controlled cooling increased the composite quality of composites placed in unsupported space by allowing the majority of the CFRTC to be placed at higher temperatures. Void content and lap shear testing of laminates manufactured in unsupported space compared to on a substrate indicate that manufacturing in unsupported space produces composites that have lower stiffness and strength. However, as the layers are built up in space the composite quality does increase due to the increasing stiffness of the successive layers which then resists deformation and improves consolidation. Further hardware development could increase composite quality of the initial CFRTC lamina placed in unsupported space. With more research and more advanced systems in place that utilize the information gained from this work, completely wet out and consolidated composite structures manufactured in unsupported space with the MAGIC system may be realized. Controlling the consolidation pressure with a force-based feedback loop could make the composite quality more consistent when placing composite laminae. Consolidation when placing unsupported composites occurs within the placement nozzle, by changing the placement system consolidation of the composite could occur without supporting structures.

As the MAGIC system evolved specimens were manufactured to investigate how the system was producing different quality parts as each major implementation was added. The best 3D printed truss core sandwich panel had an apparent compression modulus that was only 14.6% lower than the average apparent compressive modulus of the compression molded specimens, which were manufactured as a baseline for comparison. The apparent shear stiffness of the best preforming printed panel was 23% lower than the average apparent shear stiffness of the compression molded specimens. As the MAGIC system improved the composite stiffness increased by 25% in compression and 24% in shear, and it is expected that further improvements to the MAGIC system will show even greater improvements in the stiffness of the resulting composite truss core sandwich panels.

More work needs to be done to further automate the manufacturing processes with the MAGIC system. Doing more tests to quantify consolidation force and how variations in the consolidation force affect the CFRTC when placed on both the substrate and in unsupported free space are important future trials. Development of hardware to consolidate and wet out CFRTC strands during placement will be critical in producing quality composite structures. It was discovered in this work that precise control of the CFRTC temperature, as it is being placed, dramatically effects the composite quality and every step should be considered when designing a system to increase the control temperature and quickly cool the CFRTC strand. With the advent of the technology to place continuous fiber reinforced thermoplastic composite structures without the need for tooling the trajectory of the composites industry could be forever changed by making complex composites structures significantly more cost effective to manufacture.

WORKS CITED

[1] "Special Chem," Glass Transition Temperature, 2019. [Online]. Available: https://omnexus.specialchem.com/polymer-properties/properties/glass-transition-temperature. [Accessed 3 June 2019].

[2] tecnologia de los plasticos, [Online]. Available: https://tecnologiadelosplasticos.blogspot.com/2011/11/moldeo-manual-de-materiales-compuestos.html. [Accessed 30 5 2019].

[3] D. Cohen, "Infuence of filament winding parameters on composite vessel quality and strength," *Composites Part A,* vol. 28A, pp. 1034-1047, 1997.

[4] "Fibermaq consolidates filament winding portfolio," JEC Group, 23 March 2018. [Online]. Available: http://www.jeccomposites.com/knowledge/international-composites-news/fibermaq-consolidates-filament-winding-portfolio. [Accessed 30 May 2019].

[5] A. H. Miller, N. Dodds, J. M. Hale and A. G. Gibson, "High speed pultrusion of thermoplastic matrix composites," *Composites Part A,* vol. 29A, pp. 773-782, 1998.

[6] M. Valliappan, J. A. Roux and J. G. Vaughan, "Die and post-die temperature and cure in graphite/e[oxy compoiste," *Composites: Part B,* vol. 27B, no. Number 1, 1996.

[7] "Pultrusion Online," MPI, [Online]. Available: http://pultrusiononline.com/tooling. [Accessed 30 5 2019].

[8] Z. Qureshi, T. Swait, R. Scaife and H. El-Dessouky, "In situ consolidation of thermoplastic prepreg tape using automated tape placement technology: potential and possibilities," *Composites: Part B,* vol. 66, pp. 255-267, 2014.

[9] Z. August, G. Ostrander, J. Michasiow and D. Hauber, "Recent Developments in Automated Fiber Placement of Thermoplastic Composites," *SAMPE J,* vol. 50, no. 2, pp. 30-37, 2013.

[10] D. W. Radford and K. M. Hedin, "Fused Deposition Technology Applied to Thermoplastic Matrix Placement and Wetout in Filament Winding," in *20th International Conference on Composite Materials*, Copenhagen, 2015.

[11] R. Pitchumani, J. W. Gillespie and M. A. Lamontia, "Design and Optimization of a Theroplastic Tow-Placement Process with in-situ Consolidation," *Composite Materials,* vol. 31, no. 3, pp. 244-274, 1997.

[12] K. Potter, B. C. Kim and P. Weaver, "Continuous tow shearing for manufacturing variable angle tow composites," *Composites: Part A,* vol. 43, pp. 1347-1356, 2012.

[13] ElectroImpact, [Online]. Available: https://www.electroimpact.com/Products/Composites/Overview.aspx. [Accessed 30 5 2019].

[14] H. Prüβ and T. Vietor, "Design for Fiber-Reinforced Additive Manufacturing," *Journal of Mechanical Design,* vol. 137, 2015.

[15] C. Koch, L. Van Hullen and N. Rudolph, "Investigation of mechanical anisotropy of the fused filament fabrication process via customized tool path generation," *Additive Manufacturing,* vol. 16, pp. 137-145, 2017.

[16] H. Tekinalp, V. Kunc, G. Velez-Garcia, C. Duty, L. Love, A. Naskar, C. Blue and S. Ozcan, "Highly Oriented Carbon Fiber-polymer Composites via Additive Manufacturing," *Composite Science and Technology,* vol. 105, pp. 144-150, 2014.

[17] E. Bohez, "Compensating for systematic errors in 5-axis NC machining," *Computer-Aided Design,* vol. 34, pp. 391-403, 2002.

[18] S. Li, Jerard and Robert, "5-axis machining of sculptured surfaces with a flat-end cutter," *Computer-Adided Design,* vol. 26, no. 3, pp. 165-178, 1994.

[19] A. N. Dickson, J. N. Barry, K. A. McDonnell and D. P. Dowling, "Fabrication of continuous carbon, glass, kevlar fibre reinforced polymer composite using additive manufacturing," *Additive Manufacturing,* vol. 16, pp. 146-152, 2017.

[20] J. Justo, L. Tavara, L. Garcia-Guzman and F. Paris, "Characterization of 3D printed long fibre reinforced composites," *Composite Structures,* vol. 185, pp. 537-548, 2018.

[21] M. Invernizzi, G. Natale, M. Levi and S. Turri, "UV-Assisted 3D Printing of Glass and Carbon Fiber-Reinforced Dual-Cure Polymer Composites," *Materials,* vol. 9, no. 583, 2016.

[22] "Six months with Atropos," Atropos, 27 February 2017. [Online]. Available: http://piulab.it/projects/six-months-with-atropos. [Accessed 31 May 2019].

[23] M. Eichenhofer, J. Wong and P. Ermanni, "Continuous Lattice Fabrication of Ultra-Lightweight Composite Structures," *Additive Manufacturing,* vol. 18, pp. 48-57, 2017.

[24] P. Bettini, G. Alitta, G. Sala and L. D. Landro, "Fused Deposition Technique for Continuous Fiber Reinforced Thermoplastic," *Material Engineering and Performance,* vol. 26, no. 2, pp. 843-848, 2017.

[25] A. Kvalsvig, X. Yuan, J. Potgieter and P. Cao, "3D Printing of Fibre Reinforced Honeycomb Structured Composite Materials," Massy University, 2017.

[26] F. Van Der Klift, Y. Koga and A. Todoroki, "3D Printing of Continuous Carbon Fiber Thermo-Plastic Tensile Test Specimens," *Scientific Research Publishing,* vol. 6, pp. 18-27, 2016.

[27] K. Sugiyama, R. Matsuzaki and M. Ueda, "3D Printing of Composite Sandwich Structures Using Continous Fiber and Fiber Tension," *Composites Part A,* vol. 113, pp. 114-121, 2018.

[28] K. M. Warlick, "The Effect of Tow Shearing on Reinforcement Positional Fidelity in the Manufacturing of a Continuous Fiber Reinforced Thermoplastic Matrix Composite Via Pultrusion-like Processing of Commingled Feedstock," Colorado State University, Fort Collins, 2017.

[29] T. Vaneker, "Material Extrusion of Continuous Fiber Reinforced Plastic Using Commingled Yarn," *Procedia CIRP,* vol. 66, pp. 317-322, 2017.

[30] S. Liu, Y. Li and N. Li, "A novel Free-hanging 3D printing method for continuous carbon fiber reinforced thermoplastic lattice truss core structures," *Materials and Design,* vol. 137, pp. 235-244, 2018.

[31] P. Rodriguez and R. Donald, "Effect of Applied Consolidation Pressure in Direct Diigital Manufacture of Continuous Fiber Reinforced Composites," in *CAMX 2018*, Orlando, 2018.

[32] R. Evertz, "Investigation of core closeouts in fiber-reinforced sandwich laminates," Montana State University, Montana, 2000.

[33] *Hexweb Honeycomb Sandwich Design Technology,* 2000.

[34] N. Gupta, "Characterization of Flexural Properties of Syntactic Foam Core Sandwich Composites and Effect of Density Variation," *Composite Materials,* vol. 39, no. 24, pp. 2197-2212, 2005.

[35] Y. Hu, W. Li, X. An and H. Fan, "Fabrication and mechnaincal behaviors of corrugated lattice truss composite sandwich panels," *Composites Science and Technology,* vol. 125, pp. 114-122, 2016.

[36] T.-S. Lok and C. Qian-Hua, "Elastic Stiffness Properties and Behavior of Truss-Core Sandwich Panel," *Stuctural Engineering,* vol. 126, no. 5, pp. 552-559, 2000.

[37] J. Mei, J. Liu and J. Liu, "A novel fabrication method and mechanical behavior of all-composite tetrahedral truss core sandwich panel," *Composites: Part A,* vol. 102, pp. 28-39, 2017.

[38] l. Ma, H.-Y. Zheng and L.-Z. Wu, "Mechanical Properties and impulsive Response of 3D-Kagome truss core sandwich panel," in *16th International Conference of composite materials*, 2007.

[39] J. Xiong, L. Ma, S. Pan, L. Wu, J. Papadopoulos and A. Vaziri, "Shear and Bending Performance of Carbon Fiber Composite Sandwich Panels with Pyramidal Truss Core," *Acta Materialia,* vol. 60, pp. 1455-1466, 2012.

[40] T. George, V. Deshpande and H. Wadley, "Mechanical Resone of Carbon Fiber Composite Sandwich Panels with Pyramidal Truss Core," *Composites : Part A,* vol. 47, pp. 31-40, 2013.

[41] N. G. Haydn and N. G. Wadley, "Multifunctional Periodic Cellular Metals," *Philosophical Transaction of The Royal Society A,* vol. 364, pp. 31-68, 2006.

[42] L. Xiaodong, W. Linzhi, M. Li and Y. Xiangqiao, "Fabrication and mechnaical properties of composite pyramidal truss core sandwich panels with novel reinforced frames," *Reinforced Plastics & Composites,* vol. 35, no. 16, pp. 1260-1274, 2016.

[43] M. Li, L. Wu, L. Ma, B. Wang and Z. Guan, "Mechanical Response of All-composite Lattice Truss Core Sandwich Structures," *Material Science and Technology,* vol. 27, no. 6, pp. 570-576, 2011.

[44] X. Li, L. Wu, L. Ma and X. Yan, "Fabrication and mechanical properties of composite pyramidal truss core sandwich panels with nopvel reinforced frames," *Reinforced Plastics & Composites,* vol. 35, no. 16, pp. 1260-1274, 2016.

[45] J. Xiong, A. Vaziri, J. Papadopoulos and L. Wu, "Compression and Impact testing of two-layer composite pyramidal-core sandwich panels," *Composite Structures,* vol. 94, pp. 793-801, 2012.

[46] N. Wicks and J. Hutchinson, "Performance of Sandwich Plates with Truss Cores," *Mechanics of Materials,* vol. 36, pp. 739-751, 2004.

[47] "Glycol-Modified Polyethylene Terephthalate," 20 September 2018. [Online]. Available: https://www.makeitfrom.com/material-properties/Glycol-Modified-Polyethylene-Terephthalate-PETG-PET-G. [Accessed 1 June 2019].

[48] ASoM, "AZO Materials E-Glass Fiber," 30 August 2001. [Online]. Available: https://www.azom.com/article.aspx?ArticleID=764. [Accessed 1 June 2019].

[49] H. EL-Dessouky, C. Lawrence, T. McGrail and B. Broughton, "Ultra-Light Weight Thermoplastic Composites: Tow-Spreading Technology," in *European Conference on composite materials*, Venice, 2012.

[50] H. El-Dessouky and C. Lawrence, "Ultra-lightweight carbon fiber/thermoplstic composite material using spread tow technology," *Composites: Part B,* vol. 50, pp. 91-97, 2013.

[51] U. Harukazu, "JEC Composites," May 2005. [Online]. Available: http://www.jeccomposites.com/print/knowledge/international-composites-news/innovative-technology-carbon-and-aramid. [Accessed 1 June 2019].

[52] *D792 Standard Test Methods for Density and Specific Gravity (Relative Density) of Plastics by Displacement,* 2017.

[53] *D3171 Standard Test Methods for Constituent Content of Composite Materials,* 2017.

[54] *D5868 Lap Shear Adhesion for Fiber Reinford Plastic Bonding,* 2014.

[55] P. Hagstrand, F. Bonjour and J. A. E. Manson, "The influence of void content of the structural flexural performance of unidirectional glass fibre reinforced polypropylene composites," *Composites Part A: Applied science and manufacturing,* vol. 36, pp. 705-714, 2005.

[56] *C365 Standard Test Method for Flatwise Compressive Properties of Sandwich Cores,* 2019.

[57] *C273 Standard Test Method for Shear Properties of Sandwich Core Materials,* 2018.

[58] Y.-S. Lee, "Non-isoparametric tool path planning by machining strip evaluation for 5-axis scupltured surface machining," *Computer-Aided Design,* vol. 30, no. 7, pp. 559-570, 1998.

[59] L. Ye, K. Friedrich, J. Kastel and Y.-W. Mai, "Consolidation of Unidirectional CF/PEEK Composites from Commingled Yarn Prepreg," *Composites Science and Technology,* vol. 54, pp. 349-358, 1995.

[60] T. Stankovic, J. Mueller and K. Shea, "The Effect on Anisotropy on the Optimization of Additively Manufactured Lattice Structures," *Additive Manufacturing,* vol. 17, pp. 67-76, 2017.

[61] J. Xiong, L. Ma, L. Wu, J. Liu and A. Vaziri, "Mechanical Behavior and Failure of Composite Pyramidal Truss Core Sandwich Columns," *Composites: Part B,* vol. 42, pp. 938-945, 2011.

[62] J. Xiong, L. Ma, A. Vaziri, J. Yang and L. Wu, "Mechanical Behavior of Carbon Fiber Composite Lattice Core Sandwich Panels Fabricated by Laster Cutting," *Acta Materialia,* vol. 60, pp. 5322-5334, 2012.

[63] "Overview of materials for PETG Coplolyester," Matweb. [Online]. [Accessed 2 June 2019].

APPENDIX A

COMPRESSION MODULUS FORCE VS DISPLACEMENT CURVES

COMPRESSION MOLDED SPECIMENS

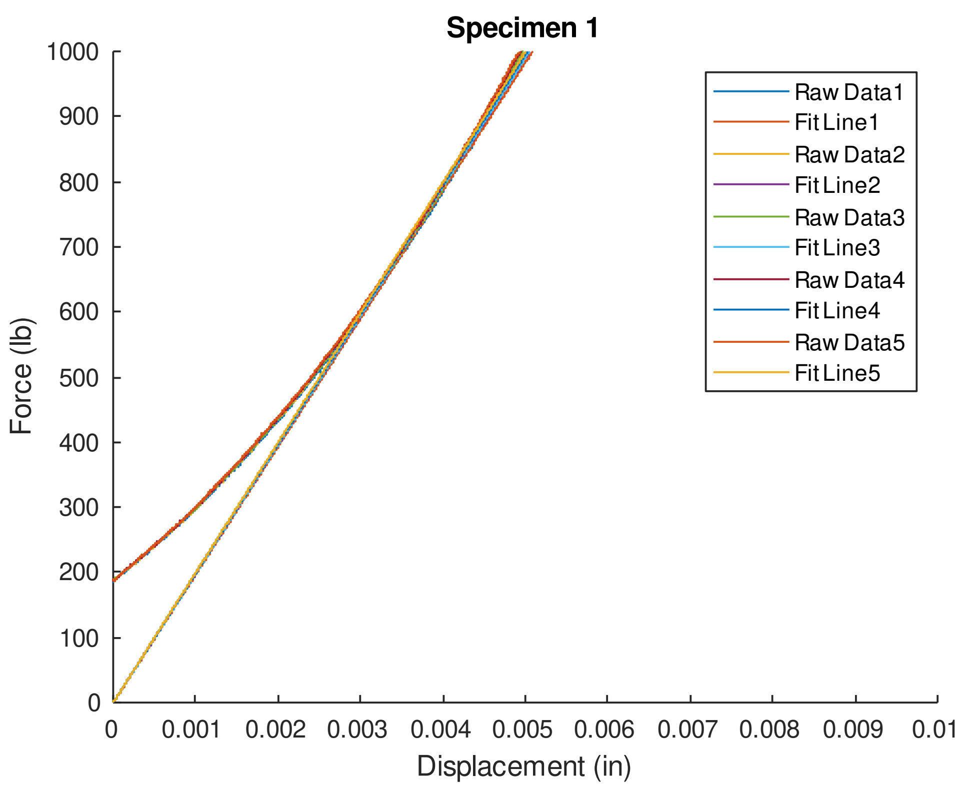

Figure 70: Compression Molded Specimen 1 (CM1)

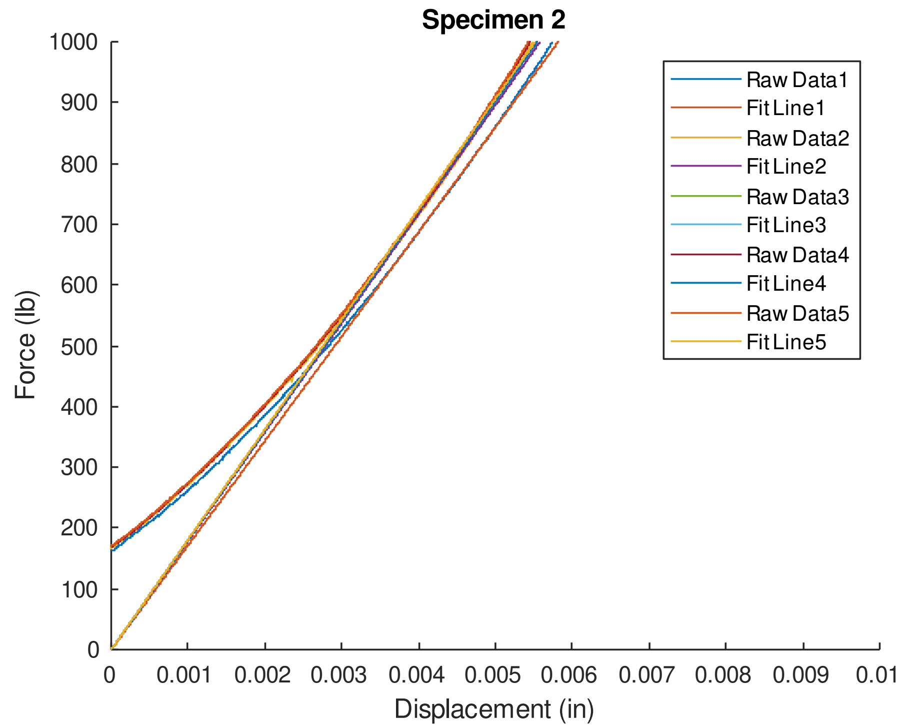

Figure 71: Compression Molded Specimen 2 (CM2)

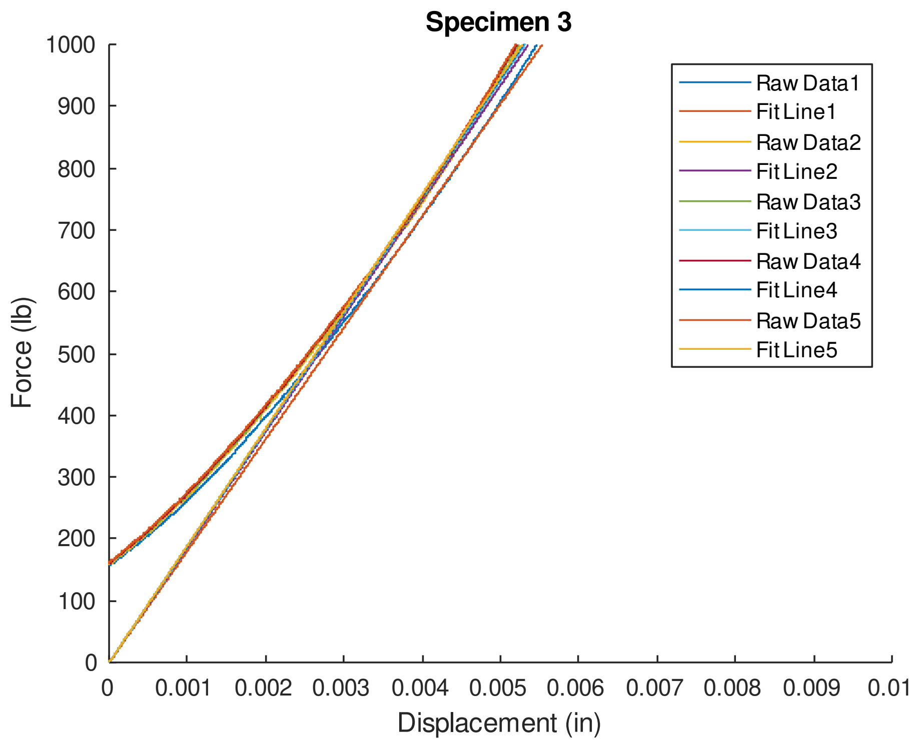

Figure 72: Compression Molded Specimen 3 (CM3)

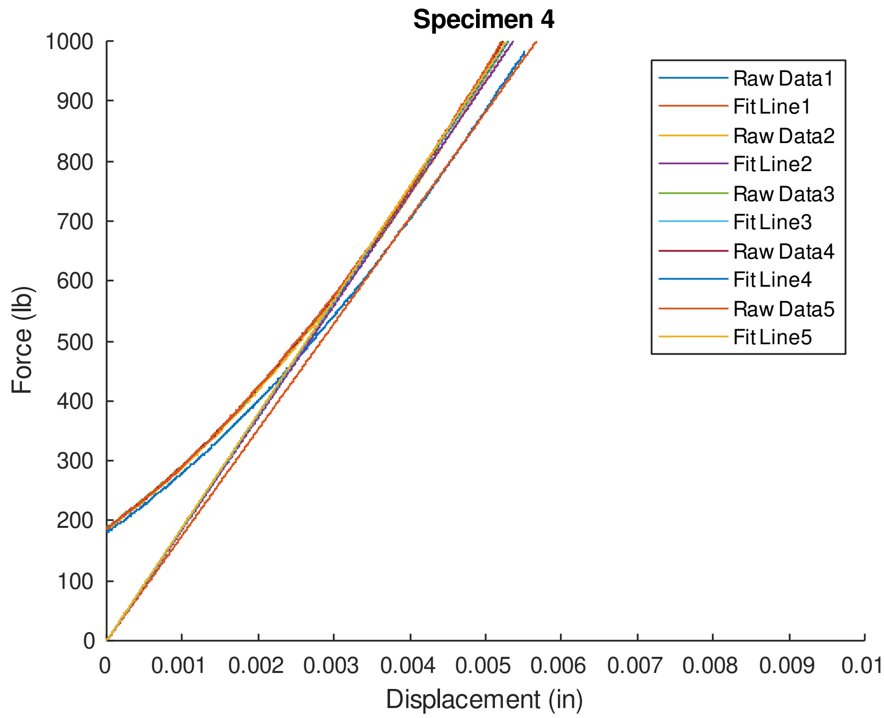

Figure 73: Compression Molded Specimen 4 (CM4)

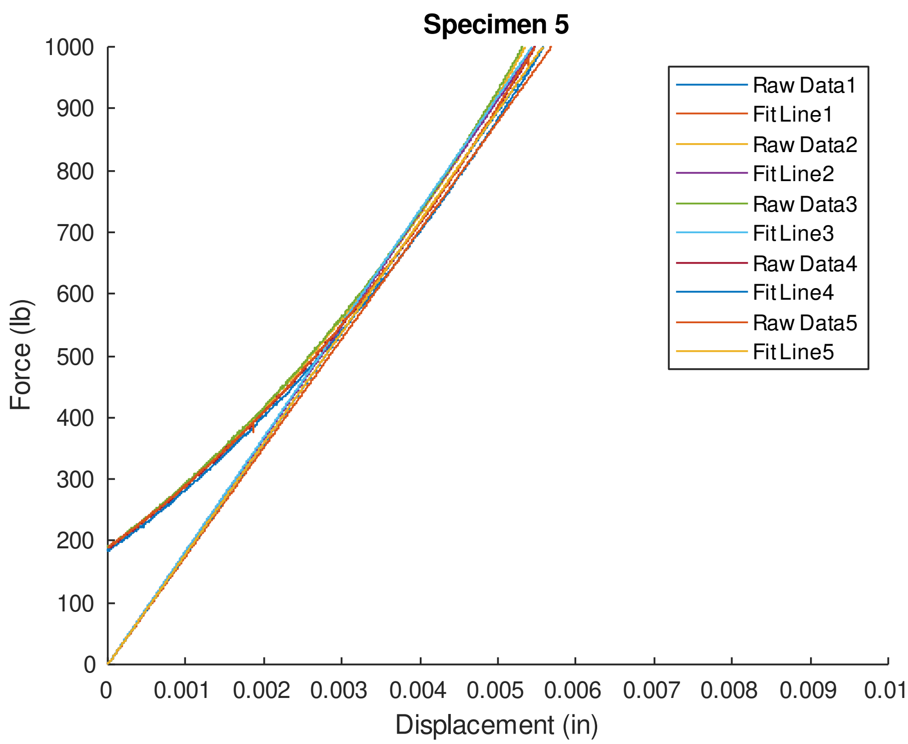

Figure 74: Compression Molded Specimen 5 (CM5)

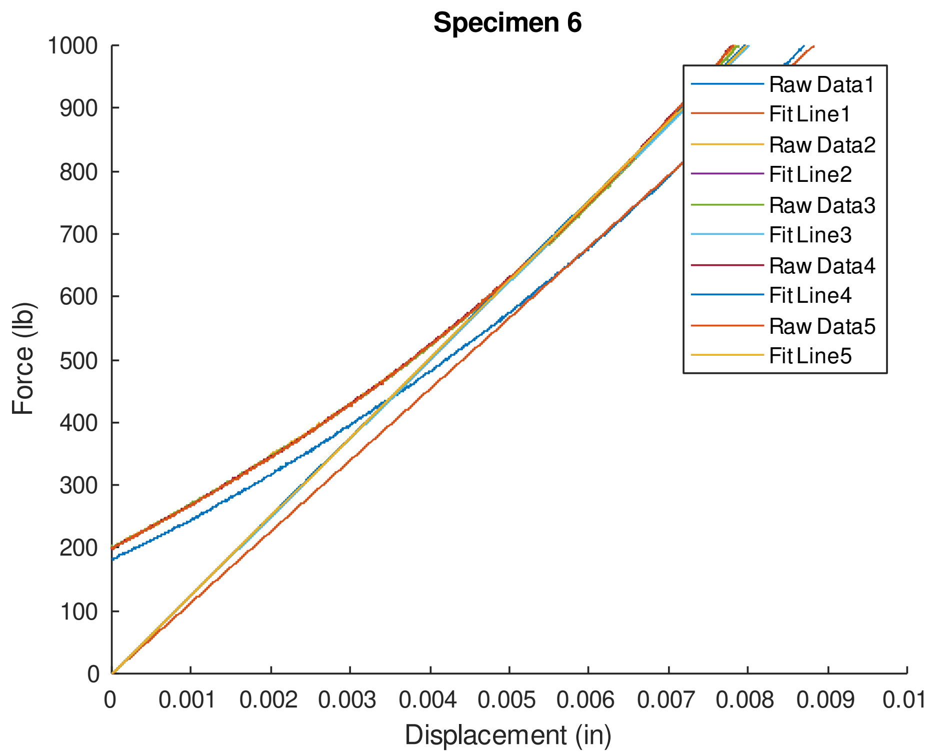

Figure 75: 3D Printed Specimen 1 (3D1)

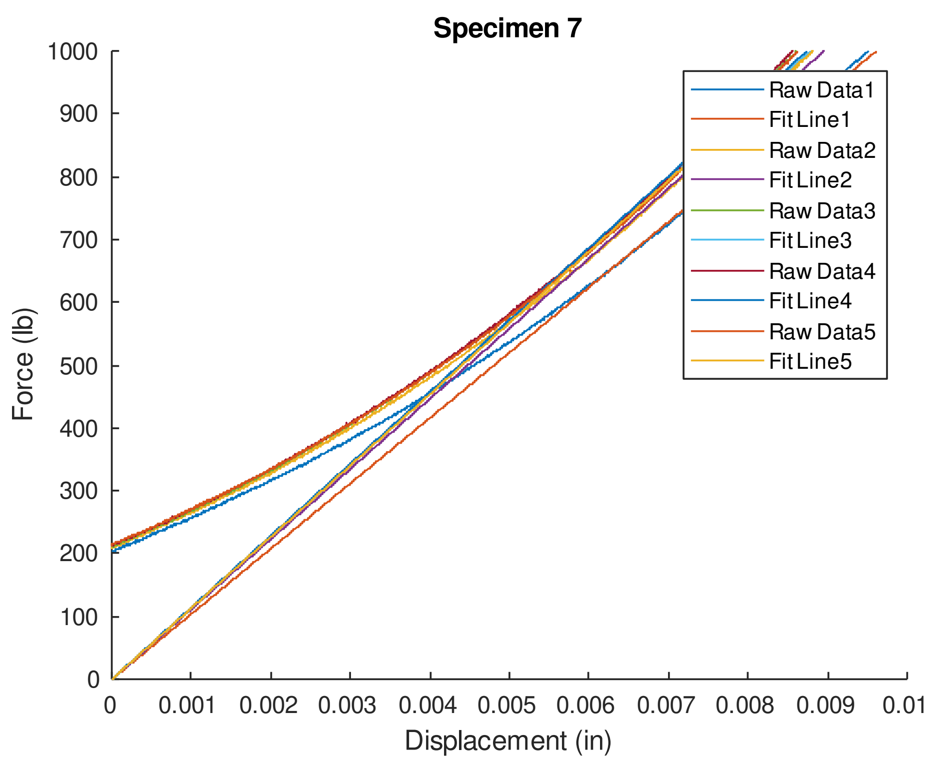

Figure 76: 3D Printed Specimen 2 (3D2)

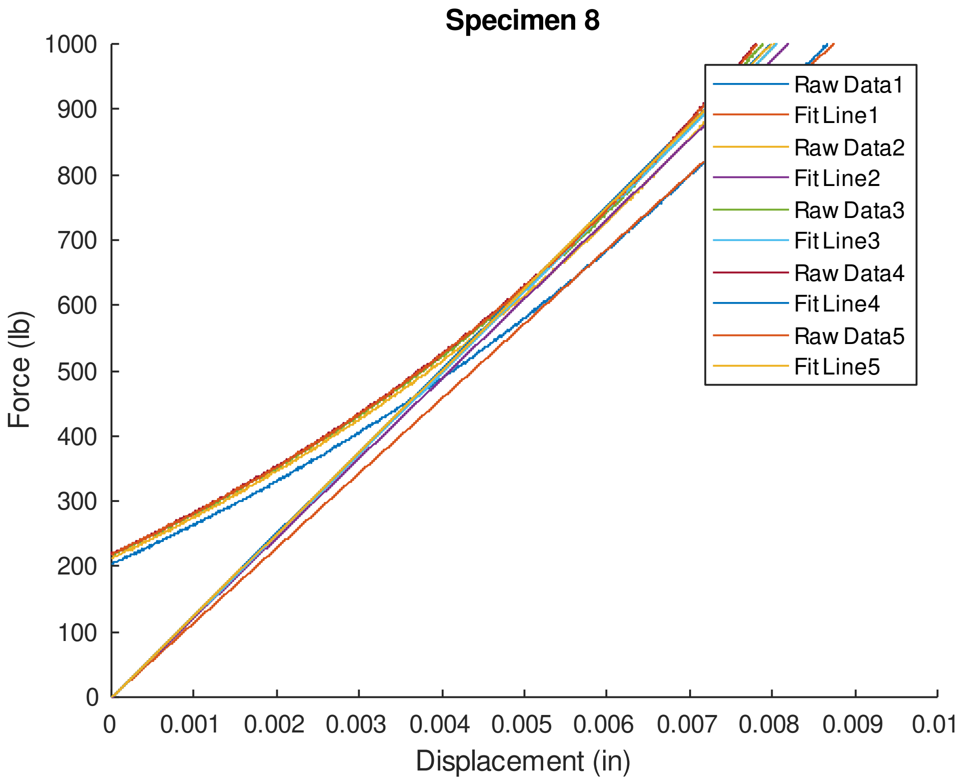

Figure 77: 3D Printed Specimen 3 (3D3)

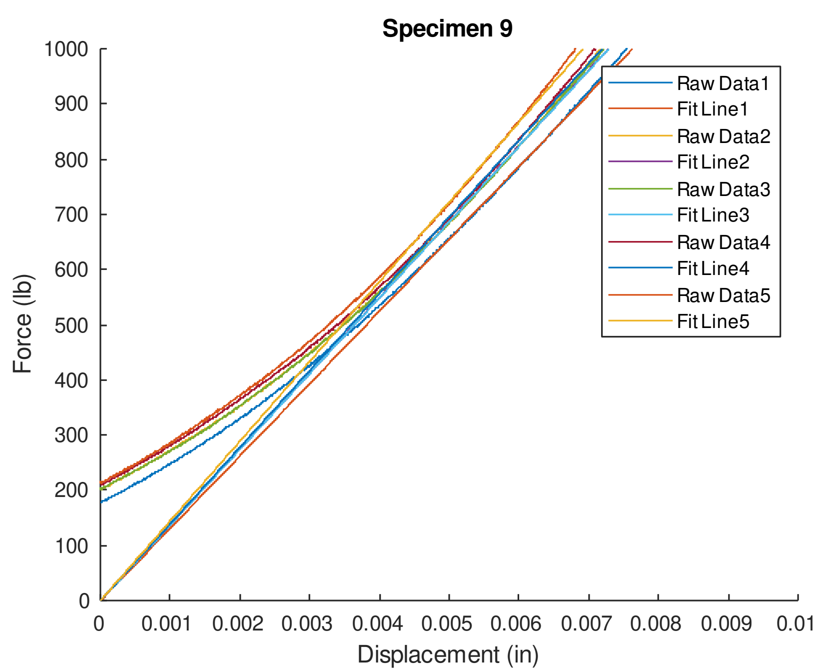

Figure 78: 3D Printed Specimen 4 (3D4)

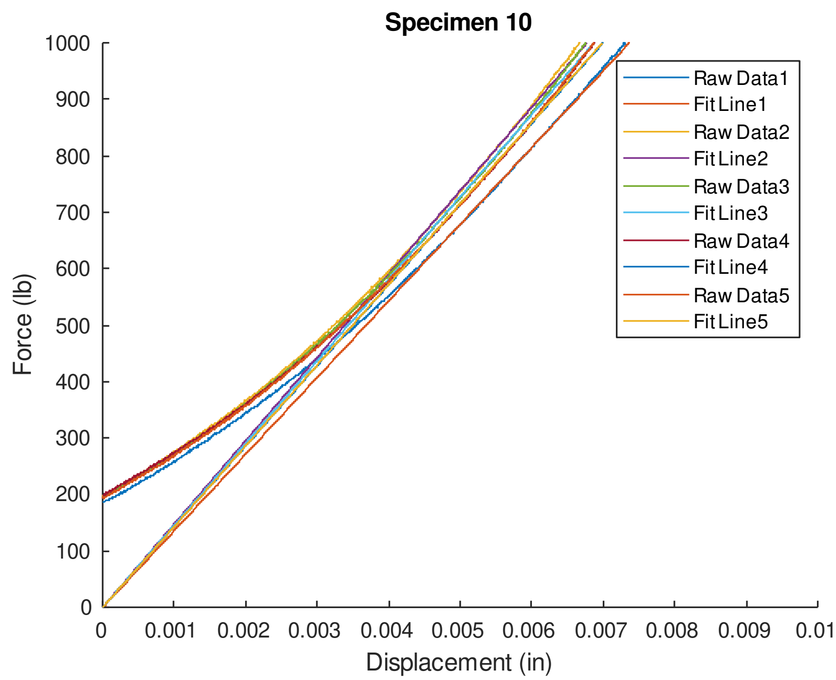

Figure 79: 3D Printed Specimen 5 (3D5)

SHEAR MODULUS FORCE VS DISPLACEMENT CURVES

COMPRESSION MOLDED

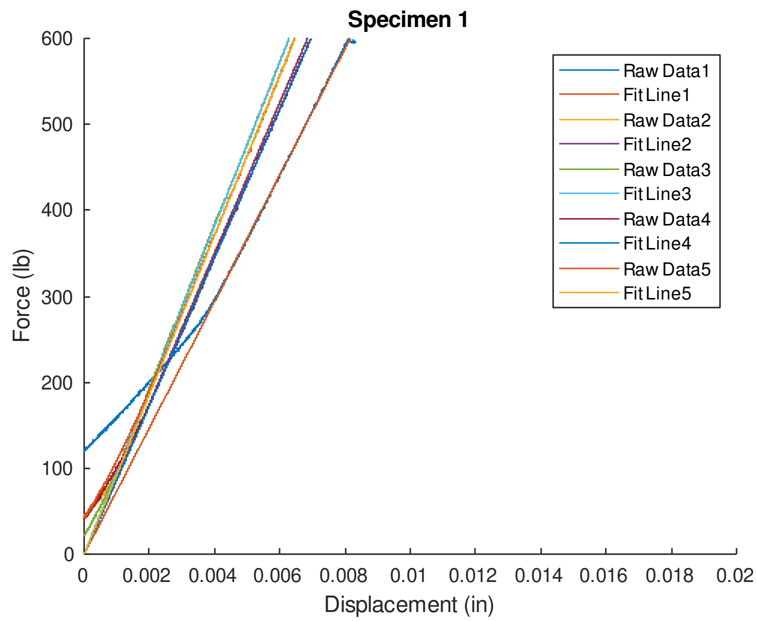

Figure 80: Compression Molded Specimen 1 (CM1)

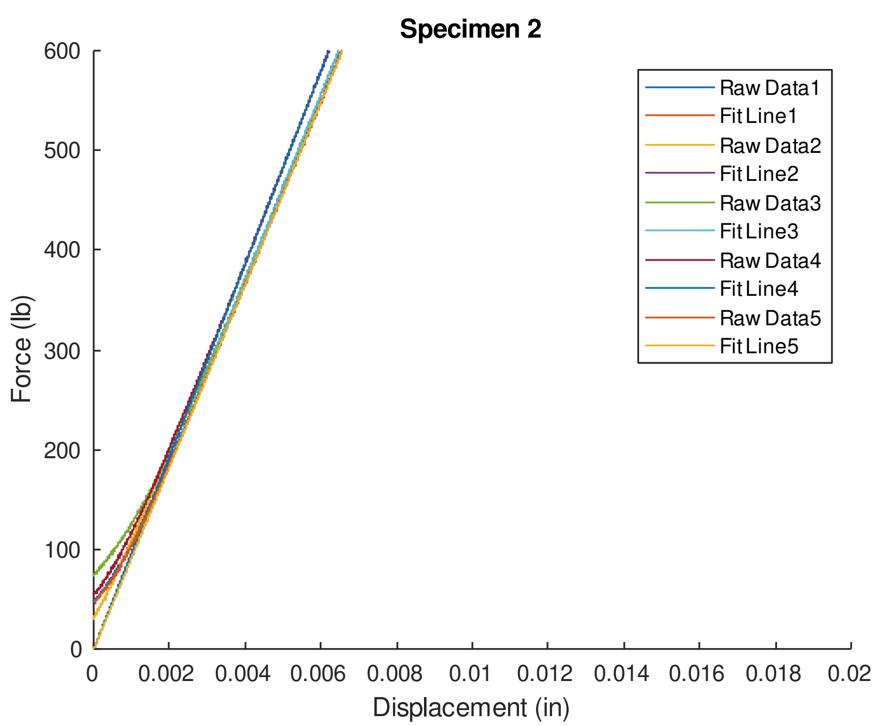

Figure 81: Compression Molded Specimen 2 (CM2)

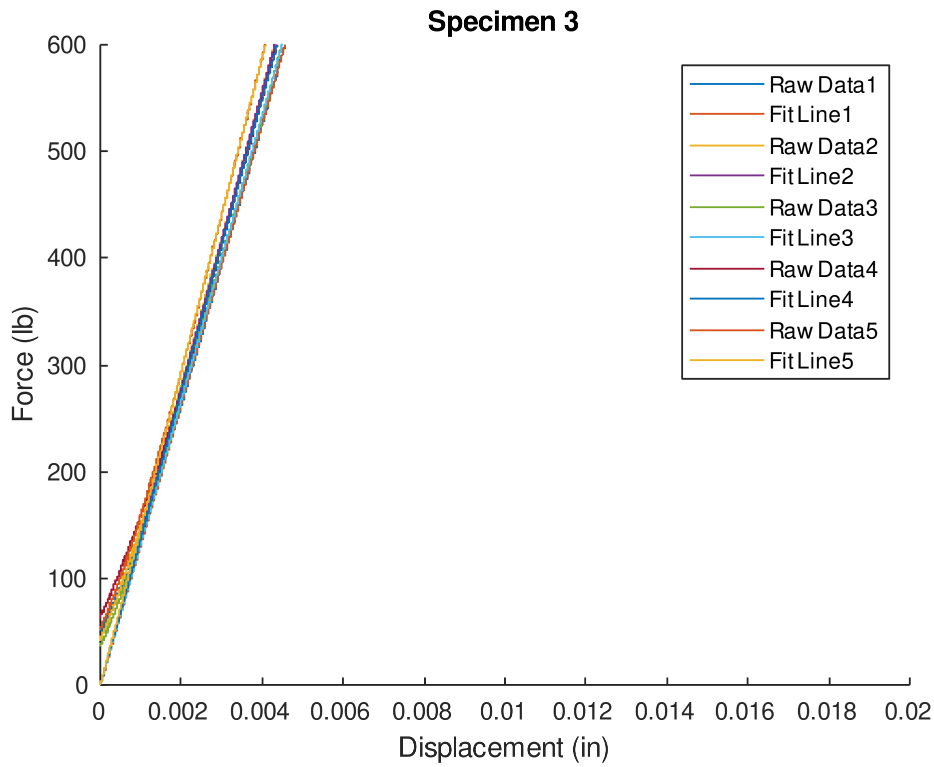

Figure 82: Compression Molded Specimen 3 (CM3)

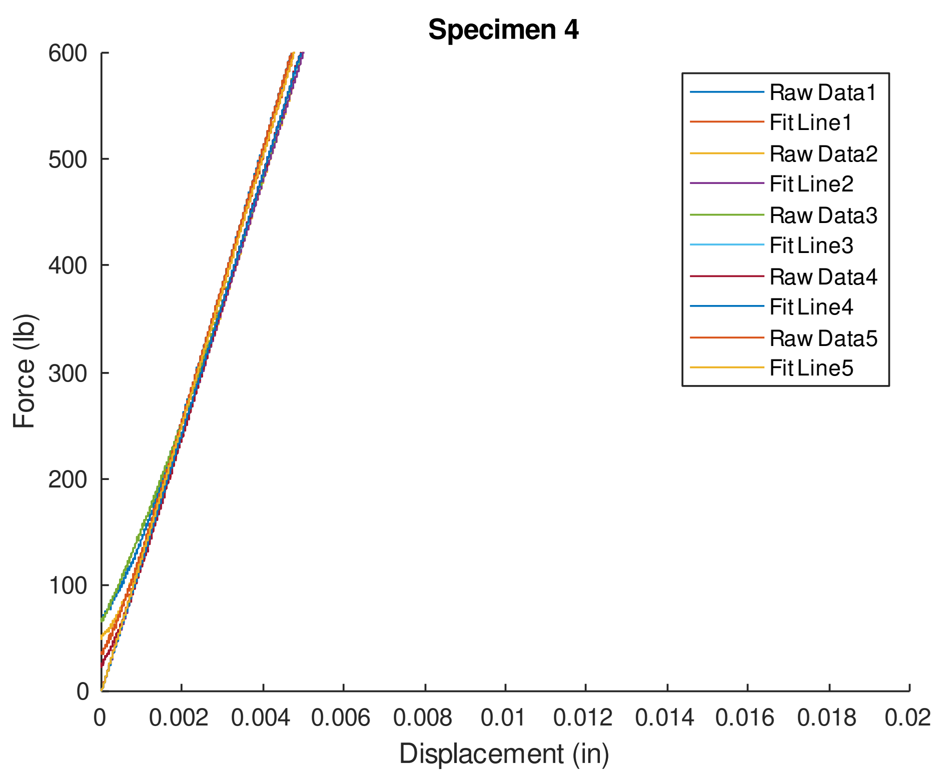

Figure 83: Compression Molded Specimen 4 (CM4)

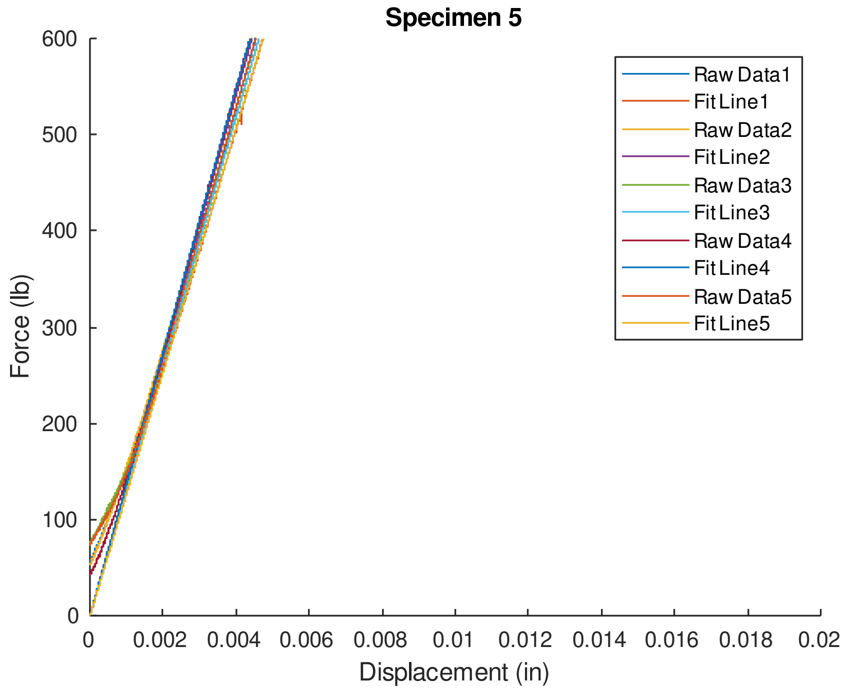

Figure 84: Compression Molded Specimen 5 (CM5)

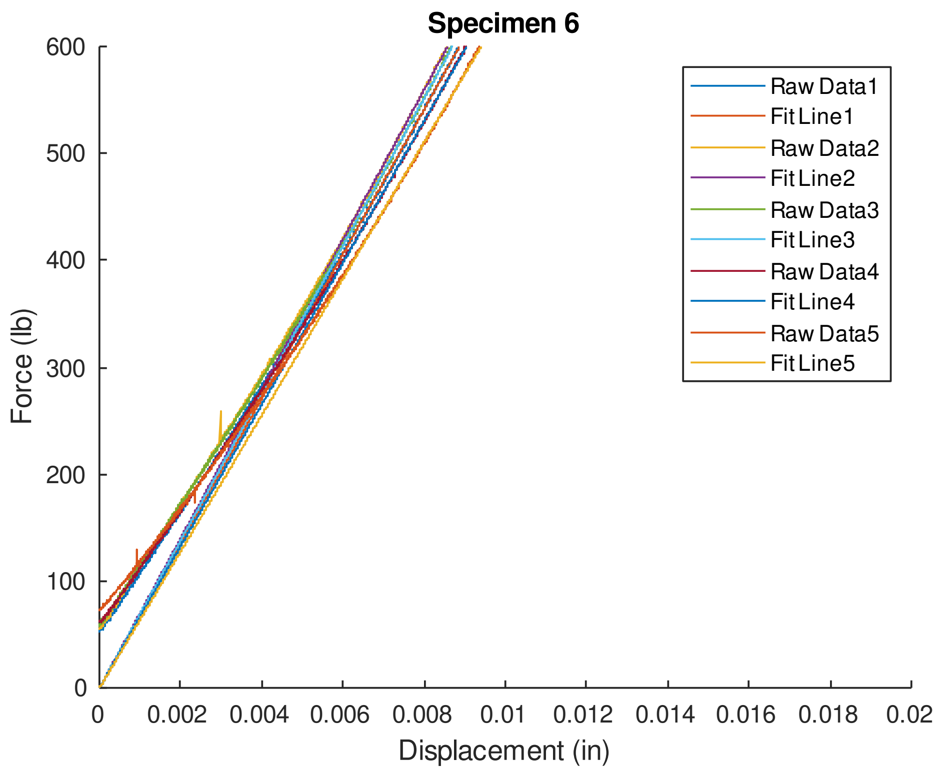

Figure 85: 3D Printed Specimen 1 (3D1)

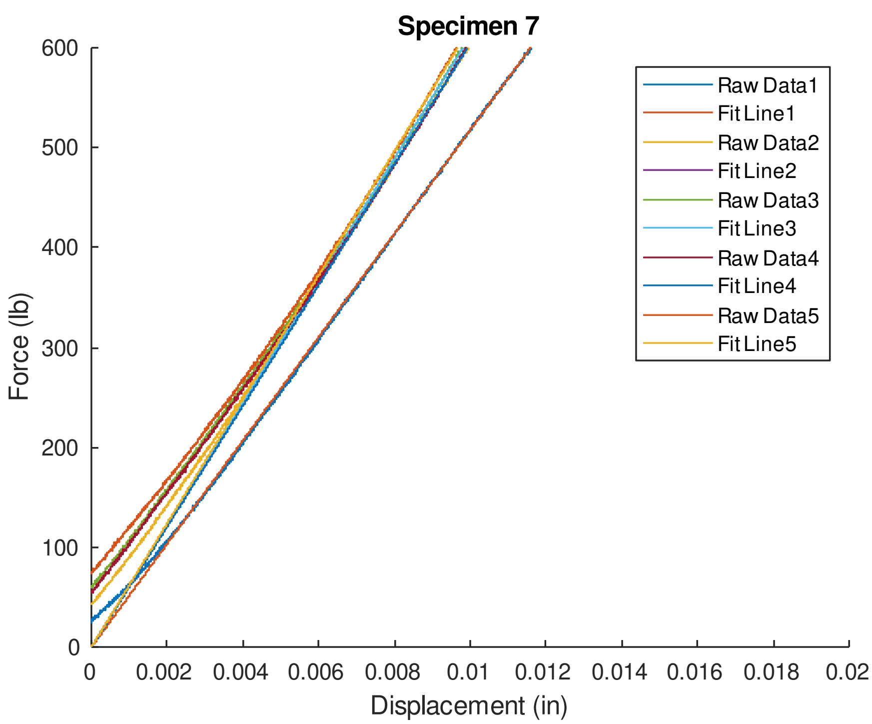

Figure 86: 3D Printed Specimen 2 (3D2)

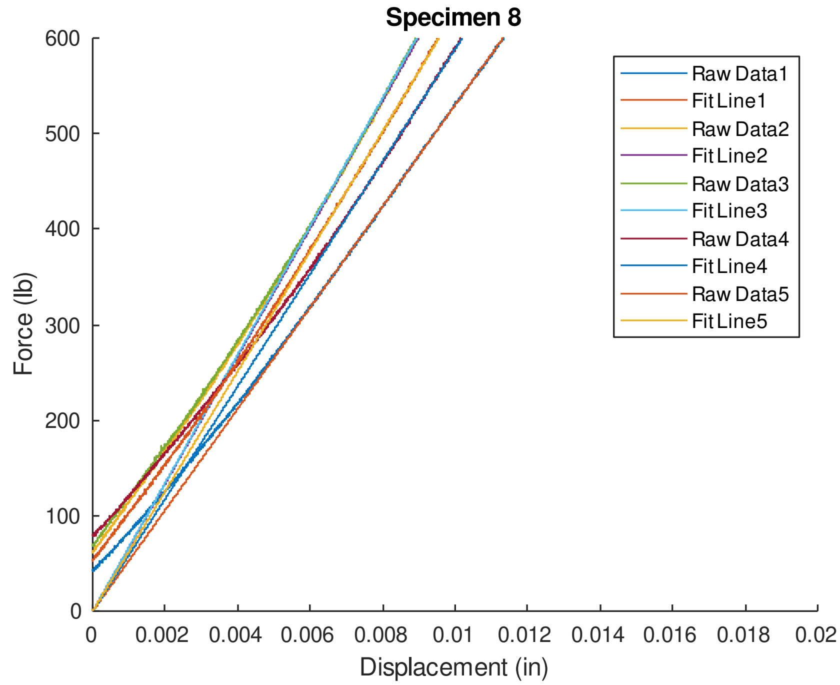

Figure 87: 3D Printed Specimen 3 (3D3)

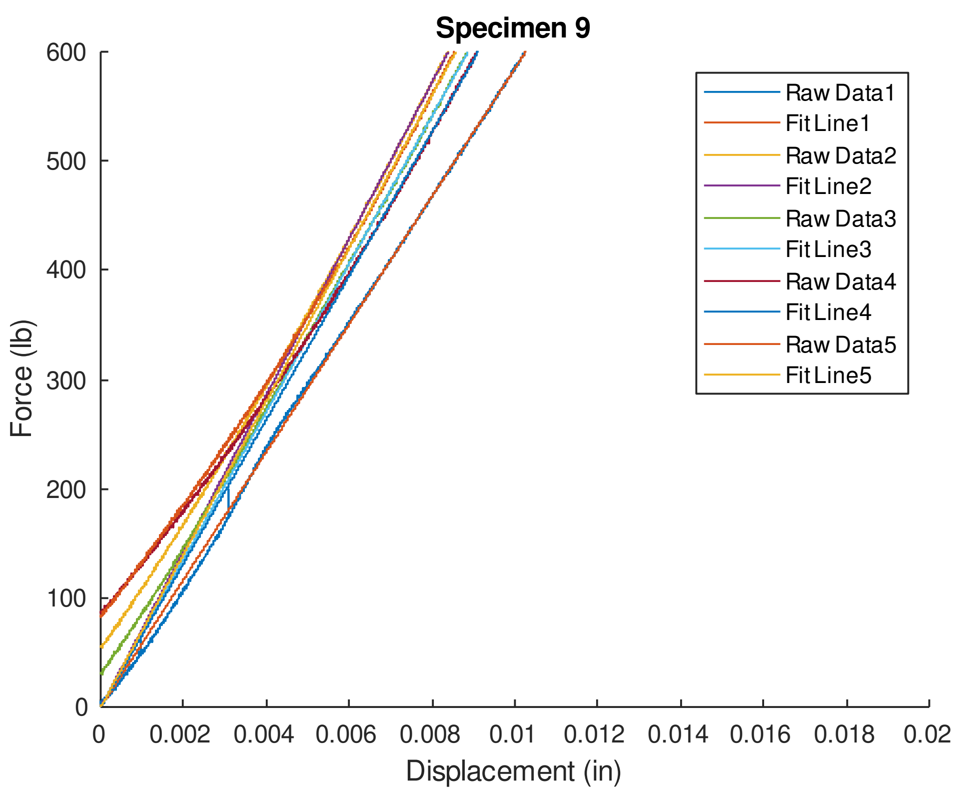

Figure 88: 3D Printed Specimen 4 (3D4)

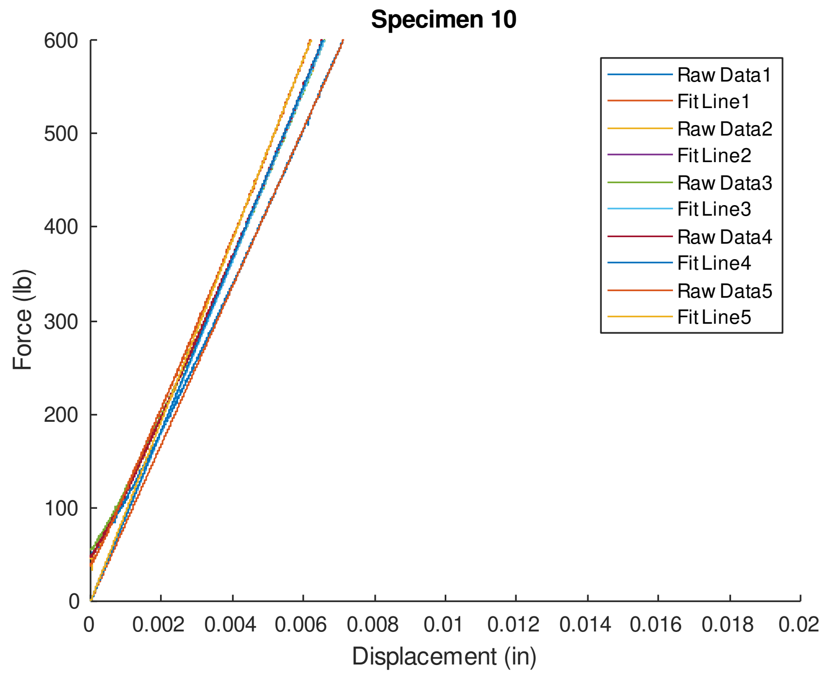

Figure 89: 3D Printed Specimen 5 (3D5)

APPENDIX B

MATLAB SCRIPT TO PARSE COMPRESSION MODULUS DATA

```
clc; clear; close all;
%% Compression Testing Math Code
% To use this program place the mech files from the compression tests in
% this file and change specCount to the number of specimens
SpecCount = 10; % Number of specimens
trialCount = 5;
%% Get Panel Information
%(Got from an excel file and moved to in file speeding up program)
%d = xlsread('SpecimenInformation.xlsx','Sheet1','B2:B11');
d =
[0.497;0.44997;0.42180;0.46440;0.455;0.497;0.48690;0.50610;0.52940;0.520];
t1= [0.10720;0.0539;0.0541;0.0561;0.0525;0.0572;0.0667;0.0655;0.0731;0.0762];
t2= [0.11450;0.0528;0.0526;0.0558;0.0542;0.0469;0.0533;0.0496;0.0605;0.0640];
b = [4.8724;5.37;5.1190;5.2273;5.1362;4.9190;4.9391;4.9241;4.8321;4.8866];
w = [4.8483;4.9160;5.1302;5.1611;5.2104;5.5824;5.5892;5.5622;5.5895;5.5849];
c =
[0.27530;0.34327;0.31510;0.35250;0.34830;0.39290;0.36690;0.391;0.39580;0.3798
0];
t = d-t1-t2;% thickness of the core
A = b.*w; % Cross sectional area of the core, I could use this or
6*7*1*10/(cos(45deg)*25.4^2)
%% The heavy lifting, or bending in this case
directory= ['01';'02';'03';'04';'05';'06';'07';'08';'09';'10'];
filenum =
['01';'02';'03';'04';'05';'06';'07';'08';'09';'10';'11';'12';'13';'14';'15';'
16';'17';'18';'19';'20';'21';'22';'23';'24';'25';'26';'27';'28';'29';'30'];

for j = 1:SpecCount
 figure
 hold on
 [m,n] = size(dir(strcat('Specimen',directory(j,:))));
 Legend = cell(m-2,1);
 for i = 1:m-2
 Set1 =
csvread(strcat('Specimen',directory(j,:),'\MECH_',filenum(i,:),'.txt'),2); %
Get the data from the text file
 % Toe correction
 T1 = find(Set1(:,3)>(600) & Set1(:,3)<(900));
 Timedef = Set1(:,1).*0.02./(2.*(60));
 %Timedef = -Set1(:,2);
 [Pol1(j,:,i),S(j,:,i)] = polyfit(Timedef(T1),Set1(T1,3),1);%Get slope for
this linear region
 Toe(1,j,i) = -Pol1(j,2,i)./Pol1(j,1,i); %Toe correction is slope/y-intercept
 %Plot the load vs displacement curve

 plot((Timedef(:)-
Toe(1,j,i)),Set1(:,3),Timedef(:),(Timedef(:)+Toe(1,j,i)).*Pol1(j,1,i)+Pol1(j,
2,i));
```

```
 title(sprintf('Specimen %d', j));
 xlabel('Displacement (in)');
 ylabel('Force (lb)');

 xlim([0 0.01]);
 ylim([0 1000]);
 % i is the load itteration
 E(i) = Pol1(j,1,i).*t(j)./A(j);
 Legend{i+i-1} = strcat('Raw Data ', num2str(i));
 Legend{i+i} = strcat('Fit Line ', num2str(i));
 end
 legend(Legend);
 E1(j) = mean(E');
 Std(j) = std(E');
 hold off
 E = [];
end
%%
figure
hold on
errorbar(E1./1000,Std./1000,'O');
title('Compressive Modulus');
xlabel('specimen number');
ylabel('Modulus (ksi)');
xlim([0 11]);
ylim([0 4]);
xticks(1:1:SpecCount);
xticklabels({'CM1','CM2','CM3','CM4','CM5','3D1','3D2','3D3','3D4','3D5'})
ax = gca;
ax.YGrid = 'on';
ax.GridAlpha = 0.75;
errorbar([1 5],
zeros(2,1)+mean(E1(1:5)'./1000),zeros(2,1)+std(E1(1:5)'./1000))
errorbar([6 10], zeros(2,1)+mean(E1(6:10)'./1000),
zeros(2,1)+std(E1(6:10)'./1000), 'Black')
hold off
```

MATLAB SCRIPT TO PARSE SHEAR MODULUS DATA

```
clc; clear; close all;
%%
% 3 Point bend testing according to ASTM 7250
% To use this program place it and shear.m in the file that has all the
% mech files then put them in the order that you need them to be in
SpecCount = 10; % Number of specimens
% Set up the number for the data graphs should be simple
% j is the specimen iteration j = 1:max specimens
%% Get Panel Information
%(Got from an excel file and moved to in file speeding up program)
%d = xlsread('SpecimenInformation.xlsx','Sheet1','B2:B11');
d =
[0.497;0.44997;0.42180;0.46440;0.455;0.497;0.48690;0.50610;0.52940;0.520;0.47
25];
t1=
[0.10720;0.0539;0.0541;0.0561;0.0525;0.0572;0.0667;0.0655;0.0731;0.0762;0];
```

```
t2=
[0.11450;0.0528;0.0526;0.0558;0.0542;0.0469;0.0533;0.0496;0.0605;0.0640;0];
b =
[4.8724;5.37;5.1190;5.2273;5.1362;4.9190;4.9391;4.9241;4.8321;4.8866;4.5];
w =
[4.8483;4.9160;5.1302;5.1611;5.2104;5.5824;5.5892;5.5622;5.5895;5.5849;5.8540
];
c =
[0.27530;0.34327;0.31510;0.35250;0.34830;0.39290;0.36690;0.391;0.39580;0.3798
0;0.4725];
t = d-t1-t2;% thickness of the core
A = b.*w; % Cross sectional area of the core, I could use this or
6*7*1*10/(cos(45deg)*25.4^2)
%% The heavy lifting, or bending in this case
directory= ['01';'02';'03';'04';'05';'06';'07';'08';'09';'10';'11'];
filenum =
['01';'02';'03';'04';'05';'06';'07';'08';'09';'10';'11';'12';'13';'14';'15';'
16';'17';'18';'19';'20';'21';'22';'23';'24';'25';'26';'27';'28';'29';'30'];
for j = 1:SpecCount
 figure
 hold on
 [m,n] = size(dir(strcat('Specimen',directory(j,:))));
 Legend = cell(m-1,1);
 for i = 1:m-2
 Set1 =
csvread(strcat('Specimen',directory(j,:),'\MECH_',filenum(i,:),'.txt'),2); %
Get the data from the text file
 % Toe correction
 T1 = find(Set1(:,3)>(400) & Set1(:,3)<(600));
 Timedef = Set1(:,1).*0.02./(2.*(60));
 %Timedef = abs(Set1(:,2));
 [Pol1(j,:,i),S(j,:,i)] = polyfit(Timedef(T1),Set1(T1,3),1);%Get slope for
this linear region
 Toe(1,j,i) = -Pol1(j,2,i)./Pol1(j,1,i); %Toe correction is slope/y-intercept
 %Plot the load vs displacement curve

 plot((Timedef(:))-
Toe(1,j,i),Set1(:,3),Timedef(:),(Timedef(:)+Toe(1,j,i)).*Pol1(j,1,i)+Pol1(j,2
,i));
 title(sprintf('Specimen %d', j));
 xlabel('Displacement (in)');
 ylabel('Force (lb)');

 xlim([0 0.02]);
 ylim([0 600]);
 % i is the load itteration
 G(i,j) = Pol1(j,1,i).*c(j)./A(j);
 Legend{i+i-1} = strcat('Raw Data ', num2str(i));
 Legend{i+i} = strcat('Fit Line ', num2str(i));
 end
 legend(Legend);
 G1(j) = mean(G(1:i,j));
 Std(j) = std(G(1:i,j));
 hold off
end
%%
```

```
figure
hold on
errorbar(G1./1000,Std/1000,'O');
title('Shear Modulus');
xlabel('specimen number');
ylabel('Modulus (ksi)');
xlim([0 11]);
ylim([0 2.5]);
xticks(1:1:SpecCount);
xticklabels({'CM1','CM2','CM3','CM4','CM5','3D1','3D2','3D3','3D4','3D5'})%,'
Hexcell'
ax = gca;
ax.YGrid = 'on';
ax.GridAlpha = 0.75;
errorbar([3 5],
zeros(2,1)+mean(G1(3:5)'./1000),zeros(2,1)+std(G1(3:5)'./1000))
errorbar([6 10], zeros(2,1)+mean(G1(6:10)'./1000),
zeros(2,1)+std(G1(6:10)'./1000), 'Black')
hold off
```

MATLAB SCRIPT TO GENERATE G-CODE – FACINGS

```
%% Code for multi angle samples
format compact; clear; clc;
%% Constants
% Sample Geometry
BW = 2.9; % mm Bandwidth, Tow Width, Road Width all the same thing
LH = 0.4; % mm Layer height or Distance between CC and the Part
SpringDef = 0.4; % mm
% Bed Geometry
BX = 270; % mm Bed X length
BY = 300; % mm Bed Y length
% Clearance Constants
EZ = 15; % Z clearance
% Change these variables
Speed = 180; % mm/min Sample Placement Speed
Rapid = 1800; % Rapid movement
Layer = 1;
SheetSizeX = 120;
SheetSizeY = 146;
Flange = 30;
fileout = 'CoolBottomFace0.gcode';
fileID = fopen(fileout,'wt'); % set up file
fprintf(fileID,'G28\nM17\nG92 E0'); % Home as first line always

%% Point Compiler
X = fliplr(BX/2-SheetSizeX/2:BW:BX/2+SheetSizeX/2);
Y = fliplr(BY/2-SheetSizeY/2:SheetSizeY:BY/2+SheetSizeY/2);
Z = LH*Layer-SpringDef;
[CX,CY,CZ] = meshgrid(X,Y,Z);
[n,m] = size(CX);
%% change this for there and back again
% to cut with this
% for i = 1:m
% CCX(1,(i-1)*n+1:i*n) = CX(:,i);
```

```
% CCY(1,(i-1)*n+1:i*n) = CY(:,i);
% CCZ(1,(i-1)*n+1:i*n) = CZ(:,i);
% end
% Dont need to cut with this
for i =1:m
 if (mod(i,n)==0)
 CCX(1,(i-1)*n+1:i*n) = CX(:,i);
 CCY(1,(i-1)*n+1:i*n) = CY(:,i);
 CCZ(1,(i-1)*n+1:i*n) = CZ(:,i);
 else
 CCX(1,(i-1)*n+1:i*n) = flipud(CX(:,i));
 CCY(1,(i-1)*n+1:i*n) = flipud(CY(:,i));
 CCZ(1,(i-1)*n+1:i*n) = flipud(CZ(:,i));
 end
end

[CLX,CLY,CLZ,E] = anglechange(CCX,CCY,CCZ);
ZC = max(max(CLZ))+EZ;
%% Point Aligner
N=1;
for i = 1:n*m % Row
 if (CLY(i) >= BY/2)
 FL = Flange;
 else
 FL = -Flange;
 end
 if (i == 1)
 % The first line of code
 % Move to safe starting point
 Xf(N) = CLX(i); % Move to X
 Yf(N) = CLY(i)+FL; % Move to Y % added FL for cooling
 Zf(N) = CLZ(i)+ZC;
 Ef(N) = E(i);
 Mf(N) = Rapid; % At a fast speed
 Cf(N) = 255; % added for cooling
 N=N+1;
 % Move Down
 Xf(N) = CLX(i); % Move to X
 Yf(N) = CLY(i)+FL; % Move to Y
 Zf(N) = CLZ(i);
 Ef(N) = E(i);
 Mf(N) = Rapid; % At a fast speed
 Cf(N) = 255;
 N=N+1;
 % Move Over
 Xf(N) = CLX(i); % Move to X
 Yf(N) = CLY(i); % Move to Y
 Zf(N) = CLZ(i);
 Ef(N) = E(i);
 Mf(N) = Speed; % At a fast speed
 Cf(N) = 255;
 N=N+1;
 elseif (i == n*m ) % The last line of code
 Xf(N) = CLX(i); % Move to X
 Yf(N) = CLY(i)+FL; % Move to Y
 Zf(N) = CLZ(i);
 Ef(N) = E(i)+40;
```

```
 Mf(N) = Speed; % At a fast speed
 Cf(N) = 255;
 N=N+1;
 Xf(N) = CLX(i); % Move to X
 Yf(N) = CLY(i)+FL; % Move to Y
 Zf(N) = ZC;
 Ef(N) = E(i)+40;
 Mf(N) = Speed; % At a fast speed
 Cf(N) = 255;
 N=N+1;
 elseif (mod(i,2) == 0)
 Xf(N) = CLX(i); % Move to X
 Yf(N) = CLY(i); % Move to Y
 Zf(N) = CLZ(i);
 Ef(N) = E(i);
 Mf(N) = Speed;
 Cf(N) = 0;
 N=N+1;
 % what I need to do is add the flange, and only cool the flange
 Xf(N) = CLX(i); % Move to X
 Yf(N) = CLY(i)+FL; % Move to Y
 Zf(N) = CLZ(i);
 Ef(N) = E(i)+40;
 Mf(N) = Speed; % At a fast speed
 Cf(N) = 255;
 N=N+1;
 % what I need to do is add the flange, and only cool the flange
 Xf(N) = CLX(i+1); % Move to X
 Yf(N) = CLY(i)+FL; % Move to Y
 Zf(N) = CLZ(i);
 Ef(N) = E(i)+40;
 Mf(N) = Speed; % At a fast speed
 Cf(N) = 255;
 N=N+1;
 % what I need to do is add the flange, and only cool the flange
 Xf(N) = CLX(i+1); % Move to X
 Yf(N) = CLY(i); % Move to Y
 Zf(N) = CLZ(i);
 Ef(N) = E(i)+40;
 Mf(N) = Speed; % At a fast speed
 Cf(N) = 255;
 N=N+1;
 end
end


%% Write G-code
% G5 S255 turn on cooling
% G5 S0 turn off cooling
for i = 1:N-1
 % added for cooling
 fprintf(fileID, '\nG1 X%3.2f Y%3.2f Z%3.2f F%3.2f S%3.2f', Xf(i), Yf(i),
Zf(i), Mf(i), Cf(i));
 if i==N-1
 fprintf(fileID,'\nG1 Z%3.2f\nG5 S0',ZC);
 end
```

```
end
fclose('all');
```

MATLAB SCRIPT FOR GENERATING G-CODE – CFRTC CORE X-DIRECTION

```
%% Code for multi angle samples
format compact; clear; clc;
%% Constants
% Sample Geometry
XBand = 10;
XGap = 40;
YBand = 44;
BW = 2; % mm Bandwidth, Tow Width, Road Width all the same thing
LH = 0.2; % mm Layer height or Distance between CC and the Part
SpringDef = 0.4; % mm
% Bed Geometry
BX = 270; % mm Bed X length
BY = 300; % mm Bed Y length
% Clearance Constants
EZ = 15; % Z clearance
% Change these variables
Speed = 100; % mm/min Sample Placement Speed
Rapid = 1800; % Rapid movement
Layer = 1;
SheetSizeX = 120;
SheetSizeY = 146;
Flange = 25;
fileout = 'CoolingTrussXStep4.gcode';
WaitTime = 4; % Seconds
fileID = fopen(fileout,'wt'); % set up file
fprintf(fileID,'G28\nM17\nG92 E0'); % Home as first line always
% Starting Constants

%% Node Information
% Set up of node points this is the center of each node
X = [];
Y = [];
Z = [];
C = [];
S = [];
End = [];
Nx = [((-XBand/2:BW:XBand/2)+BX/2)-XGap ((-XBand/2:BW:XBand/2)+BX/2) ((-
XBand/2:BW:XBand/2)+BX/2)+XGap];
Ny = [BY/2-YBand*3/2;BY/2-YBand/2;BY/2+YBand/2; BY/2+YBand*3/2]';
%Ny = [BY/2-YBand BY/2 BY/2+YBand];
[NodeX,NodeY] = meshgrid(fliplr(Nx),Ny);
% Node Constants and diagram =)
% TopLength
% H2 H4
% Overshoot/--.--\ Height
% /H3NP |
% / |
% / | Base Length
%______/ |_______
% H1 H5
```

```
Height = 11;
BaseLength = 5;
TopLength = 12;
Overshoot =0;
% Forward
HP(1,1) = -TopLength/2-(Height-5);
HP(2,1) = -TopLength/2-1;
HP(3,1) = -TopLength/2;
HP(4,1) = TopLength/2+3;
HP(5,1) = TopLength/2+(Height-1);
%Backward
HP(1,2) = -TopLength/2-(Height-5);
HP(2,2) = -TopLength/2-3;
HP(3,2) = TopLength/2;
HP(4,2) = TopLength/2+1;
HP(5,2) = TopLength/2+(Height-1);

CP(1,1) = 255;
CP(2,1) = 0;
CP(3,1) = 0;
CP(4,1) = 0;
CP(5,1) = 255;

SP(5) = WaitTime;
ZP(1) = LH-SpringDef;
ZP(2) = Height;
ZP(3) = Height;
ZP(4) = Height;
ZP(5) = LH-SpringDef;
[Gridx,Gridy] = size(NodeX);
% The Y
for Gy = 1:Gridy
 if (mod(Gy,2)==0)
 j = 1;
 else
 j = 2;
 end
 for Gx = 1:Gridx
 if Gx == 1
 X = [X,NodeX(Gx,Gy)];
 Y = [Y,NodeY(Gx,Gy)-Flange];
 Z = [Z,ZP(3)];
 C = [C,255];
 S = [S,SP(3)];
 End = [End,0];
 for i = 3:5
 X = [X,NodeX(Gx,Gy)];
 Y = [Y,NodeY(Gx,Gy)+HP(i,j)];
 Z = [Z,ZP(i)];
 if (i == 3)
 C = [C,255];
 else
 C = [C,CP(i)];
 end
 S = [S,SP(i)];
 End = [End,0];
```

```
 end
 elseif Gx == Gridx
 for i = 1:3
 X = [X,NodeX(Gx,Gy)];
 Y = [Y,NodeY(Gx,Gy)+HP(i,j)];
 Z = [Z,ZP(i)];
 C = [C,CP(i)];
 S = [S,SP(i)];
 End = [End,0];
 end
 X = [X,NodeX(Gx,Gy)];
 Y = [Y,NodeY(Gx,Gy)+Flange];
 Z = [Z,ZP(3)];
 C = [C,255];
 S = [S,SP(3)];
 End = [End,1];
 else
 for i = 1:5
 X = [X,NodeX(Gx,Gy)];
 Y = [Y,NodeY(Gx,Gy)+HP(i,j)];
 Z = [Z,ZP(i)];
 C = [C,CP(i)];
 S = [S,SP(i)];
 End = [End,0];
 end
 end
 end
 CX(Gy,:) = X; X = [];
 CY(Gy,:) = Y; Y = [];
 CZ(Gy,:) = Z; Z = [];
end


%% Point Compiler
[n,m] = size(CX);
for i =1:n
 if (mod(i,2)==0)
 CCX(1,(i-1)*m+1:i*m) = CX(i,:);
 CCY(1,(i-1)*m+1:i*m) = CY(i,:);
 CCZ(1,(i-1)*m+1:i*m) = CZ(i,:);
 else
 CCX(1,(i-1)*m+1:i*m) = fliplr(CX(i,:));
 CCY(1,(i-1)*m+1:i*m) = fliplr(CY(i,:));
 CCZ(1,(i-1)*m+1:i*m) = fliplr(CZ(i,:));
 end
end
[CLX,CLY,CLZ,E] = anglechange(CCX,CCY,CCZ);
ZC = max(max(CLZ))+EZ;
%% Point Aligner
[n,m]=size(CLX);
N=1;
for i = 1:n*m % Row
 if (i == 1)
 % Move to safe starting point
 Xf(N) = CLX(i); % Move to X
 Yf(N) = CLY(i); % Move to Y
```

```
 Zf(N) = ZC;
 Ef(N) = E(i);
 Mf(N) = Rapid; % At a fast speed
 Sf(N) = S(i);
 Cf(N) = C(i);
 N=N+1;
 end
 % Move to the desired point then rotate in to the ideal position
 Xf(N) = CLX(i); % Move to X
 Yf(N) = CLY(i); % Move to Y
 Zf(N) = CLZ(i);
 Ef(N) = E(i);
 Mf(N) = Speed;
 Cf(N) = C(i);
 Sf(N) = S(i);
 N=N+1;
 if (End(i)==1) % Indicates and end point
 if (i == n*m ) % End of code
 Xf(N) = CLX(i); % Move to X
 Yf(N) = CLY(i); % Move to Y
 Zf(N) = ZC;
 Ef(N) = E(i)+40;
 Mf(N) = Speed; % At a fast speed
 Cf(N) = C(i);
 Sf(N) = S(i);
 N=N+1;
 else % End of a line
 % Move Up
% Xf(N) = CLX(i); % Move to X
% Yf(N) = CLY(i); % Move to Y
% Zf(N) = ZC;
% Ef(N) = E(i)+40;
% Mf(N) = Speed; % At a fast speed
% Sf(N) = S(i);
% N=N+1;
% % Move over rapidly
% Xf(N) = CLX(i+1); % Move to X
% Yf(N) = CLY(i+1); % Move to Y
% Zf(N) = ZC;
% Ef(N) = E(i)+40;
% Mf(N) = Rapid; % At a fast speed
% Sf(N) = S(i);
% N=N+1;
 end
 end
end
time = max(max(E))/Speed/60

%% Start Writing G-code
for i = 1:N-1
 fprintf(fileID, '\nG1 X%3.2f Y%3.2f Z%3.2f F%3.2f S%3.2f', Xf(i), Yf(i),
Zf(i), Mf(i), Cf(i));
 if Sf(i) ~= 0
 fprintf(fileID, '\nG4 S%3.2f',Sf(i));
 end
end
fprintf(fileID, '\nG1 Z30 S0');
```

```
fclose('all');
```

MATLAB SCRIPT FOR GENERATING CFRTC SCAFFOLDING

```
%% Code for multi angle samples
format compact; clear; clc; fclose('all');
%% Constants
% Sample Geometry
BW = 2.9; % mm Bandwidth, Tow Width, Road Width all the same thing
LH = 0.2; % mm Layer height or Distance between CC and the Part
SpringDef = 0.4; % mm
% Bed Geometry
BX = 270; % mm Bed X length
BY = 300; % mm Bed Y length
% Clearance Constants
EZ = 15; % Z clearance
% Change these variables
Speed = 180; % mm/min Sample Placement Speed
Rapid = 1800; % Rapid movement
Layer = 1;
SheetSizeX = 120;
SheetSizeY = 146;
Flange = 25;
fileout = 'CoolingScafXStep1.gcode';
fileID = fopen(fileout,'wt'); % set up file
fprintf(fileID,'G28\nM17\nG92 E0'); % Home as first line always

%% Node Information
Height = 10;
ZP = [Height];
% HPoints for the truss
%% Point Compiler
Y1 = [(BY-SheetSizeY)/2;(BY+SheetSizeY)/2];
DX = 8.964/2;
XNP = [BX/2-SheetSizeX/2:40:BX/2+SheetSizeX/2]';
%XNP = [BX/2-40;BX/2;BX/2+40];
N = 1;
% criss
[m,n] = size(XNP);
for i = 1:m
 if i == 1
 X(N) = XNP(i)+DX;
 N = N + 1;
 elseif ((i ~= 1) && (i ~= m))
 X(N) = XNP(i)-DX;
 N = N + 1;
 X(N) = XNP(i)+DX;
 N = N + 1;
 elseif i == m
 X(N) = XNP(i)-DX;
 N = N + 1;
 end
end
```

```
Z = [Height];
[CX,CY,CZ] = meshgrid(X',Y1,Z);
[n,m] = size(CY);
% for i = 1:n
% CCX(1,(i-1)*m+1:i*m) = CX(i,:);
% CCY(1,(i-1)*m+1:i*m) = CY(i,:);
% CCZ(1,(i-1)*m+1:i*m) = CZ;
% end
for i =1:m
 if (mod(i,n)==0)
 CCX(1,(i-1)*n+1:i*n) = CX(:,i);
 CCY(1,(i-1)*n+1:i*n) = CY(:,i);
 CCZ(1,(i-1)*n+1:i*n) = CZ(:,i);
 else
 CCX(1,(i-1)*n+1:i*n) = flipud(CX(:,i));
 CCY(1,(i-1)*n+1:i*n) = flipud(CY(:,i));
 CCZ(1,(i-1)*n+1:i*n) = flipud(CZ(:,i));
 end
end
[CLX,CLY,CLZ,E] = anglechange(CCX,CCY,CCZ);
ZC = max(max(CLZ))+EZ;
%% Point Aligner
N=1;
for i = 1:n*m % Row
 if (CLY(i) >= BY/2)
 FL = Flange;
 else
 FL = -Flange;
 end
 if (i == 1)
 % The first line of code
 % Move to safe starting point
 Xf(N) = CLX(i); % Move to X
 Yf(N) = CLY(i)+FL; % Move to Y % added FL for cooling
 Zf(N) = CLZ(i)+ZC;
 Ef(N) = E(i);
 Mf(N) = Rapid; % At a fast speed
 Cf(N) = 255; % added for cooling
 N=N+1;
 % Move Down
 Xf(N) = CLX(i); % Move to X
 Yf(N) = CLY(i)+FL; % Move to Y
 Zf(N) = CLZ(i);
 Ef(N) = E(i);
 Mf(N) = Rapid; % At a fast speed
 Cf(N) = 255;
 N=N+1;
 % Move Over
 Xf(N) = CLX(i); % Move to X
 Yf(N) = CLY(i); % Move to Y
 Zf(N) = CLZ(i);
 Ef(N) = E(i);
 Mf(N) = Speed; % At a fast speed
 Cf(N) = 255;
 N=N+1;
 elseif (i == n*m ) % The last line of code
 Xf(N) = CLX(i); % Move to X
```

```
 Yf(N) = CLY(i)+FL; % Move to Y
 Zf(N) = CLZ(i);
 Ef(N) = E(i)+40;
 Mf(N) = Speed; % At a fast speed
 Cf(N) = 255;
 N=N+1;
 Xf(N) = CLX(i); % Move to X
 Yf(N) = CLY(i)+FL; % Move to Y
 Zf(N) = ZC;
 Ef(N) = E(i)+40;
 Mf(N) = Speed; % At a fast speed
 Cf(N) = 255;
 N=N+1;
 elseif (mod(i,2) == 0)
 Xf(N) = CLX(i); % Move to X
 Yf(N) = CLY(i); % Move to Y
 Zf(N) = CLZ(i);
 Ef(N) = E(i);
 Mf(N) = Speed;
 Cf(N) = 0;
 N=N+1;
 % what I need to do is add the flange, and only cool the flange
 Xf(N) = CLX(i); % Move to X
 Yf(N) = CLY(i)+FL; % Move to Y
 Zf(N) = CLZ(i);
 Ef(N) = E(i)+40;
 Mf(N) = Speed; % At a fast speed
 Cf(N) = 255;
 N=N+1;
 % what I need to do is add the flange, and only cool the flange
 Xf(N) = CLX(i+1); % Move to X
 Yf(N) = CLY(i)+FL; % Move to Y
 Zf(N) = CLZ(i);
 Ef(N) = E(i)+40;
 Mf(N) = Speed; % At a fast speed
 Cf(N) = 255;
 N=N+1;
 % what I need to do is add the flange, and only cool the flange
 Xf(N) = CLX(i+1); % Move to X
 Yf(N) = CLY(i); % Move to Y
 Zf(N) = CLZ(i);
 Ef(N) = E(i)+40;
 Mf(N) = Speed; % At a fast speed
 Cf(N) = 255;
 N=N+1;
 end
end
%time = max(max(E))/Speed/60

%% Start Writing G-code
for i = 1:N-1
 fprintf(fileID, '\nG1 X%3.2f Y%3.2f Z%3.2f F%3.2f S%3.2f', Xf(i), Yf(i),
Zf(i), Mf(i),Cf(i));
 if i==N-1
 fprintf(fileID,'\nG1 Z%3.2f',ZC);
 end
end
```